AD-A112 855 MINNESOTA UNIV MINNEAPOLIS DEPT OF ELECTRICAL ENGIN--ETC F/G 20/3
INVESTIGATION OF PYROELECTRIC AND PYROMAGNETIC DETECTION.(U)
APR 74 A VAN DER ZIEL DAAK02-72-C-0398

UNCLASSIFIED NL

1 of 2

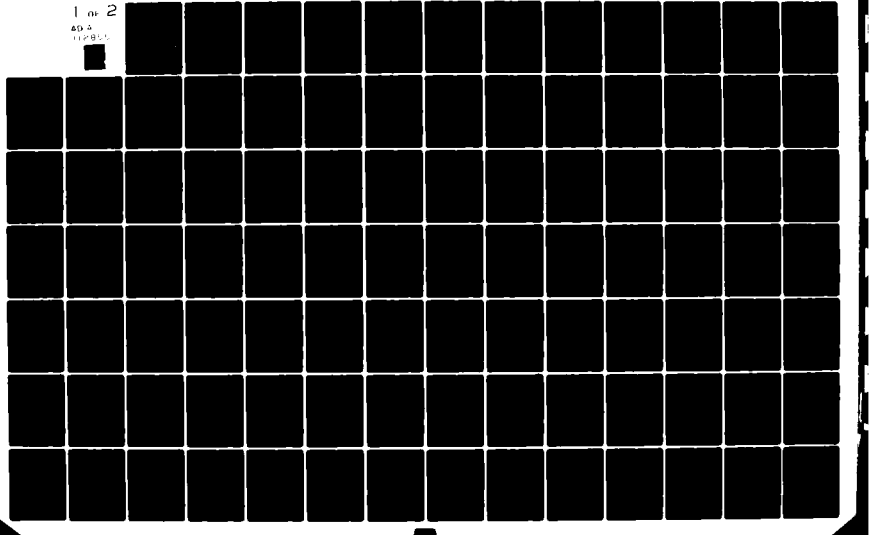

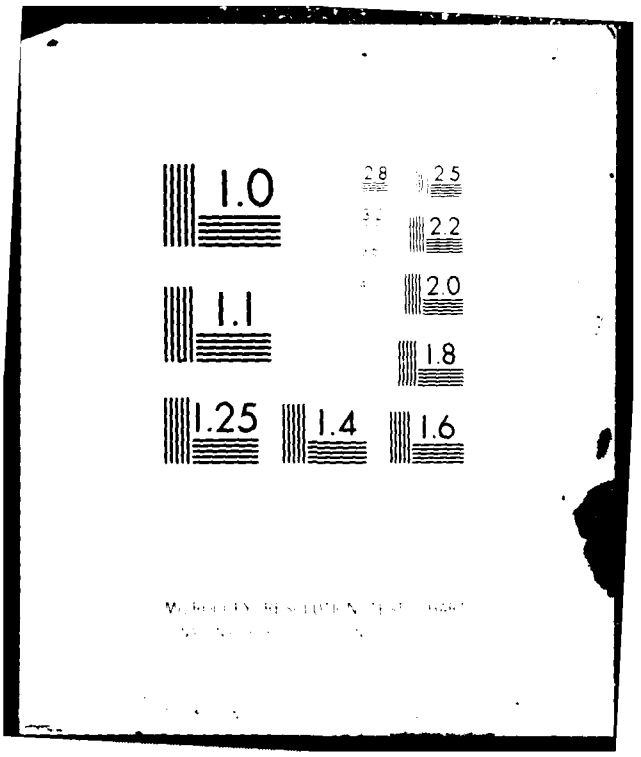
1.0
1.1
1.25
1.4
1.6
1.8
2.0
2.2
2.5

INVESTIGATION OF PYROELECTRIC AND PYROMAGNETIC DETECTION

Final Report

April 1974

by

A. van der Ziel

612--373-2460

Department of Electrical Engineering
University of Minnesota
Minneapolis, Minnesota 55455

Sponsored by

Advanced Research Projects Agency
ARPA Order No. 2192
Program Code No. 2M10
DAAK 02-72-C-0398

The views and conclusions contained in this document are those of the authors and should not be interpreted as necessarily representing official policies either expressed or implied, of the Advanced Research Projects Agency of the U. S. Government.

INVESTIGATION OF PYROELECTRIC AND PYROMAGNETIC DETECTION

Final Report

April 1974

by

A. van der Ziel

612--373-2460

Department of Electrical Engineering
University of Minnesota
Minneapolis, Minnesota 55455

Sponsored by

Advanced Research Projects Agency
ARPA Order No. 2192
Program Code No. 2M10
DAAK 02-72-C-0398

FOREWORD

This investigation was conducted from April 1, 1973 to March 31, 1974 by the Department of Electrical Engineering, University of Minnesota, under Contract DAAK 02-72-C-0398 monitored by Dr. P. Stickley, Advanced Research Projects Agency. The contracting officers representative is Mr. F. Pepito, Night Vison laboratory, Fort Belvoir, Virginia. This work was performed by A. van der Ziel, J. H. Judy, V. Singh, H. D. Park and S. J. Lee of the Electrical Engineering Department, and J. F. Wertz, F. Dravnieks, K. Mosuro of the Chemistry Department.

A. van der Ziel
Principal Investigator

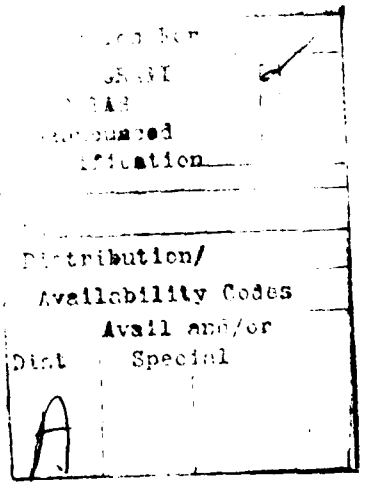

SUMMARY

A full discussion is given of Mr. V. Singh's capacitive bolometer work, ~~which was submitted~~ in partial fulfillment of the requirements for the Ph.D. degree. Capacitive bolometer detectors using TGS, and operating in the paraelectric region close to the Curie point, are shown to be comparable in performance for infrared detection with the best thermal detectors. An excess polarization noise was observed that adversely influences the NER.

A full discussion is given of the theoretical work performed under the contract. Most of ~~this~~ work deals with the molecular field model, developed under the contract. This model gives the right order of magnitude of $p/\epsilon^{1/2}$, which is the figure of merit of the pyroelectric detector; a more refined calculation for TGS gives agreement between theory and experiment within 10%. The three level model, if realized experimentally, might give better performance near the Curie temperature. The other hope for improvement of pyroelectric detectors lies in decreasing tan δ. Procedures for making contacts and synthesizing ceramic samples are outlined. Au-Cr contacts give reproducible and reliable performance.

TABLE OF CONTENTS

	Page
Summary	1
Part I Capacitive Bolometer Work	
1. Theory	2
1.1 Thermal Response	
1.2 d.c. Capacitive Bolometer	
1.3 a.c. Capacitive Bolometer	
2. Noise Equivalent Power (NEP)	5
2.1 NEP due to Temperature Fluctuations	
2.2 NEP of d.c. Capacitive Bolometer	
2.3 NEP of a.c. Capacitive Bolometer	
2.4 NEP of Pyroelectric Detector	
2.5 A Numerical Calculation for TGS	
3. Results and Discussion	10
3.1 Dielectric Measurements	
3.2 Sensitivity Measurements	
3.2.1 d.c. Bolometer	
3.2.2 a.c. Bolometer	
3.3 Noise Measurements	
Part II Theoretical Work	
1. The Pyroelectric Detector	23
2. Note on Dielectric Losses	26
3. Generalized Molecular Field Theory of the Pyroelectric Effect and Capacitive Bolometer Effect	30
4. Molecular Field Theory of Ferroelectricity and its Application	34
5. A Three-Energy Level Model of the Noise Equivalent Power Figure of Merit p/ϵ-1 of $BaTiO_3$	42
6. Accurate Calculation of $p/(\epsilon-1)^{1/2}$ in TGS	46
7. Solar Power Generation with the Pyroelectric Effect	51
Part III Materials Work	
1. Contact Study on PLZT (12-40/60)	57
2. Pyroelectric Materials Preparation	61

List of Figures

		Page
Fig. 1	D.C. capacitive bolometer circuit	67
Fig. 2	A.C. capacitive bolometer circuit	68
Fig. 3	Experimental set-up for measuring d.c. bolometer sensitivity	69
Fig. 4	Set-up for measuring a.c. bolometer sensitivity	70
Fig. 5	Set-up for noise measurement in d.c. bolometer	71
Fig. 6	Capacitance versus temperature in TGS capacitor	72
Fig. 7	1/C versus temperature in TGS capacitor	73
Fig. 8	TGS #42, 1/C versus temperature	74
Fig. 9	tan δ versus temperature TGS-#40	75
Fig. 10	tan δ and capacitance versus temperature for SBN	76
Fig. 11	tan δ, capacitance C and conductance G_p versus temperature for $BaTiO_3$	77
Fig. 12	Series resistance of $BaTiO_3$ versus temperature	78
Fig. 13	Capacitance C versus field E in TGS	79
Fig. 14	Dissipation factor tan δ versus field E in TGS	80
Fig. 15	D.C. bolometer sensitivity for TGS#40 versus E	81
Fig. 16	D.C. bolometer sensitivity for TGS#40 versus E	82
Fig. 17	D.C. bolometer sensitivity versus E for TGS#42	83
Fig. 18	Induced polarization versus field in TGS	84
Fig. 19	Inverse of sensitivity versus temperature in TGS	85

Fig. 20 Inverse of sensitivity versus temperature in TGS#40 86

Fig. 21 Pyroelectric sensitivity and capacitive bolometer sensitivity versus field (TGS#40) 87

Fig. 22a Pyroelectric sensitivity for TGS#40 versus temperature, field as parameter 88

Fig. 22b Pyroelectric sensitivity for TGS#40 versus temperature at 1.6 KV/cm 89

Fig. 23 Pyroelectric sensitivity and noise resistance R_n versus temperature for TGS#42 90

Fig. 24 Sensitivity versus frequency for TGS#40 91

Fig. 25 Sensitivity versus field for SBN#2 at room temperature 92

Fig. 26 Sensitivity versus field for SBN#2 at room temperature 93

Fig. 27 Noise resistance R_n versus field in TGS#40 at 55°C 94

Fig. 28 Noise resistance R_n versus field in TGS#40 at 51°C 95

Fig. 29 Noise resistance R_n versus frequency TGS#40 96

Fig. 30 Noise resistance R_n in TGS#42 versus field 97

Fig. 31 NEP and D* versus field in TGS#42 for capacitive bolometer mode 98

Fig. 32 NEP and D* versus temperature in TGS#42 for zero field 99

Fig. 33 Noise resistance R_n and series resistance R_s versus field for SBN#2 100

Fig. 34 Sensitivity versus a.c. field for TGS#30 101

Fig. 35 Schematic diagram of pyroelectric detector 102

Fig. 36 Graphical determination of the saturation polarization, if any 103

Fig. 37 $P_s(t)/P(o)$ plotted versus T/T_c for the classical and the two-level cases 104

Fig. 38 D* versus w for PLZT samples with Cr-Au contacts 105

Part I Capacitive Bolometer Work

The Capacitive Bolometer Effect in TGS*

V. P. Singh and A. van der Ziel

Department of Electrical Engineering

University of Minnesota

Minneapolis, Minnesota 55455

Summary

Capacitive bolometer detectors using ferroelectric material and operating in the paraelectric region are shown to be sensitive, low noise, rugged and easy to make devices for infra-red detection. Sensitivity of 110 volts/watt at 15 Hz and specific detectivity $D^*=1.6 \times 10^8 \frac{cm(Hz)^{1/2}}{watt}$ at modulation frequency of 100 Hz were obtained.

---

*Supported by ARPA contract.

1. Theory

Consider a capacitive element consisting of a thin film of a ferroelectric material like TGS with metal electrodes on both sides. Also assume that it can be maintained at any steady temperature T within a wide range including the Curie temperature. Now let this device be exposed through a small window to an infra-red radiation of intensity $\Delta W \sin \omega t$ watts. This would lead to a change in the device temperature.

1.1 Thermal Response

To determine the device temperature accurately one should solve the one-dimensional heat flow equation.[1] However, it can be shown[2] that the detector response to modulated radiation obtained from this equation differs insignificantly from the results obtained for the uniformly heated lumped model. Thermal response may therefore by given by

$$C_H \frac{d\Delta T}{dt} + G_H \Delta T = \eta \Delta W \sin \omega t \qquad (1.1a)$$

where η is the absorption efficiency; $C_H = \rho C_p A d$ is the heat capacity of detector; ρ is its density, C_p its specific heat, A its area and d is the thickness; G_H is the equivalent heat conductance of the device.

Steady state solution of Eq. (1.1a) is

$$\Delta T = \frac{\Delta W}{G_H} \frac{1}{(1 + \omega^2 \tau_H^2)^{1/2}} \text{ Sin } (\omega t - \varphi) \qquad (1.1b)$$

where $\tau_H = C_H/G_H$ and tan $\varphi = \omega\tau_H$.

1.2 d.c. Capacitive Bolometer

The schematic diagram is shown in Fig. 1. We will consider the operation in paraelectric phase and also the device will be assumed to behave as a perfect capacitive element (tan $\delta = 0$). Thus the whole of d.c. voltage drop V is across the detector. Let R_L be very large so that $\omega C_d R_L >> 0$, where C_d is the d.c. capacitance of the device. Then if v is the voltage across the capacitor and q the charge on electrode surface

$$\Delta q = C_d \Delta v + v \Delta C_d \qquad (1.2a)$$

Letting $\Delta q = 0$ because we have an effective open circuit.

$$\Delta v = -v \frac{\Delta C_d}{C_d}$$

Now $v = V + \Delta v \approx V$

and $\Delta v = v_o$

$$v_o = - \frac{V}{C_d} \left(\frac{\partial C_d}{\partial T} \Delta T + \frac{\partial C_d}{\partial v} \Delta v\right) \qquad (1.2b)$$

In the linear dielectric region $\frac{\partial C_d}{\partial v} = 0$, so that

$$v_o = - \frac{v}{C_d} \frac{\partial C_d}{\partial T} \frac{\eta \Delta W \text{Sin}(\omega t - \varphi)}{G_H (1+\omega^2 \tau_H^2)^{1/2}} \qquad (1.2c)$$

One can also express[3] v_o in terms of the induced polarization P. If E be the device field, then

$$\Delta E = -\Delta P/\epsilon_o$$

$$v_o = \Delta E.d = - \frac{d}{\epsilon_o} \Delta P$$

$$v_o = -\frac{d}{\epsilon_o}\left(\frac{\partial P}{\partial T}\Delta T + \frac{\partial P}{\partial E}\Delta E\right)$$

Assuming $\frac{\partial P}{\partial E} >> \epsilon_o$

$$v_o = -d\,\frac{\partial P/\partial T}{\partial P/\partial E}\,\frac{\eta\Delta W \sin(\omega t-\varphi)}{G_H(1+\omega^2\tau_H^2)^{1/2}} \qquad (1.2d)$$

This is a more general expression for d.c. bolometer response. In linear dielectric region Eq. (1.2d) reduces to (1.2c) so that the capacitive bolometer effect is essentially an induced pyroelectric effect. At large fields when the material no longer behaves like a linear dielectric, one must stick to Eq. (1.2d). Using thermodynamic theory of ferroelectrics one may write

$$E = 2A(T-T_C)P + 4BP^3 + 6CP^5 + \ldots \qquad (1.2e)$$

substituting in (1.2d)

$$v_o = d(2AP)\,\frac{\eta\Delta W \sin(\omega t-\varphi)}{G_H(1+\omega^2\tau_H^2)^{1/2}} \qquad (1.2f)$$

technical sensitivity S is therefore given as

$$S = \left|\frac{v_o}{\Delta W}\right| = kP \qquad (1.2g)$$

where the constant k is,

$$k = \frac{2dA}{G_H(1+\omega^2\tau_H^2)^{1/2}} \qquad (1.2h)$$

1.3 a.c. Capacitive Bolometer

Figure 2 shows the schematic diagram of an a.c. bolometer with resonant circuit and suppressed carrier. If r_c be made equal to the series resistance representing device losses, then the circuit is completely balanced except for the variation in the capacitance of device due to incident radiation. At the tuning frequency ω_1

$$\omega_1^2 LC_o = 1 \tag{1.3a}$$

where C_o is the detector capacitance in the linear dielectric region, one can easily show that the demodulator output v_o is given as

$$v_o = \frac{V_1}{2} Q \frac{1}{C_o} \frac{\partial C_o}{\partial T} \frac{\eta \Delta W \sin(\omega t - \varphi)}{G_H (1+\omega^2 \tau_H^2)^{1/2}} \tag{1.3b}$$

where Q is the quality factor of the resonant circuit. This expression is identical to the d.c. bolometer response given by Eq. (1.2c) except for Q; V_1 is the amplitude of a.c. carrier voltage while V was the d.c. voltage; factor 2 in the denominator reflects the loading due to the balancing circuit.

2. Noise Equivalent Power (NEP)

2.1 NEP due to Temperature Fluctuations

Noise due to spontaneous fluctuations in device temperature is essential to all thermal detectors and therefore to the ferroelectric detector whether operating in pyroelectric mode or in d.c. or a.c. capacitive bolometer mode. If P_1 be the

r.m.s. incident power, then the r.m.s. value of temperature variation is, from Eq. (1.1b)

$$\Delta T = \frac{\eta P_1}{(G_H^2+\omega^2 C_H^2)^{1/2}}$$

Thermal Sensitivity a(f), therefore is,

$$a(f) = \left|\frac{\Delta T}{P}\right| = \frac{\eta}{(G_H^2+\omega^2 C_H^2)^{1/2}} \qquad (2.1a)$$

The spectral intensity of noise is[5]

$$S_T(f) = \frac{4kT^2 G_H}{(G_H^2+\omega^2 C_H^2)^{1/2}} \qquad (2.1b)$$

The NEP, P_{eq} is therefore given as

$$(P_{eq})_{temp} = \frac{[S_T(F)]^{1/2}}{a(F)} = \frac{1}{\eta}(4kT^2 G_H)^{1/2} \qquad (2.1c)$$

Letting $G_H = 2(4\sigma_B T^3)A$

where A is the area and σ_B is Stephen-Boltzmann's constant

$$(P_{eq})_{temp} = \frac{1}{\eta}(32\, k\, \sigma_B T^5)^{1/2}\sqrt{A} \qquad (2.1d)$$

2.2 NEP of d.c. Capacitive Bolometer

The sensitivity may be obtained from Eq. (1.2c). Substituting $C_d = \frac{\beta}{T-T_C}$ in the linear dielectric region above Curie temperature and assuming $\omega^2 C_H^2 >> G_H^2$

$$a(f) = \left|\frac{v_o}{P_1}\right| = \frac{\eta V}{\rho C_p A d\omega} \quad \frac{1}{T-T_C} \tag{2.2a}$$

Spectral intensity of noise due to dielectric losses is

$$S_V(f) = \frac{4kT \tan\delta}{\omega C} \tag{2.2b}$$

Therefore

$$(P_{eq})_{diel} = \sqrt{\frac{4kT}{\epsilon_o}} \frac{\rho C_p}{\eta} \sqrt{\frac{\tan\delta}{\epsilon}} \sqrt{\frac{Ad\omega}{v/d}} (T-T_C) \tag{2.2c}$$

From Eq. (2.1d) and (2.2c)

$$(P_{eq})_{d.c.\ bolo} = \frac{\sqrt{A}}{\eta} \sqrt{\frac{4kT}{\epsilon_o} \frac{\rho^2 C_p^2}{\eta^2} \frac{\tan\delta}{\epsilon} \frac{d}{(v/d)^2} \omega (T-T_C)^2 + 32kT^5} \sqrt{B} \tag{2.2d}$$

2.3 NEP of a.c. Capacitive Bolometer

From Eq. (1.3b) again letting $C = \frac{\beta}{T-T_C}$ and $\omega^2 C_H^2 >> G_H^2$, we get for sensitivity

$$a(f) = \frac{\eta (v/d)}{2\rho C_p A\omega} \quad \frac{1}{T-T_C} \tag{2.3a}$$

By inspection of the circuit one sees immediately that

$$S_V(f) = \frac{A}{\sqrt{2}} \sqrt{4kT (\gamma_c + \gamma_L} \tag{2.3b}$$

Assuming $\gamma_L << \gamma_c$ and substituting $\gamma_c = \frac{\tan\delta}{\omega_1 C_o}$ where ω_1 is the carrier frequency

$$(P_{eq})_{diel} = \sqrt{\frac{4kT}{\epsilon_o}} \frac{\rho C_p}{\eta} \sqrt{\frac{\tan\delta}{\epsilon}} \frac{\sqrt{Ad}}{v/d} (T-T_C) \sqrt{\frac{\omega}{\omega_1}} \tag{2.3c}$$

Comparing this to Eq. (2.2c) we see that it is smaller by a factor $\sqrt{\frac{\omega}{\omega_1}}$ if certain material characteristics remain frequency independent over the audio range which is indeed the case. From Eqs. (2.1d) and (2.3c)

$$(P_{eq})_{a.c.\ bolo} = \frac{\sqrt{A}}{\eta}\sqrt{\frac{4kT}{\epsilon_o}\frac{\rho^2 C_p^2}{\eta^2}\frac{\tan\delta}{\epsilon}\frac{d}{(v/d)^2}\frac{\omega^2}{\omega_1}(T-T_c)^2+32kT^5\sigma_B} \qquad (2.3d)$$

2.4 NEP of Pyroelectric Detector

$$I_{sc} = A\frac{d\Delta P}{dt} = j\omega pA\Delta T$$

where p is the pyroelectric co-efficient

$$v_o = \frac{I_{sc}}{j\omega C} = \frac{pA}{C}\frac{\eta P_1}{(G_H^2+\omega^2 C_H^2)^{1/2}}$$

Letting $\omega^2 C_H^2 >> G_H^2$, the sensitivity is given as

$$a(f) = \frac{\eta p}{\omega\rho C_p d} \qquad (2.4a)$$

$$S_V(f) = \frac{4kT\tan\delta}{\omega C} \qquad (2.4b)$$

$$(P_{eq})_{diel} = \sqrt{4kT\epsilon_o}\sqrt{\frac{\epsilon\tan\delta}{p\eta}}\rho C_p\sqrt{\omega Ad} \qquad (2.4c)$$

From Eq. (2.1d) and (2.4c)

$$(P_{eq})_{pyro} = \frac{\sqrt{A}}{\eta}\sqrt{4kT\epsilon_o\frac{\epsilon\tan\delta}{p^2}\rho^2 C_p^2\omega Ad+32kT^5\sigma_B} \qquad (2.4d)$$

As for the choice of material to minimize NEP, $\frac{\sqrt{\epsilon}}{p}$ is expected to be constant (within a factor of 2). Therefore tanδ is the main parameter to play with in addition to density and specific heat.

2.5 A Numerical Calculation for TGS

Let the area of device be 1 mm^2 and its thickness 50 microns; loss factor tanδ = .02; modulation frequency of radiation intensity

f = 10 Hz; for the pyroelectric detecor we would assume room temperature to be the operating temperature, T = 300°K and ϵ = 40; the pyroelectric coefficient of TGS at room temperature is $p = 2 \times 10^{-4} \frac{\text{coul}}{\text{m}^2 \cdot \text{K}}$. For capacitive bolometers we take the operating temperature to be 50°C so that $T-T_c$ = 1°C. Since the Curie Weiss law is followed by TGS, $\epsilon = \beta = 3200$ at this temperature. Bias field of 10 $\frac{\text{kV}}{\text{cm}}$ will be used; for a.c. bolometer a carrier frequency of 1 kHz is taken. We take $\eta = 1$, $\rho = 1.69 \times 10^3 \frac{\text{Kg}}{\text{m}^3}$, $C_p = 0.97 \times 10^3 \frac{\text{Joules}}{°\text{K Kg}}$ for TGS.

Then $(P_{eq})_{temp} = 9.4 \times 10^{-12} \frac{W}{\sqrt{Hz}}$ at T = 323°K

$(P_{eq})_{temp} = 6.5 \times 10^{-12} \frac{W}{\sqrt{Hz}}$ at T = 300°K

$(P_{eq})_{d.c.bolo} = 15.5 \times 10^{-12} \frac{W}{\sqrt{Hz}}$

$(P_{eq})_{a.c.\ bolo} = 9.5 \times 10^{-12} \frac{W}{\sqrt{Hz}}$

$(P_{eq})_{pyro} = 16 \times 10^{-12} \frac{W}{\sqrt{Hz}}$

$(P_{eq})_{temp}$ is of course the lowest NEP obtainable from a ferroelectric detector. It is seen that it can be realized only in the a.c. capacitive bolometer mode. Noise due to dielectric losses dominates in d.c. capacitive bolometer as well as in pyroelectric detector and their NEP's are comparable.

3. Results and Dicussion

The measurement set up used for d.c. bolometer sensitivity, a.c. bolometer sensitivity and d.c. bolometer noise are shown in Figs. 3, 4, and 5 respectively. The diagrams are self-explanatory (see Ref. 6 for further details).

Here the results of measurements made on TGS devices T40 and T42 and the SBN device are reported and interpreted in the light of theory described earlier. Device T40 has a thickness of 50 microns and electrode area of 4 mm^2; T42 is 325 microns thick and also 4 mm^2 in area; SBN device is 100 microns thick and has an electrode area of 6.25 mm^2. All electrodes were vacuum evaporated chromium and gold.

3.1 Dielectric Measurements

Figure 6 shows the capacitance vs. temperature characteristic of T40. A sharp peak is seen at 47°C which therefore is the Curie temperature of this device. The ratio of peak capacitance to room temperature capacitance was 400. The maximum amplitude of a.c. measuring field in these devices was 8V/cm.

In Fig. 7 inverse of capacitance is plotted against temperature. The linear variation in paraelectric region shows that the Curie-Weiss law is obeyed with the Curie constant $\beta = 2820°K$. This relatively lower value of β suggests an order-disorder type transition in TGS. At room temperature the relative dielectric constant of this

device, after poling was 40 and its dissipation factor 0.02. Figure 8 shows the 1/C vs. temperature characteristic of T42; its Curie temperature is seen to be 49.8°C and θ = 31 30°K. Slight divergence in θ and T_c of these devices may be attributed to the difference in materials which were obtained from two different sources; material for T40 was purchased from Isomet Corporation while crystals for T42 were grown by Mr. Fritz Dravnieks.

Figure 9 shows the variation of dissipation factor (tan δ) with temperature in the vicinity of Curie point in T40. Variation of tan δ over a broader temperature range is shown in Figs. 10 and 11 for crystal SBN and ceramic barium titanate respectively. The minimum in the loss tangent at Curie temperature implies that the increase in capacitance there is much sharper than the increase in parallel conductance of the device; this is illustrated in Fig. 12.

Figure 12 shows the temperature variation of the series loss resistance R_s $(=\frac{\tan\delta}{\omega C})$ of the device. This is an important parameter because the device noise is primarily due to noise in this resistance.

Figures 13 and 16 show the variation of device capacitance with the d.c. bias field in the paraelectric region in TGS. At temperature farther from Curie temperature, TGS acts like a linear dielectric; however it becomes non-linear at high fields near the Curie temperature. Also, the capacitance goes down while tan δ

increases with the field; this would shoot R_s up and thus increase the noise. This non-linear dielectric behavior can be explained[7] using the phenomenological theory of Ferroelectricity.

3.2 Sensitivity Measurements

3.2.1 d.c. Bolometer

The d.c. bolometer sensitivity of device T40 operating in the paraelectric region is shown in Figs. 15 and 16 while Fig. 17 shows the sensitivity of T42. It is seen that at temperatures farther from Curie temperature, sensitivity increases linearly with the applied bias field. Sensitivity clearly increases as the operating temperature approaches θ. However, near the Curie temperature sensitivity first varies linearly with the field but tends to saturate at higher fields. Since we are operating above Curie temperature, no hysteresis is observed; all these curves are symmetrical with respect to the bias field direction.

These results are in good agreement with the d.c. bolometer theory developed earlier. It was shown that d.c. bolometer effect is essentially an induced pyroelectric effect and that bolometer sensitivity is directly proportional to induced polarization. From Thermodynamic theory, one can calculate the induced polarization as a function of applied field using Eq. (1.2e). Constant A is determined from

$$2A(T-T_o) = \chi = \frac{T-T_o}{\beta}$$

letting $\beta = 3130$ we get

$$A = 1.82 \times 10^{7} \frac{\text{meter}}{\text{Farad}^{\circ}\text{C}}$$

which is in good agreement with the Triebwasser's[7] value. Constants B and C have also been evaluated earlier[7] from measurements on the spontaneous polarization of TGS. $B = 1.62 \times 10^{11}$ and $C = 0.61 \times 10^{14}$ in MKS units. Using these values, induced polarization is plotted against E in Fig. 18. A linear variation is seen for large values of $(\theta-\theta_c)$ while non-linearities set in near Curie temperatures

Now $S = kP$

where S is the sensitivity, P is the induced polarization and k is a constant given by Eq. (1.2h)

$$k = \frac{2Ad}{G_H(1+\omega^2\tau_H^2)^{1/2}}$$

By letting $k = 19 \frac{V/W}{\mu\text{Coul/cm}^2}$ for T40 one can fit the theoretical curve with the measured sensitivity as shown in Fig. 16; the value of k for device T42 is $105 \frac{V/W}{\mu\text{Coul/cm}^2}$. Note that the ratio of k values for these two devices is roughly equal to the ratio of their thickness which are 50 and 325 microns respectively. Good agreement between theory and measurements shows that the constants B and C determined from the spontaneous polarization measurements satisfactorily describe the nonlinearity in the d.c. bolometer sensitivity in the paraelectric region; this further validates the induced polarization as the cause of bolometer response.

Figures 19 and 20 shows the variation of bolometer sensitivity with the operating temperature at relatively low bias fields. At low values of E, the P-E characteristic is linear and the sensitivity is expected to vary inversely as $T-T_c$; this directly follows from Eqs. (1.2g) and (1.2e). This is experimentally confirmed in Figs. 19 and 20.

Figure 21 shows the onset of pyroelectric response as the temperature is decreased below the Curie temperature. At T = 46.3°C one not only observes the bolometer response at zero field (signifying the presence of spontaneous polarization) but the response actually decreases with the applied field in contrast to induced pyroelectric effect. This reduction in pyroelectric response is probably due to the "clamping" of domains in the presence of field. Figures 22(a) and (b) show the variation of sensitivity with temperature in paraelectric as well as ferroelectric regions as the device is gradually cooled. The pyroelectric response which varies as $\frac{1}{C}\frac{\partial Ps}{\partial T}$ is directly proportional to the spontaneous polarization P_s. This explains the sharp rise in sensitivity just below the Curie temperature when the device is moving into its ferroelectric phase. However, the maximum in sensitivity a few degrees below Curie temperature is not well understood. It may have something to do with the way the device gets polarized as it is slowly cooled. Figure 23 shows the sensitivity-temperature characteristic for T42 as the device is gradually heated from room temperature without any applied field.

Figure 24 shows the frequency response of the pyroelectric detector T40 at room temperature. The sensitivity was measured after poling the device; it is seen to very approximately as the inverse of frequency over the range (10-100) Hz. This is from the theory of pyroelectric detector. Since the thermal time constant of TGS detector is of the order of a second αC_H is much greater than g_H for modulation frequency of 10 Hz or higher. This leads to 1/f variation of sensitivity.

In the device T42 the maximum d.c. bolometer sensitivity measured is 110 V/W at 50°C with the bias field of 6 KV/cm. This is slightly higher than 98 V/W which is its sensitivity as a pyroelectric detector at room temperature. In device T40 on the other hand, maximum sensitivity measured is only 16.5 V/W at 49.5°C and 14 KV/cm, smaller than the pyroelectric sensitivity of 39 V/W; of course much higher values can be achieved by moving the operating temperature nearer to 47°C, the Curie point.

Figures 25 and 26 show the measurements on a pyroelectric detector using SBN at room temperature. The pyroelectric response is again seen to go down at large externally applied electric fields. Slope of the straight line in Fig. 26 is unity indicating a 1/f variation of sensitivity as is theoretically expected. The room temperature sensitivity of this detector without any applied field is 114 V/W, at the modulation frequency of 15 Hz.

3.2.2 a.c. Bolometer

Figure 34 shows the sensitivity of a.c. bolometer. A TGS device 325 microns thick was used in the balancing circuit described earlier. However, the performance of this bolometer was not satisfactory for the following reason. Since a large carrier must be used in order to have strong enough bias for high sensitivity, balancing circuit had to be used in order to cancel the carrier at the output. But the oven in which the device was placed was not very stable; its temperature fluctuated in response to environmental changes. For operating temperature near T_c this small variation in temperature leads to a considerable capacitance variation thus unbalancing the delicate balance. For this reason a steady signal output could not be achieved in the vicinity of Curie temperature; the problem of course becomes more serious at higher fields when the carrier is even stronger.

The results reported are therefore at temperatures away from T_c; but then only lwo sensitivity can be achieved. As shown by theoretical calculation, a.c. bolometer has great potential, but further work must await the availability of an extremely temperature stable oven.

3.3 Noise Measurements

The equivalent noise resistance of T40 was measured at room temperature after poling the device. Its value was 84 kΩ at a frequency of 1 KHz. Since the device had a capacitance of 28 pF

and loss tangent .02, its series resistance R_s $(=\frac{\tan\delta}{\omega C})$ is 110 KΩ. However the measured noise resistance R_n is smaller than the device loss resistance because of the loading due to the input capacitance of the preamplifier. This becomes significant for low capacitance devices. The input capacitance of preamplifier was determined from other measurements to be 4.2 pF. Then the corrected value for R_n would be

$$R_n' = R_n \left(\frac{C_d+C_i}{C_d}\right)^2 \qquad (3.3a)$$

where C_d is the device capacitance and C_i is the input capacitance of pre-amplifier. Substituting the values for T40 from above

$$R_n' = 112\ K\Omega \approx R_s$$

Devices with larger capacitance like the SBN detector did not need this correction. This device had a capacitance of 65 pF and dissipation factor of .04 at f = 100 Hz at room temperature. Therefore R_s is 0.98 MΩ. Its noise equivalent resistance was measured as 1.26 MΩ.

Figures 27 shows R_s and R_n measured for a TGS device in the paraelectric region at a relatively large value of $T-T_c$. There is sharp increase in R_n with the applied field, followed by saturation; R_s remains practically constant. Figure 28 shows R_n and R_s measured for a smaller value of $T-T_c$. R_s now increases with increasing bias (tan δ is an increasing function while C is decreasing function of bias field as seen also in Figs. 13 and 14)

but R_n increases even faster. Since the bias electric field across the device is kept constant, the noise must be caused by spontaneous fluctuations in the device polarization. It is well known for a material with a relative dielectric constant $\varepsilon = \varepsilon' - j\varepsilon''$ under equilibrium conditions that Nyquist's theorem can be expressed in terms of polarization fluctuations with a spectrum[8]

$$S_p(f) = \frac{4kT\varepsilon_o\varepsilon''}{\omega Ad} \tag{3.3b}$$

If under applied field the device would still show thermal noise we would have instead

$$S_p(f) = \frac{4kT\varepsilon_o\varepsilon''(E)}{\omega Ad} \tag{3.3c}$$

where the imaginary part ε'' of the dielectric constant may now depend upon field. But actually the noise should be larger than thermal noise so that we may write[9]

$$S_p(f) = \frac{4kT\varepsilon_o\varepsilon''(E)}{\omega Ad}\, g(E) \tag{3.3d}$$

where $g(E)$ is a function of E that is unity at zero bias and larger for E not equal to zero.

Just as Eq. (3.3c) leads to an open circuit noise voltage with a spectram

$$S_V(f) = 4kTR_s(E) \tag{3.3e}$$

So Eq. (3.3d) will lead to

$$S_v(f) = 4kT\, R_s(E)g(E) = 4kT\, R_n(E) \tag{3.3f}$$

thus

$$g(E) = \frac{R_n(E)}{R_s(E)} \tag{3.3g}$$

A theoretical evaluation of g(E) to fit the measurements is now being attempted.

However it is clear from the dielectric and noise measurements mentioned above that the primary source of noise in these detectors, in absence of applied field, is the thermal noise due to dielectric losses; the 1/f variation of R_n shown in Fig. 29 further supports it.

Figure 30 shows R_n in the d.c. bolometer using T42, as a function of bias field. The sensitivity of this bolometer at various values of E is already known from Fig. 17. Therefore, its NEP may be calculated from the relation

$$P_{eq} = \frac{\sqrt{4kT\ R_n}}{S} \quad \frac{\text{Watt}}{\sqrt{\text{Hz}}} \tag{3.3h}$$

Figure 31 plots the NEP of T42 as a function of field at two temperatures in the paraelectric region. Compare this with the theoretical expression of Eq. (2.2d). It is hard to determine the temperature dependence of P_{eq} quantitatively because tan δ and ϵ are complex functions of T. Qualitatively, of course, it is very advantageous to operate in the vicinity of T_c because then not only is $(T-T_c)$ small but R_s is reduced drastically too. Equation (2.2d) predicts 1/E variation of NEP; from Fig. 31 we see that D* $(=\frac{\sqrt{A}}{NEP})$ does vary linearly with E up to 8 KV/cm at 60°C.

However, nearer to Curie temperature at 52.7°C, the linearity is completely lost. This is of course because of saturation of sensitivity, increasing $R_s(E)$ and increasing $g(E)$. There is little one can do about the sensitivity saturation because that is limited by the characteristics of ferroelectric materials. However there is room for improvement in the dielectric losses and also the understanding of $g(E)$ is quite important. Because of these factors the minimum NEP observed in T42 is only $1.26 \times 10^{-9} \frac{W}{\sqrt{Hz}}$. However it is lesser than the NEP of the same device used as a pyroelectric detector at room temperature, which is $1.71 \times 10^{-9} \frac{W}{\sqrt{Hz}}$.

Figure 23 shows the R_n for this device in the pyroelectric mode; variation of R_n as well as S with temperature is shown. NEP calculated from Fig. 23 is plotted against temperature in Fig. 32; sharp decrease in R_n makes the operation near Curie temperature very promising.

Figure 33 shows the $R_s(E)$ and $R_n(E)$ at room temperature in the pyroelectric SBN detector indicating that the enhancement of device noise with field occurs not only in paraelectric region but also in the ferroelectric region. The specific detectivity of SBN pyroelectric detector is $0.27 \times 10^8 \frac{cm\sqrt{Hz}}{W}$ at room temperature and modulation frequency of 100 Hz.

Figure 34 shows the sensitivity of an a.c. TGS bolometer.

References

1. Blackburn, H., and Wright, H. C., Infra-red Physics 10, pp. 191-197 (1970).

2. van der Ziel, A., and Liu, S. T., J. Appl. Phys. 43, pp. 4260-4261, (Oct. 1972).

3. Singh, V. P., Ph.D. Thesis, Elec. Engr. Dept., University of Minnesota, pp. 45.

4. Ref. 3, p. 68.

5. van der Ziel, A., Noise, Prentice Hall Inc., Englewood Cliffs, New Jersey, pp. 332.

6. Ref. 3, Chapter 5.

7. Treibwasser, S., IBM J. Research Development, 2, pp. 212, (1958).

8. Burgess, R. E., Can. J. Phys. 36, p. 1569 (1958).

9. Singh, V. P., and van der Ziel, A., to be published.

Part II Theoretical Work

1. The Pyroelectric Detector

Figure [35] shows a poled ferroelectric capacitor of area A and thickness d. Let the material have a small-signal dielectric constant Σ, then the device capacitance $C = \Sigma\Sigma_o A/d$, where Σ_o is the dielectric constant of free space. Let the front face be painted black to absorb the incoming radiation. Let the front face have a heat loss conductance $g_H = \eta \cdot 4\sigma T^3 A$ by radiation and the back face a heat loss conductance $g_H' = \eta' \cdot 4\sigma T^3 A$, where η and η' are the emissivities of front and back face, respectively.

The heat response of the detector due to incident radiation $P_1 \exp(j\omega t)$ is given by

$$C_H \frac{d\Delta T}{dt} + (g_H + g_H')\Delta T = \eta P_1 \exp(j\omega t) \tag{1}$$

where $C_H = c_o d_o A w$, c_o being the specific heat per gram and d_o the density of the material. Putting $\Delta T = \Delta T_o \exp(j\omega t)$ and solving for ΔT_o yields

$$\Delta T_o = \frac{\eta P_1}{j\omega C_H + g_H + g_H'} \tag{2}$$

The thermal time constant $\tau_H = C_H/(g_H + g_H')$ is generally of the order of 1 second and ω is usually of the order of 10-100 per sec so that $\omega^2 \tau_H^2 >> 1$. Therefore

$$\Delta T_o \simeq \frac{P_1}{j\omega C_H} = \frac{P_1}{j\omega c_o d_o A d} \tag{2a}$$

Now the polarization P_s of the polarized ferroelectric material decreases with increasing temperature. The charge on the capacitor is $Q = AP_s$ and hence the short-circuited current is

$$I_d(t) = \frac{dQ}{dt} = A\frac{dP_s}{dt} = A\frac{dP_s}{dT}\cdot\frac{dT}{dt} = -Ap j\omega \Delta T_o \exp(j\omega t) =$$

$$-I_{do}\exp(j\omega t) \qquad (3)$$

where $p = -dP_s/dT$ is the pyroelectric coefficient. Since the ac current is proportional to $d\Delta T/dt$, rather than to ΔT, the response of the detector is very fast. The current amplitude

$$I_{do} = Ap j\omega \Delta T_o = \frac{p\eta P_l}{c_o d_o d} \qquad (3a)$$

is therefore independent of frequency for $\omega\tau_H >> 1$.

The voltage developed across the capacitor C has an amplitude

$$V_{do} = \frac{I_{do}}{\omega C} = \frac{p\eta}{\omega c_o d_o \Sigma\Sigma_o A} P_l \qquad (4)$$

The <u>voltage response</u> thus decreases with increasing frequency.

The limiting noise of the device is generally the noise of dielectric losses. The spectral intensity is

$$S_i(f) = 4kT\omega C\tan\delta = 4kT\omega\frac{\Sigma\Sigma_o A}{d}\tan\delta$$

where $g = \omega C\tan\delta$ is the loss conductivity of the capacitor and $\tan\delta$ is its loss factor. The noise equivalent power P_{eq}, defined by

$$I_{do} = [S_i(f)]^{1/2} \qquad (6)$$

yields

$$P_{eq} = \frac{[S_i(f)]^{1/2} c_o d_o d}{p\eta} = \frac{c_o d_o}{p\eta}(4kT\,\Sigma\Sigma_o\tan\delta)^{1/2}(wdA)^{1/2} \qquad (7)$$

so that

$$D^* = \frac{A^{1/2}}{P_{eq}} = \frac{p\eta}{c_o d_o} \frac{1}{(4kT\ \Sigma\Sigma_o \tan\delta)^{1/2} (\omega d)^{1/2}} \tag{7a}$$

It thus pays to go to thinner samples.

The figure of merit of the detector is therefore

$$\frac{p}{(\Sigma \tan\delta)^{1/2}} \tag{7b}$$

Can this be improved by going to a different temperature? Usually not, for $p/\Sigma^{1/2}$ is independent of temperature, and $\tan\delta$ is not strongly temperature dependent. Can one improve D^* by going to a different material? Unfortunately not, for $p/\Sigma^{1/2}$ turns out to be nearly independent of the material. The only improvement lies in a lower tan δ.

2. Note on Dielectric Losses

It is the aim of this note to show that the theory of dielectric losses in low-loss dielectrics is easily extended to high-loss dielectrics and that the results thus obtained can qualitatively explain the observed loss behavior.

It is well known that in many low-loss dielectrics the loss factor, tan δ is practically independent of frequency over a wide frequency range. This is usually interpreted by assuming that some of the polarizable atoms, molecules, or trapped electrons have a wide distribution of time constants (τ) of the form[+]

$$g(\tau)d\tau = (g_o/\tau)d\tau \qquad \text{for } \tau_1 < \tau < \tau_2 \qquad (1)$$
$$= 0 \qquad \text{otherwise.}$$

where $g_o = 1/\ln(\tau_2/\tau_1)$, the loss factor, tan δ, is then found to be practically independent of frequency for $1/\tau_2 < \omega < 1/\tau_1$.

In lossy dielectrics, however, tan δ often decreases slowly with increasing frequency over a wide frequency range, and this requires an explanation. To give one we assume a model with two types of polarizable atoms, molecules, or trapped electrons. The first, of density N_o and polarizability α_o, give an instantaneous response,

---

[+]If τ is determined by a variable activation energy E_a so that $\tau = \tau_o \exp(E_a/kT)$, then Eq. (1) corresponds to a distribution in E_a of the form $dE_a/(E_{a2}-E_{a1})$ for $E_{a1} < E_a < E_{a2}$, and zero otherwise. If it is determined by tunneling through a variable distance x so that $\tau = \tau_o \exp(\alpha x)$, then Eq. (1) corresponds to a distribution in x of the form $dx/(x_2-x_1)$ for $x_1 < x < x_2$, and zero otherwise. The factor g_o, which is $1/\ln(\tau_2/\tau_1)$, is determined by the normalization condition

$$\int_0^\infty g(\tau)d\tau = 1.$$

whereas the second, of density N_1 and average polarizability α_1, respond slowly with a distribution of time constants, $g(\tau)$.

The dynamic Clausius-Mossotti equation may then be written

$$\frac{\epsilon-1}{\epsilon+2} = \frac{N_o\alpha_o}{3\epsilon_o} + \frac{N_1\alpha_1}{3\epsilon_o}\int_o^\infty \frac{g(\tau)d\tau}{1+j\omega\tau} \tag{2}$$

Rewriting Eq. (2) in terms of the static dielectric constant, ϵ_s, and the high-frequency dielectric constant, ϵ_∞, yields

$$\frac{\epsilon-1}{\epsilon+2} = b + (a-b)\int_o^\infty \frac{g(\tau)d\tau}{1+j\omega\tau} \tag{3}$$

$$= b + (a-b)(I_1-jI_2)$$

where

$$a = \frac{\epsilon_s-1}{\epsilon_s+2} = (N_o\alpha_o + N_1\alpha_1)/3\epsilon_o,\quad b = \frac{\epsilon_\infty-1}{\epsilon_\infty+2} = N_o\alpha_o/3\epsilon_o,$$

and I_1 and I_2 represent the real and imaginary parts of the integral, respectively.

The integration in Eq. (2) yields

$$I_1 = 1 - \frac{g_o}{2}\ln\left(\frac{1+\omega^2\tau_2^2}{1+\omega^2\tau_1^2}\right), \text{ and}$$

$$I_2 = g_o[\tan^{-1}\omega\tau_2 - \tan^{-1}\omega\tau_1] \tag{4}$$

where $g_o = \dfrac{1}{\ln(\tau_2/\tau_1)}$.

Solving Eq. (3) for ϵ yields

$$\epsilon = \epsilon' - j\epsilon'' \tag{5}$$

$$= -2 - \frac{3}{(b-1)+(a-b)(I_1-jI_2)}$$

where ϵ' and ϵ'' represent the real and imaginary parts of ϵ, respectively. Consequently, we obtain

$$\tan\delta = \frac{\epsilon''}{\epsilon'} \tag{6}$$

$$= 3(a-b)I_2/[(1-b)(1+2b)+(1-4b)(a-b)I_1-2(a-b)^2(I_1^2+I_2^2)]$$

If we assume $\tau_2 >> \tau_1$, Eq. (4) reduces to

$$I_1 \simeq -g_o \ln(\omega\tau 1) \ , \ I_2 \simeq \pi g_o/2 \tag{7}$$

for $1/\tau_2 < \omega < 1/\tau_1$, and hence Eq. (6) becomes

$$\tan\delta = 3(a-b)I_2/[(1-b)(1+2b)+(1-4b)(a-b)I_1-2(a-b)^2 I_1^2] \tag{8}$$

where we have neglected the I_2^2 term in Eq. (6) because $\tau_2 >> \tau_1$.

We see from Eq. (8) that $\tan\delta$ decreases with increasing frequency since I_1 is positive for the frequency range under consideration.

For $\omega = 1/\tau_2$ we have

$$(\tan\delta)_{1/\tau_2} = 3(a-b)\pi g_o/[2(1-a)(1+2a)]$$

$$= \frac{\epsilon_s-\epsilon_\infty}{\epsilon_\infty} \left(\frac{\pi g_o}{2}\right) \frac{\epsilon_s+2}{\epsilon_\infty+2} \cdot \frac{\epsilon_\infty}{\epsilon_s} \ .$$

For $\omega = 1/\tau_1$ we have

$$(\tan\delta)1/\tau_1 = 3(a-b)\pi g_o/[2(1-b)(1+2b)]$$

$$= \frac{\epsilon_s-\epsilon_\infty}{\epsilon_\infty} \left(\frac{\pi g_o}{2}\right) \frac{\epsilon_\infty+2}{\epsilon_s+2} \ .$$

If $(\epsilon_s-\epsilon_\infty)$ and ϵ_∞ are comparable, and $\tau_2 \sim 1$ sec and $\tau_1 \sim 10^{-8}$ sec, loss factors of the order of 0.1 become feasible. But in that case $\tan\delta$ decreases slowly over the frequency range $1/\tau_2 < \omega < 1/\tau_1$ and this decrease is the more pronounced the larger $(\epsilon_s-\epsilon_\infty)/\epsilon_\infty$.

This simple model is also formally appropriate for ferroelectric crystals such as used in pyroelectric detectors and capacitive bolometers. In such materials tan δ is usually of the order of $0.01 \sim 0.1$, which is well within the range covered by the above model.

3. Generalized Molecular Field Theory of the Pyroelectric Effect and Capacitive Bolometer Effect

In the pyroelectric effect the significant parameter is p/ϵ, or, if $\epsilon >> 1$, we may write

$$\frac{p}{\epsilon} \simeq \left(\frac{p}{\epsilon-1}\right) = \epsilon_o \frac{\partial P/\partial T}{\partial P/\partial E} \tag{1}$$

where $p = \partial P/\partial T$ is the pyroelectric coefficient and $P=P_s$, whereas $\epsilon-1 = \frac{1}{\epsilon_o}\frac{\partial P}{\partial E}$.

In the capacitive bolometer of electrode distance d

$$v_d(t) = \frac{\partial P/\partial T}{\partial P/\partial V_o}\ \Delta T = d\,\frac{\partial P/\partial T}{\partial P/\partial E}\,\Delta T(t) \tag{2}$$

since $E = V_o/d$. Both problems thus have in common that the quantity of interest is

$$\frac{\partial P/\partial T}{\partial P/\partial E} \tag{3}$$

To evaluate this expression, we assume that the polarization P is a function $f(E_\ell/T)$ of the local field E_ℓ, where T is the absolute temperature,

$$E_\ell = E + \frac{\lambda P}{\epsilon_o} \tag{4}$$

and λ is a kind of Lorentz factor. We thus have

$$P = f(E_\ell/T) = f\left(\frac{E+\lambda P/\epsilon_o}{T}\right) \tag{5}$$

The function f need not be further specified at the moment.

We call this the <u>generalized molecular field theory</u> of the effects.

If f' denotes the derivative, we have

$$\frac{\partial P}{\partial T} = f'\left[-\frac{(E+\lambda P/\epsilon_o)}{T^2} + \frac{\lambda}{\epsilon_o T}\frac{\partial P}{\partial T}\right]$$

or

$$\frac{\partial P}{\partial T} = -\frac{f'}{(1-f'\lambda/\epsilon_o T)}\left(\frac{E+\lambda P/\epsilon_o}{T^2}\right) \tag{6}$$

$$\frac{\partial P}{\partial E} = f'\left[\frac{1 + (\lambda/\epsilon_o)\,\partial P/\partial E}{T}\right]$$

or

$$\frac{\partial P}{\partial E} = \left(\frac{f'}{1-f'\lambda/\epsilon_o T}\right)\frac{1}{T} \tag{7}$$

Therefore

$$\frac{\partial P/\partial T}{\partial P/\partial E} = -\frac{E + \lambda P/\epsilon_o}{T} \tag{8}$$

We thus see that the explicit form of f is not important; all that matters is that it is a function of $\left(\frac{E+\lambda P/\epsilon_o}{T}\right)$

We now turn to the pyroelectric effect. Here E=0 and $P=P_s$. Hence

$$\frac{P}{\epsilon-1} = \epsilon_o\left(\frac{\lambda P_s/\epsilon_o}{T}\right) = -\frac{\lambda P_s}{T} \tag{9}$$

This is generally valid as long as (5) is valid.

We must now get rid of λ. To that end we consider $T > T_c$ but close to T_c and assume E to be small. Then P is a linear function of E_ℓ.

$$P = a\epsilon_o E_\ell = a\frac{(\epsilon_o E+\lambda P)}{T} \tag{10}$$

where a is a constant that needs to be expressed in measurable parameters

$$P\left(1-\frac{a\lambda}{T}\right) = \frac{a\epsilon_o E}{T} \quad , \text{ or } P = \frac{a\epsilon_o E}{T-a\lambda} \tag{11}$$

But we know that in this case

$$\frac{P}{\epsilon_o E} = \frac{C}{T-T_c} \tag{12}$$

where C is Curie's constant and T_c is the Curie temperature. Therefore

$$T_c = a\lambda \qquad a = C, \text{ or } \lambda = \frac{T_c}{C} \tag{13}$$

Hence

$$\frac{p}{\epsilon-1} = -\frac{T_c}{T}\frac{P_s}{C} \tag{14}$$

A similar relationship was first found by S.T. Liu[1], derived for $T \simeq T_c$, and consequently the factor T_c/T was missing. The factor is important, however, for devices with a high Curie temperature; they should have a higher value of $p/(\epsilon-1)$ at room temperature.

We now turn to the capacitive bolometer effect for $T > T_c$. Since $\lambda P >> \epsilon_o E$, we have

$$\frac{\partial P/\partial T}{\partial P/\partial E} \simeq \frac{\lambda P/\epsilon_o}{T}$$

so that

$$v_d(t) = -\frac{\lambda d}{\epsilon_o T} P\Delta T(t) \tag{15}$$

This equation is generally valid as long as $\epsilon_o E << P$.

We now assume E to be small. Then P varies linearly with E and, according to (11)

$$v_d(t) = -\frac{\lambda d}{\epsilon_o C}\left(\frac{\epsilon_o EC}{T-T_c}\right)\Delta T(t) = \left(\frac{V_o}{T-T_c}\right)\Delta T(t) \simeq -V_o\frac{\Delta T(t)}{T-T_c} \tag{16}$$

in agreement with previous results. The response is then linear in V_o. For large values of V_o the response $v_d(t)$ saturates. This must come about because the polarization P in (15) saturates. Experimentally $|V_d(t)|_{sat}$ increases strongly with decreasing $T-T_c$; this then must mean that the saturated value for P increases strongly with decreasing $T-T_c$. This can only be verified theoretically if the function $f(\frac{E+\lambda P/\epsilon_o}{T})$ is further specified.

References:

1. S.T. Liu, Evaluation of Curie Constants of Ferroelectric Crystals from Pyroelectric Response, Presented at 3d International Meeting on Ferroelectricity, Edinburgh, Scotland, Sept. 10-14, 1973.

4. Molecular Field Theory of Ferroelectricity and its Application

In the preceding section we discussed the case that the polarization P(T) was an arbitrary function of E_ℓ/T) where $E_\ell = E + \lambda P/\epsilon_o$ is the local field, λ the Lorentz factor, T the absolute temperature and E the applied field. We were then able to give a generally valid expression for $p/(\epsilon-1)$, where p is the pyroelectric coefficient and ϵ the relative dielectric constant; $p/(\epsilon-1)$ is a figure of merit for the signal response of a pyroelectric detector.

In the expression for the noise equivalent power another figure of merit must be introduced; it is $p/(\epsilon-1)^{1/2}$. It is therefore necessary to give a general expression for $p/(\epsilon-1)^{1/2}$. In contrast to the previous case, explicit expressions for the function of (E_ℓ/T) must now be used.

To that end we assume that each molecule has a permanent electric moment μ. There are now several possibilities:

a) The dipoles can orient themselves in arbitrary directions (classical approach). This leads to the following expression for the polarization

$$P(T) = P(o)L(x);\ L(x) = \coth x - \frac{1}{x};\ x = \frac{\mu E \ell}{kT} \qquad (1)$$

where $P(o) = N\mu$ is the total polarization when all dipoles are aligned. μ the dipole moment, N the number of dipoles per unit

volume, k = Boltzmann's constant. This gives the classical molecular field theory of ferroelectricity.

b) There are several preferred directions of polarization. The simplest case is that the dipoles can orient themselves parallel or antiparallel a preferred direction. In that solution

$$P(T) = P(o)\tanh x. \qquad (2)$$

This is the two-level molecular field theory of ferroelectricity.

It should, of course, be understood that more complicated directions of polarization are possible. For example, in $BaTiO_3$ these are the parallel, antiparallel and perpendicular directions; of the latter there are four equivalent orientations. Therefore the total number of orientations is 6, corresponding to two preferred directions along each cubic axis.

By solving Eqs. (1) and (2) for E=0, one obtains P/P(o) as a function of T. Graphically this is done in Fig.36, from which we see that the line $P(T)/P(o) = a(T)x$ meets the curve L(x) or tanh(x). We see that there are two possibilities for properly chosen values of T:

a) The two curves meet at a non-zero value of x, and hence of P(T). In other words we have spontaneous polarization. This is called the ferroelectric regime.

b) The two curves intersect at x=0 only. Hence P(T)=0, so that we have no spontaneous polarization. This is called the paraelectric regime.

c) In between there is a temperature $T=T_c$ where the line $P(T)/P(0) = a(T)x$ is tangent to $L(x)$ or $\tanh x$ at $T=0$. This is called the Curie temperature.

Figure 37 shows $P_s(T)/P(0)$ plotted versus T_c/T for the classical and for the two-level theory. Also shown are measured points for TGS, matched at $T/T_c = 0.88$.

Besides the classical and the two-level theories there is also the thermodynamic theory which assumes E to be a non-linear function of the polarization P.

Since P changes sign if E changes sign, E must be an odd function of P. The thermodynamic theory of ferroelectricity thus writes

$$E = \beta(T-T_c)P + b\,P^3 + \ldots \tag{3}$$

We then see that for $T < T_c$ this gives spontaneous polarization P_s for $E = 0$. This yields

$$\beta(T-T_c) + bP_s^2 = 0 \qquad P_s = \left[\frac{\beta}{b}\,(T_c-T)\right]^{1/2} \tag{4}$$

$$p = \frac{\partial P_s}{\partial T} = -\left(\frac{\beta}{b}\right)^{1/2} \frac{1}{(T_c-T)^{1/2}} \tag{5}$$

$$\epsilon-1 = \frac{1}{\epsilon_o\,\partial E/\partial P} = \frac{1/\epsilon_o}{\beta(T-T_c)+3bP_s^2} = \frac{1/\epsilon_o}{2\beta(T_c-T)} \tag{6}$$

Consequently

$$\frac{P}{(\epsilon-1)^{1/2}} = -\frac{1}{2}\left(\frac{\beta}{b}\right)^{1/2}(2\beta\epsilon_o)^{1/2} = -\beta\left(\frac{\epsilon_o}{2b}\right)^{1/2} \tag{7}$$

In order to evaluate this expression we must evaluate β and b. We do this for the two models described by Eqs. (1) and (2).

We first discuss the classical case described by Eq. (1). For small values of x the equation may be written as

$$\frac{P(T)}{P(0)} = \frac{1}{3} x - \frac{1}{45} x^3 + \ldots \tag{8}$$

Suppose x is quite small, $E \neq 0$ and T is sufficiently large. We then have

$$P = \frac{1}{3} P(0)\, x = \frac{1}{3} \frac{N_\mu^2}{kT} \left[E + \frac{\lambda P}{\epsilon_o}\right] \tag{9}$$

or $$P(T)\left[1 - \frac{1}{3} \frac{N_\mu^2 \lambda}{\epsilon_o kT}\right] = \frac{1}{3} \frac{N_\mu^2}{kT} E$$

$$P(T) = \frac{\frac{1}{3} N_\mu^2/(\epsilon_o k)}{T - T_c} \epsilon_o E = \frac{C}{T - T_c} \epsilon_o E \tag{10}$$

where

$$T_c = \frac{N_\mu^2 \lambda}{3\epsilon_o k}, \quad C = \frac{1}{2} \frac{N_\mu^2}{\epsilon_o k} = \frac{T_c}{\lambda} \tag{10a}$$

T_c is the Curie temperature and C is called the Curie constant. The derivation holds for $T > T_c$. For $T < T_c$ spontaneous polarization occurs; this must be discussed separately.

We can invert Eq. (8) as follows

$$x = 3 \frac{P}{P(0)} + \frac{9}{5} \left[\frac{P}{P(0)}\right]^3 + \ldots \tag{11}$$

or $$E + \frac{\lambda P}{\epsilon_o} = \frac{3kT}{\mu^2 N} P + \frac{9}{5} \left[\frac{P}{P(0)}\right]^3 + \ldots$$

since $P(0) = N\mu$, so that

$$E = \left(\frac{3kT}{\mu^2 N} - \frac{\lambda}{\epsilon_o}\right) P + \frac{9}{5} \frac{kT}{N^3 \mu^4} P^3 + \ldots \tag{12}$$

This is of the form (3), and

$$\beta = \frac{3k}{\mu^2 N}, \quad b = \frac{9}{5}\frac{kT}{N^3\mu^4} \tag{13}$$

Consequently

$$\frac{P}{(\epsilon-1)^{1/2}} = \frac{3k}{N\mu^2}\left(\frac{\epsilon_o}{2}\frac{5N^3\mu^4}{9kT}\right)^{1/2} = \left(\frac{5}{2}\epsilon_o\frac{Nk}{T}\right)^{1/2} \tag{14}$$

Next we discuss the two-level case. For small values of x, Eq. (2) may be written

$$\frac{P(T)}{P(o)} = x - \frac{1}{3}x^3 + \ldots \tag{15}$$

Suppose x is quite small, $E \neq 0$ and T sufficiently large. We then have

$$P = P(0)x = \frac{N\mu^2}{kT}\left(E + \frac{\lambda P}{\epsilon_o}\right) \tag{16}$$

or $$P\left[1 - \frac{N\mu^2\lambda}{\epsilon_o kT}\right] = \frac{N\mu^2}{kT}E$$

so that

$$P(T) = \frac{N\mu^2/\epsilon_o k}{T-T_c}\epsilon_o E = \frac{C}{T-T_c}\epsilon_o E \tag{17}$$

where T_c is the Curie temperature and C the Curie constant

$$T_c = \frac{N\mu^2\lambda}{\epsilon_o k}; \quad C = \frac{N\mu^2}{\epsilon_o k} = \frac{T_c}{\lambda} \tag{17a}$$

This derivation holds again for $T>T_c$; spontaneous polarization occurs for $T<T_c$; this must again be discussed separately.

The two models thus differ in the values of T_c and C; in the classical case T_c and C are a factor 3 smaller than in the two-level case.

We can invert Eq. (15) as follows

$$x = \frac{P}{P(0)} + \frac{1}{3}\left[\frac{P}{P(0)}\right]^3 + \ldots \tag{18}$$

or $$E + \frac{\lambda P}{\epsilon_o} = \frac{kT}{\mu^2 N} P + \frac{kT}{3\mu^4 N^3} P^3 + \ldots$$

so that

$$E = \left(\frac{kT}{\mu^2 N} - \frac{\lambda}{\epsilon_o}\right) P + \frac{kT}{3\mu^4 N^3} P^3 + \ldots \tag{19}$$

This is of the form (3) so that

$$\beta = \frac{k}{\mu^2 N} \; ; \quad b = \frac{kT}{3\mu^4 N^3} \tag{20}$$

Consequently

$$\frac{p}{(\epsilon-1)^{1/2}} = \frac{k}{\mu^2 N}\left(\frac{\epsilon_o}{2}\frac{3\mu^4 N^3}{kT}\right)^{1/2} = \left(\frac{3}{2}\,\epsilon_o\,\frac{Nk}{T}\right)^{1/2} \tag{21}$$

This differs from (14) only by a factor $(5/3)^{1/2} = 1.29$; this difference between the two models is relatively small.

We should make one correction for our results given in Eqs. (14) and (21). The derivations are only correct relatively close to the Curie temperature T_c. Therefore, it is perhaps better to replace T by T_c in Eqs. (14) and (21). We then have: Classical Theory:

$$\frac{p}{(\epsilon-1)^{1/2}} = \left(\frac{5}{2}\,\epsilon_o\,\frac{Nk}{T_c}\right)^{1/2} \tag{22}$$

Two level theory: $$\frac{p}{(\epsilon-1)^{1/2}} = \left(\frac{3}{2}\,\epsilon_o\,\frac{Nk}{T_c}\right)^{1/2} \qquad (23)$$

We must now find the suitable expression for N, the density of dipoles. It is easily seen that

$$N = \frac{A\rho}{W} \qquad (24)$$

where A is Avagadro's number, ρ is the density and W the molecular weight. Evaluating the numbers we have

$$\frac{P}{(\epsilon-1)^{1/2}} = 13.5 \times 10^{-9} \left(\frac{\rho}{\frac{W}{100}\cdot\frac{T_c}{100}}\right)^{1/2} \frac{\text{Coulomb}}{\text{cm}^2\ ^\circ\text{k}} \qquad (25)$$

for the classical theory and for the two level theory

$$\frac{P}{(\epsilon-1)^{1/2}} = 10.5 \times 10^{-9} \left(\frac{P}{\frac{W}{100}\cdot\frac{T_c}{100}}\right)^{1/2} \frac{\text{Coulomb}}{\text{cm}^2\ ^\circ\text{K}} \qquad (25a)$$

The results obtained are shown in Table I for Eq. (25a)

Table I

Material	ϵ(20°C) (exp)	p(20°C) (exp)	$p/(\epsilon-1)^{1/2}$ (exp)	ρ	W	T_C	$P/(\epsilon-1)^{1/2}$ (calc)
TGS	40	2×10^{-8}	3.2×10^{-9}	1.69	323	322	4.3×10^{-9}
$LiTaO_3$	46	2.4×10^{-8}	3.5×10^{-9}	7.50	234	900	6.3×10^{-9}
SBN(x=0.5)	400	7.4×10^{-8}	3.5×10^{-9}	5.33	394	380	6.3×10^{-9}
PLZT(x=0.65)	1400	11×10^{-8}	3×10^{-9}	7.82	324	45	7.6×10^{-9}

It is suspected that if p and ϵ were measured closer to T_c, the value of $p/(\epsilon-1)^{1/2}$ would be closer to the value predicted by Eq. (25).

We have also expanded E versus P to higher order terms; one then obtains correction factors for $p/(\epsilon-1)^{1/2}$ that become significant farther away from the Curie temperature T_c. The changes, through significant, are not very large.

Table I was constructed under the assumption that a dipole unit consists of 1 molecule. This is probably not the case for some structures. If n molecules form <u>one</u> dipole, the effective molecular weight is n times as large. The calculated value of $p/(\epsilon-1)^{1/2}$ could thus lie closer to the experimental value. This must be checked with the actual structure of the material.

It should also be noted that $p/(\epsilon-1)^{1/2}$ is a factor 1.29 smaller for the two-level theory. This theory would thus bring the value for TGS down to 4.3×10^{-9} Coulomb per cm^2 per °K, which is quite close.

It should also be noted that $p/(\epsilon-1)^{1/2}$ does not depend on $T-T_c$. Little is therefore gained by operating closer to the Curie temperature. Also $p/(\epsilon-1)^{1/2}$ does not depend very strongly upon the material, in agreement with experiment.

The final conclusion is therefore that the calculated value of $p/(\epsilon-1)^{1/2}$ gives the right order of magnitude, and that closer agreement might be obtained by further refinements of the theory.

5. A Three-Energy Level Model of the Noise Equivalent Power Figure of Merit $p/\sqrt{\epsilon-1}$ of $BaTiO_3$,

Above the Curie point, the crystal structure of $BaTiO_3$ is cubic with a titanium ion at the center, eight barium ions at the corners, and six oxygen ions at the face centers in an octahedral configuration. The mechanical distortion due to the displacement of barium and oxygen ions cannot destroy pair cancellation of dipole moments. However, the large barium ions create a large hole at the body center so that the small titanium ion is free to rattle around in the hole. Hence, a net dipole moment can result only by a unilateral displacement of the titanium ion with respect to the negative oxygen surroundings and there are six possible directions for dipole moment.

The local field, $\vec{E}_\ell$, acting on the titanium ion can be written in the form

$$\vec{E}_\ell = \vec{E} + \lambda\vec{P}/\epsilon_o$$

where $\vec{E}$ is an applied field in the c-axis direction.

The ferroelectric phase below T_c of $BaTiO_3$ may be thought of as a paraelectric phase in which the local electric field E_ℓ acts. The polarization of $BaTiO_3$ in the paraelectric phase should therefore have the same temperature dependence as that of any other paraelectric material except the fact that the local electric

field E_ℓ is not constant, but decreases as the temperature increases. Now that the dipole orientation of $BaTiO_3$ is quantized, the number of dipoles pointing in the directions parallel, antiparallel, and perpendicular to $\vec{E}_\ell$ can be obtained.

Assuming that the polarization is proportional to the Boltzmann factor $e^{-w/kT}$ where $w = -\vec{\mu} \cdot \vec{E}_\ell$, the equilibrium populations in the three levels are given by

$$\frac{N\uparrow}{N} = \frac{e^{x}}{e^{x} + 4e^{0} + e^{-x}} \quad \text{(parallel)}$$

$$\frac{N\perp}{N} = \frac{4e^{0}}{e^{x} + 4e^{0} + e^{x}} \quad \text{(perpendicular)}$$

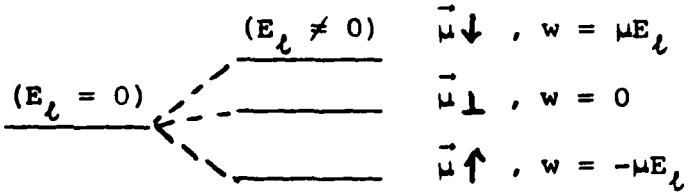

$$\frac{N\downarrow}{N} = \frac{e^{-x}}{e^{x} + 4e^{0} + e^{-x}}$$

where $x = \mu E_\ell / kT$, $\vec{\mu}\uparrow = -\vec{\mu}\downarrow = \vec{\mu}$, and $N = N\uparrow + N\perp + N\downarrow$. Thus we get a polarization

$$\vec{P} = (N\uparrow - N\downarrow)\vec{\mu}.$$

Note that the dipole moments perpendicular to the field cancel each other in pairs because they point in opposite directions in pairs and by symmetry their magnitudes are equal to each other. Accordingly, the total polarization becomes

$$\vec{P} = \vec{\mu}N \left(\frac{e^{x} - e^{-x}}{e^{x} + 4e^{0} + e^{-x}} \right)$$

Far away from saturation of the polarization, i.e., $x \ll 1$, $\mu E_\ell \ll kT$, $\vec{P}$ simplifies to

$$\frac{P(T)}{P(0)} = \frac{1}{3} x - \frac{1}{540} x^5$$

where $P(0) = \mu N$.

Writing x in terms of P(T) and solving for P(T) yields

$$P(T) = \frac{C}{T - T_c} \cdot \epsilon_o E$$

where $T_c = \lambda \mu^2 N/3\epsilon_o k$ is the Curie temperature and $C = \mu^2 N/3\epsilon_o k$ is the Curie constant.

Inverting the expression for P(T)/P(0) yields

$$x = 3 \left[\frac{P(T)}{P(0)}\right] + \frac{27}{20} \left[\frac{P(T)}{P(0)}\right]^5 ,$$

so finally, the applied electric field becomes

$$E = \frac{3k}{\mu^2 N} (T - T_c) P(T) + \frac{27}{20} \cdot \frac{kT}{\mu^6 N^5} P(T)^5 .$$

The spontaneous polarization $P_s(T)$ as obtained by setting E = 0, is

$$P_s(T) = P(0) \left[\frac{20}{9} \cdot \frac{(T_c - T)}{T}\right]^{1/4}$$

in which a spontaneous polarization occurs for $T < T_c$. The pyroelectric coefficient P and $\sqrt{\epsilon - 1}$, where ϵ is the relative dielectric constant, are obtained as follows

$$P = \frac{dP_s(T)}{dT} \qquad 45$$

$$= -\frac{5\mu N}{9} \cdot \frac{T_c}{T^2} \left[\frac{20}{9} \cdot \frac{(T_c - T)}{T}\right]^{-3/4}$$

$$\sqrt{\epsilon - 1} = \left[\frac{1}{\epsilon_o (E/P)}\right]_{P = P_s}$$

$$= [\mu^2 N / 12 \epsilon_o k (T_c - T)]^{1/2}$$

Finally, the noise equivalent power figure of merit $p/\sqrt{\epsilon-1}$ becomes

$$p/\sqrt{\epsilon-1} = -(\epsilon_o N k)^{1/2} \cdot \frac{T_c}{T} \left[\frac{5}{4} \cdot \frac{1}{T(T_c - T)}\right]^{1/4}.$$

At a temperature near the curie temperature, the NEP figure of merit may be approximated by

$$p/\sqrt{\epsilon-1} = -\left(\frac{\sqrt{5}}{2} \cdot \epsilon_o \cdot \frac{Nk}{T_c}\right)^{1/2} \left(\frac{T_c}{T_c - T}\right)^{1/4}$$

This resulting expression is different by the factors $\left[\frac{T_c}{5(T_c - T)}\right]^{1/4}$ and $\left[\frac{5}{9} \frac{T_c}{(T_c - T)}\right]^{1/4}$, from the classical case and the two-level case, respectively, reported in the last quarterly technical report. A comparison of these three models will be attempted with the experimental results obtained with TGS.

Since P_{eq} is inversely proportional to $P/\epsilon^{1/2}$, it would in this case be advantageous to operate close to T_c.

6. Accurate Calculation of $p/(\epsilon-1)^{1/2}$ in TGS.

In the preceding parts dealing with the molecular field theory for the classical, and the quantized two and three energy-level models we used a Taylor expansion of $P/\mu N = f(x)$ in x. However, this Taylor expansion does not always converge; for example, the Taylor expansion for tanh x does not converge for $x > 1$.

In this part, therefore, we make a more general approach using the generalized molecular field theory. In this case the polarization P(E,T) is given by

$$P(E,T) = f(E_\ell/T) \tag{1}$$

where $E_e \equiv E + \lambda P/\epsilon_o$ is the local field at the location of a dipole in the crystal and E is an applied field. Then we have

$$(\partial P/\partial T)_E = -[f'/(1-f'\lambda/\epsilon_o T)][(E + \lambda P/\epsilon_o)/T^2], \text{ and}$$

$$(\partial P/\partial E)_T = [f'/(1-f'\lambda/\epsilon_o T)][1/T]$$

where f' is the derivative of $f(E_\ell/T)$ with respect to its argument. Hence, for $\epsilon \gg 1$

$$p/\epsilon_r^{1/2} \simeq p/(\epsilon_r-1)^{1/2} = \epsilon_o^{1/2}(\partial P/\partial T)_E/(\partial P/\partial E)_T$$

We note that the definition of the pyroelectric coefficient p used here is more general and practical than $p \equiv (\partial P/\partial T)_{E=o}$, i.e., $\partial P_s/\partial T$ which has been used conventionally. Thus,

$$p/(\epsilon_r-1)^{1/2} = -[\epsilon_o/(1/f' - \lambda/\epsilon_o T)]^{1/2}[(E + \lambda P)/\epsilon_o T^{3/2}]$$

Now we assume that the crystal has no intrinsic bias which is true for TGS under consideration.

Then, for E = o we get

$$p/(\epsilon_r-1)^{1/2} = -[\epsilon_o/(1/f_o' - \lambda/\epsilon_o T)]^{1/2}[\lambda P_s/\epsilon_o T^{3/2}] \qquad (2)$$

where f_o' is the value of f' at E = o.

Since f_o' and P_s are functions of temperature we cannot say anything about the temperature-dependence of $p/(\epsilon_r-1)^{1/2}$ without specifying the function $f(E_\ell/T)$. We must also note that Eq. (2) is only valid for the dielectric constant measured at E = o and T = const. In practice, however, the dielectric constant is measured using a small ac field ($\sim$ 50 cps.) and hence the adiabatic correction is necessary

Now we apply Eq. (2) to the two-level model with

$$P(E,T) = \mu N \tanh x. \qquad (3)$$

where N is the number of dipoles per m^3 and $x = \frac{\mu E \ell}{KT}$. Comparing Eq. (1) with Eq. (3) we identify that

$$f(kx/\mu) = \mu N \tanh x.$$

Thus,

$$f'(Kx/\mu) = (\mu^2 N/K)\ d(\tanh x)/dx$$

$$= (\mu^2 N/K)\ \mathrm{sech}^2 x.$$

Hence, we obtain

$$f_o' = (\mu^2 N/K)\ \mathrm{sech}^2(\mu\lambda P_s/\epsilon_o KT).$$

Substitution of $\lambda = T_c/C$ with Curie constant, $C = N\mu^2/\epsilon_o K$, which was

derived previously, gives

$$f_o' = (\mu^2 N/K)\ \mathrm{sech}^2(\mu T_c P_s/\epsilon_o CKT) \tag{4}$$

and,

$$p/(\epsilon_r-1)^{1/2} = -[\epsilon_o/(1/f_o' - T_c/\epsilon_o CT)]^{1/2}[T_c P_s/\epsilon_o CT^{3/2}] \tag{5}$$

In order to test the validity of our final result, Eq. (5), we evaluated it numerically using the P_s vs. T graph whose data were obtained by S. Triebwasser [IBM Journal of R and D, July 1958]. With T_c = 322.8°K, and $C = (\mu^2 N)/\epsilon_o K$ = 3200°K we get

$\mu^2 N/K = \epsilon_o C = 2.83 \times 10^{-8}$ coul.^{2} °K/joule m,

$\mu = 1.12 \times 10^{-29}$ coul. m,

$\mu T_c = \epsilon_o CK = 9.33 \times 10^3$ m^2 °K/coul.,

$T_c/\epsilon_o C = 1.15 \times 10^{10}$ joule m/coul^2.

Substituting these constants in Eqs. (4) and (5) yields

$$f_o' = 2.83 \times 10^{-8}\ \mathrm{sech}^2(9.33 \times 10^3 P_s/T)\ \text{coul}^2\ °K/\text{joule m} \tag{6}$$

$$p/(\epsilon_r-1) = -[8.85 \times 10^{-12}/(1/f_o' - 1.15 \times 10^{10}/T)]^{1/2}$$
$$[1.15 \times 10^{10} P_s/T^{3/2}]\ \text{coul/m}^2 °K \tag{7}$$

Note that $-p/(\epsilon_r-1)^{1/2} = 3.39 \times 10^{-5}$ coul/m^2°K at T = 294.7°K is in good agreement with the value of 3.2×10^{-5} coul/m^2°K at T = 293°K which was obtained in the laboratory.

According to our numerical results $-p/(\epsilon_r-1)$ increases very slowly until the temperature increases very close to T_c and then it blows up, which can be clearly explained by looking at Triebwasser's two experimental curves, $1/\epsilon$ vs. T, and P_s vs. T and calculating $-p/(\epsilon_r-1)$ directly. Since $-(\partial P_s/\partial T) = -\tan\bar{\theta}$ along the P_s vs. T

T (°K)	P_s ($\times 10^{-2}$ coul/m^2)	P_s/T ($\times 10^{-5}$ coul/m^2°K)	$P_s/T^{3/2}$ ($\times 10^{-6}$ coul/m^2°K$^{3/2}$)	f_o' ($\times 10^{-8}$ coul^2°K/joule m)	$-p/(\epsilon-1)^{1/2}$ ($\times 10^{-5}$ coul/m^2°K)
294.7	2.70	9.16	5.34	1.47	3.39
299.8	2.53	8.44	4.87	1.61	3.42
304.5	2.33	7.65	4.39	1.75	3.424
308.5	2.21	7.16	4.08	1.86	3.44
311.1	2.05	6.59	3.74	1.98	3.48
312.5	1.93	6.18	3.49	2.06	3.49
314.5	1.83	5.82	3.28	2.14	3.53
316.4	1.66	5.25	2.95	2.25	3.54
318.4	1.42	4.46	2.50	2.39	3.58
320.2	1.16	3.62	2.02	2.57	3.64
322.2	0.68	2.110490379	1.175765217	2.723047485	3.960656927
322.6	0.34	1.053936764	0.5867895518	2.799228335	7.269007019
322.7	0.03	0.09296560273	0.05175148383	2.830212915	not defined

curve is a slowly increasing function of T until T becomes very close to T_c and ϵ-1, therefore $(\epsilon_r-1)^{1/2}$ is a decreasing function until $T = T_c$. Hence, we can imagine that $-p/(\epsilon_r-1)^{1/2}$ will show a very sharp peak at $T = T_c$.

Previously, for two-level model in a series expansion, we obtained

$$p/(\epsilon_r-1 = 1.05 \times 10^{-2}[\rho/WT_c]^{1/2} = 4.32 \times 10^{-5} \text{ coul/m}^2\text{°K}$$

which is independent of temperature contrary to the experimental result. Also, it is clear that the thermodynamic theory using

$$G = G_o + \beta(T-T_o)P^2/2 + P^4 + \delta P^6/6 + \ldots.$$

which is appropriate only for the ferrcelectric crystals with only one spontaneous polarization axis, can be successfully applied to TGS as Triebwasser did and it will, therefore, not be adequate for the spontaneous polarization which has components in more than one axial direction.

Consequently, as long as the polarization axes are known and so $P(E,T) = f(E_\ell/T)$ is determined, our generalized molecular field theory must be a good tool to treat the ferroelectric phenomena.

7. SOLAR POWER GENERATION WITH THE PYROELECTRIC EFFECT

by A. van der Ziel*

Electrical Engineering Department

University of Minnesota

Minneapolis, Minnesota 55455

Summary: It is shown with the help of a small-signal model that the pyroelectric effect cannot be used for an efficient generation of electrical power from solar radiation.

*Supported by ARPA Contract. This research was performed while on leave of absence at the EE Department, University of Florida, Gainesville, Florida 32611.

It is the aim of this note to show that the pyroelectric effect is not very suitable for generating electrical power efficiently, because the impedance level is so high. In our discussion we use a small signal model[1] that may not be very accurate but that should be good enough to give the order of magnitude of the expected effect.

Let incoming light of power density P be chopped at the rate f per sec and let $\omega = 2\pi f$. Let $P_1 \exp(j\omega t)$ be the power density of frequency ω (we neglect harmonics) incident upon poled pyroelectric capacitor of electrode area A and electrode distance d. Let $C_H = cAd$ be the heat capacity of the device, where c is the specific heat per cm^3. Let $g_H = \eta 4\sigma A T^3$ and $g_H' = \eta' 4\sigma A T^3$ be the heat loss conductances by radiation of the front and back face, respectively; here η and η' are the emissivities of front and back face, $\sigma = 5.67 \times 10^{-12}$ Watt $cm^{-2} {}^\circ K^{-4}$ is the Stefan-Boltzmann constant and T the temperature. Then the temperature variation $\Delta T = \Delta T_o \exp(j\omega t)$ has an amplitude[1]

$$\Delta T_o = \frac{\eta P_1 A}{j\omega C_H + g_H + g_H'} = \frac{\eta P_1 A}{j\omega C_H [1 + 1/(j\omega T_H)]} \tag{1}$$

where T_H is the thermal time constant of the device

$$T_H = \frac{C_H}{g_H + g_H'} = \frac{cd}{(\eta + \eta') 4\sigma T^3} \tag{1a}$$

The short-circuited current $I_{do} \exp(j\omega t)$ of the device has an amplitude[1]

$$I_{do} = \frac{A \partial P_s}{\partial t} = \frac{A \partial P_s}{\partial T} \frac{dT}{dt} = \frac{\eta A p P_1}{cd [1 + 1/(j\omega T_H)]} \tag{2}$$

where $p = \partial P_s / \partial T$ is the pyroelectric coefficient of the capacitor and P_s is its spontaneous polarization.

Let now a load resistance R be connected in parallel with the capacitance $C = \epsilon\epsilon_o A/d$ of the device; here ϵ is the relative dielectric constant and $\epsilon_o = 8.85 \times 10^{-14}$ F/cm. Then the power dissipated in this load is

$$P_d = \frac{1}{2} \frac{|I_{do}|^2 R}{1+\omega^2 C^2 R^2} \tag{3}$$

This has a maximum for $R = 1/(\omega C)$ and the value P_{max} is

$$P_{max} = \frac{|I_{do}|^2}{4\omega C} = \frac{\eta^2 p^2 (P_1 A)^2}{4c^2 d^2 [1+1/(\omega^2 T_H^2)]\omega\epsilon\epsilon_o A/d} \tag{4}$$

This, in turn, has an optimum value for $\omega = 1/T_H$ and that optimum value P_{opt} is given by

$$\frac{P_{opt}}{A} = \frac{\eta^2 p^2 P_1^2}{8c(\eta+\eta')4\sigma T^3 \epsilon\epsilon_o} \tag{5}$$

which is independent of the thickness d. Consequently, the conversion efficiency η_p is

$$\eta_p = \frac{P_{opt}/A}{P} = \frac{\eta^2 p^2 (P_1/P)^2 P}{8c(\eta+\eta')4\sigma T^3 \epsilon\epsilon_o} \tag{6}$$

We now bear in mind that $p/\sqrt{\epsilon} \simeq 3 \times 10^{-9}$ Coulomb $cm^{-2} {}^\circ K^{-1}$ for most pyroelectric materials[2] and that c = 2 Joule cm^{-2} is a representative value for the specific heat per cm^3. Putting $\eta = 1$, $\eta' = 0$, $T = 300^\circ K$ and $P_1/P = 0.50$, which is probably somewhat optimistic, and bearing in mind that $P \simeq 0.10$ Watt cm^{-2} for unfocused sunlight yields

$$\eta = 0.025\%$$

This efficiency is so small that it can be safely concluded that pyroelectric capacitors are not very suitable as power generators using unfocused sunlight.

Since η_p is proportional to the incident power density P, better efficiencies would be obtained by <u>focusing</u> the solar radiation onto the pyroelectric detector. However, in that case the variation in temperature will be so large that the small signal theory becomes a very poor approximation; it must be replaced by a large-signal theory. It is highly doubtful, however, that attractive efficiencies can be obtained in this manner, because the impedance level of the power generator is inherently high.

References

1. E. H. Putley, The Pyroelectric Detector, in R. K. Willardson and A. C. Beer, Semiconductors and Semimetals, Vol. 5, Academic Press, New York (1970), pp. 259-285.

2. S. T. Liu, Private communication.

Part III. Materials Work

1. Contact Study on PLZT (12-40/60)

From the same material of PLZT (12-40/60), four different types of contacts: vacuum evaporation of 15 Å cf Cr and 4000 Å of Au, gold fired at 800°C (Dupont DP8760), silver fired at 480°C (Dupont 4887) and silver paste, were investigated. The thickness of the samples was varied from 30 mils down to 2 mils.

The contact of Cr+Au vacuum evaporation gave the best results. The measurement of capacitance vs. temperature gave a Curie temperature of about 140°C and the Curie temperature varied 1-2°C from 140°C with variation of thickness from 30 mils down to 2 mils. Repetition of the measurement did not change the Curie temperature. The ratio of the capacitance at the Curie temperature to that at room temperature ranged from 8.8 to 9.8 from 30 mils down to 2 mils. The dissipation factor tan δ varied from 0.015 at room temperature to 0.018 just few degrees below the Curie temperature. The shape of capacitance versus temperature curves was conserved when the measurements were repeated and the thickness was varied. In other words, the measurements were fully reproducible.

The silver-fired contact gave a Curie temperature a few degrees higher or lower than 140°C. The difference could be due to diffusion processes on the surface during the contacting. It was worse in the gold-fired case, probably because of the higher processing temperature. The ratio of the Curie temperature capacitance to the capacitance at

room temperature was in the range of 7.0 to 7.8. The value of tan δ fluctuated over a wide range.

The gold-fired contact gave similar results to the silver-fired case, but the variation of Curie temperature was in the range of 5 to 6°C difference from 140°C and the maximum capacitance was about 6-7 times larger than the room temperature value. The tan δ showed wider variations. In the silver paste case, the Curie temperature and tan δ were not changed much but the maximum capacitance at the Curie temperature was only 1.5 times larger than at room temperature.

Some samples were annealed before making contacts. The samples were annealed at 850°C for Au-fired contacts, 520°C for Ag-fired contacts and 400°C for Cr+Au vacuum evaporation. For the fired contact cases, the capacitance at Curie temperature were increased, however, for the vacuum evaporated Cr+Au contact the capacitance decreased somewhat.

Before poling the device, the loss factor tan δ was 0.015 at room temperature and slowly increased to 0.018 at about Curie temperature. After poling the device, the annealed devices gave a higher loss factor, specially for the fired-contact cases. The worst case gave a value of tan δ of about 10 times larger than before poling the device. It also showed that the lossy device had a slightly higher voltage responsivity.

When all the devices were poled, the Curie temperature was slightly raised. That means when the capacitance was measured, one should not apply too high input voltage, especially when the sample is very thin All our measurements were done with 5 mV peak to peak input which did not effect the determination of the Curie temperature.

The results of detectivity measurements for various thickness, various contacts and for the annealed and without annealed cases are shown in Table 1. The value of 7.6×10^7 cm$(cps)^{1/2}$/watt was the highest one obtained at 100 cps. The device was 2.1 mil thick with Cr+Au contacts. It appears that Cr+Au contacts gave the best results and that one whould avoid heating the material during the contacting process.

Theoretically, the D* varies with $(w)^{-\frac{1}{2}}$ where w is the thickness of the device. The plot of D* vs. w from 2 mil to 30 gave a slope of -0.54 compared with the theoretical value of -0.50.

In conclusion, one should avoid any fired-contact on pyroelectric material to preserve the material characteristic and to obtain higher detectivity.

Currently we plan to repeat the same experiment on $BaTiO_3$ and SBN devices.

Table 1 D* Measurement

Device no's	Thickness mils	Area $10^{-2}cm^2$	Capacitor pf	tan δ	Annealing before worked	Contact	Light Response 10^{-4}, volt rms	Voltage Response v/w	NEP 10^{-9}	D* 10^7
1	2.1	1.51	506	0.074	No	Cr+Au	3.4	36 v/w	1.62	7.61
18	2.1	1.51	426	0.026	No	Cr+Au	2.2	24	1.68	7.31
2	3.5	2.48	376	0.039	No	Cr+Au	3.2	22	2.49	6.56
3	4.5	5.23	676	0.052	No	Cr+Au	3.4	11	4.4	5.2
4	4.5	2.48	277	0.02	No	Cr+Au	2.2	14	3.05	5.16
5	4.5	2.48	225	0.015	Yes	Cr+Au	2.6	17	2.58	6.1
7	4.5	2.48	257	0.122	No	Ag Fired 500°C	1.4	91	12.2	0.129
8	4.5	2.48	235	0.08	Yes	"	2.0	13	7.2	2.19
13	4.5		390	0.166	Yes	"				
6	4.5	2.48	212	0.177	No	Au-Fired 800°C	1.2	7.8	16.1	0.98
9	4.5	3.00	372	0.034	No	"	2.0	13	4.8	4.4
10	4.5	2.48	238	0.12	Yes	"	2.0	13	8.82	1.79
11	4.5	2.48	235	0.032	Yes	"	2.2	14	4.09	3.85
12	4.6		721	0.21	Yes	"				
14	11.6	5.23	241	0.04	No	Au-Cr	2.4	7.4	7.74	2.96
15	20.1	5.23	166	0.042	No	Au-Cr	2.4	7.4	8.96	2.56
16	30	5.23	111	0.042	No	Au-Cr	2.4	7.4	0.125	1.83
17	4.5	2.48	204	0.067	No	Silver Paste	1.0	6.5	0.138	1.12

2. Pyroelectric Materials Preparation.

Several different types of materials have been synthesized and in some cases heat treated. One of the specifications on some of the materials requested was that the Curie temperature should be close enough to room temperature so that at will one could work either in the ferroelectric or the paraelectric regions.

One of the systems for which data on Curie temperature vs. composition was available was the $BaTiO_3$ - $SrTiO_3$ system. It was our experience, as was confirmed by others, that by mixing these two compounds in proper proportions, one could, after proper thermal treatments, obtain a pyroelectric material with Curie temperature in a wide temperature region around the room temperature.

We prepared a system $(Ba_{0.6}, Sr_{0.4})$ TiO_3 for which a Curie temperature = 0°C was predicted. The $BaTiO_3$ and $SrTiO_3$ powders were milled in a jar mill for 18 hours within pure H_2), then after drying, milled again with acetone for 4 hours, dried, heated at 900°C, crushed and ground. It was submitted to the Ceramics Division of Honeywell Co. for hot pressing. The result was a sample about 25 mm diameter and 6 mm thick, exhibiting good ferroelectric characteristics, with a Curie temperature of about 5°C measured.

A second hot pressing of a little different composition: $(Ba_{0.68}, Sr_{0.32})\ TiO_3$ by the same Honeywell group was a dismal failure, apparently from heating at too low a temperature.

We decided to develop our own heat treatments using the apparatus available in our laboratory. The technical difficulty of the problem is to obtain relatively high (more than 1400°C) temperature in presence of open air atmosphere. We observe that when the (Ba, Sr) TiO_3 ceramics are heated in vacuum or argon atmosphere (in these conditions a temperature 1400°C can be obtained in our laboratory easily using the HF - induction heater) the samples change the color from light to dark due to the loss of oxygen, and starts to be a semiconductor, losing their ferroelectric properties. But when the dark samples were reheated at approximately 1000°C in open air or oxygen atmosphere, the light color was regained, together with the pyroelectric properties.

From that we concluded that when a (Ba, Sr) TiO_3 powder would be pressed at room temperature in a pellet (using approximately 20,000 psi pressure) and the pellet heated in argon atmosphere at = 1400°C, in this way forming a dark colored partially deoxidized

semiconductor, this dark material could be transformed in normal (Ba, Sr) TiO_3 ceramic after reheating it at 1000°C within air or oxygen atmosphere.

We experimented intensively in this way preparing many samples. The heating in argon formed dark, rigid material which, after the reheating in open air or oxygen became a light uniformly colored non-conductive ceramic, but unfortunately this (Ba, Sr) TiO_3 - ceramic does not exhibit pyroelectric properties. Apparently the crystalline microstructure formed at high temperature when the material is partially deoxidized is not identical with the normal structure formed from the pressed powder of normal (Ba, Sr) TiO_3 which has not been reduced.

We constructed an electrical furnace which can be operated near 1400°C in open air as the upper limit. (The furnace was damaged in trying to operate it above 1400°C.)

When pellets were pressed at room temperature (16 mm diameter and a 2 mm thickness after pressing at 20,000 psi) were heated at around 1350°C in open air, the final (Ba, Sr) TiO_3 ceramics obtained in this way show a distinct dielectric constant maximum peak near to the predicted Curie temperature.

In this way samples of the following constitution were prepared:

$(Ba_{0.68}, Sr_{0.32})\ TiO_3$

$(Ba_{0.75}, Sr_{0.25})\ TiO_3$

$BaTiO_3$ (not mixed)

After the heat treatment all the samples were ground and polished with the silicon carbind Wetordry papers to approximately 0.3 -- 0.5 mm thickness.

All the (Ba, Sr) TiO_3 samples exhibit distinct dielectric peaks near the predicted Curie temperatures, but their tan δ factors are not very low.

The pure $BaTiO_3$ - ceramic at Curie temperature (= 100°C) has an excellent tan δ - factor (= 0.012), too.

Repeating all the procedures mentioned above we tried to prepare a Ba $(Ti_{0.85}, Sn_{0.15})\ O_3$ - ceramic sample by mixing in corresponding proportions the $BaTiO_3$ - and $BaSnO_3$ - powders. The predicted Curie temperature of this ceramic should be around 18°C.

$BaTiO_3$ - powders are commercially available, but the $BaSnO_3$ we prepared ourselves using the reaction:

$$BaCO_3 + SnO_2 \xrightarrow[\text{heat}]{} BaSnO_3 + CO_2\ (\text{gas})$$

Our Ba (Ti, Sn) O_3 - ceramic has good ceramic-like appearance, but it exhibited a very low and flat peak in the dielectric constant vs. temperature curve around 11°C so that practically it is unusable as pyroelectric sample.

The reasons for that could be twofold:

a) For the preparation of $BaSnO_3$ - ceramic the heating at 1450°C for 1 hour is recommended in air atmosphere. We could not reach so high a temperature.

b) It is possible that our homemade $BaSnO_3$ is not of the quality required (in practice this reaction between two powders in solid state form might not be easily accomplished due to the contact between the $BaCO_3$ and SnO_2 powders; and the reaction in H_2O - solution is impossible bacause both the reagents are insoluble).

We have made a number of single crystals of the material Tl_3AsSe_3, as well as some smaller crystals of the related compound In_3AsSe_3. These are closely related to the naturally occuring materials Ag_3AsS_3 (proustite) and Ag_3SbS_3 (pyrargyrite) which have been used in studies of nonlinear optics. Both the thallium selenoarsenites and the indium selenoarsinite were prepared by heating the elements in the appropriate ratios. The thallium compound is a semiconductor, for which superb pyroelectric properties had been reported; however, the pyroelectric coefficient measurements were latter retracted by Deis and Roland. The intent in the preparation of the indium compound was to obtain a material of sufficiently larger band gap so that its resistivity would be greatly reduced. In this direction, it is now projected that we should make the compounds Ag_3AsS_3 and Ag_3SbS_3,

which are reported to have band gaps of 2.0 and 1.8 eV respectively. Their pyroelectric properties, if any are unknown; we shall prepare them for evaluation by Professor van der Ziel's group.

Our most recent project is the preparation of $Pb_5(Ge,Si)_3O_{11}$, which is said to have a Curie point of 84°C. Thus far only very small crystals have been made by the Czochralski technique.

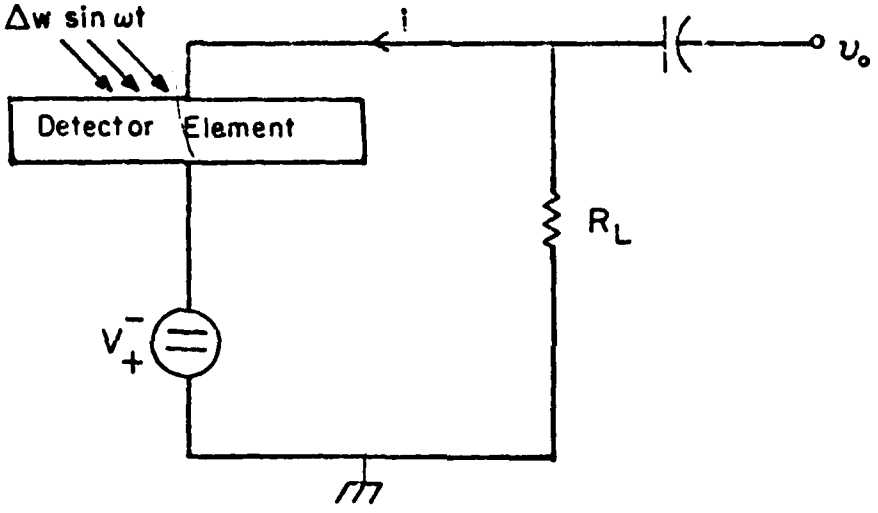

Fig. 1

D.C. capacitive bolometer circuit

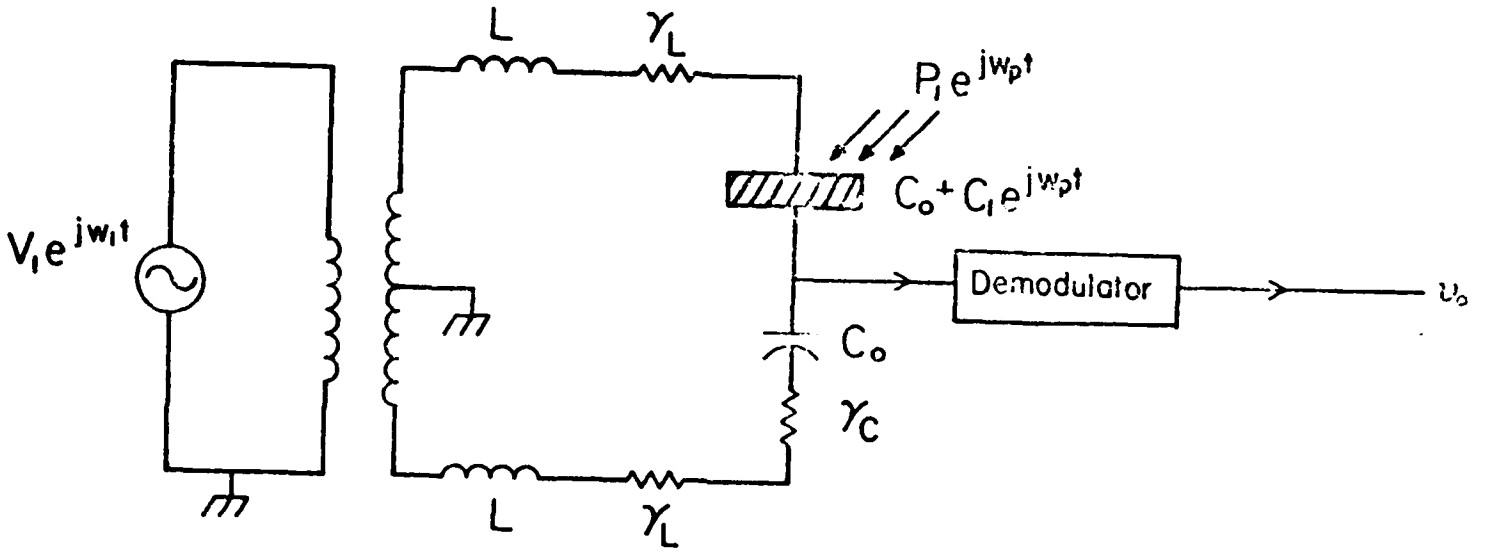

Fig. 2

A.C. capacitive bolometer circuit

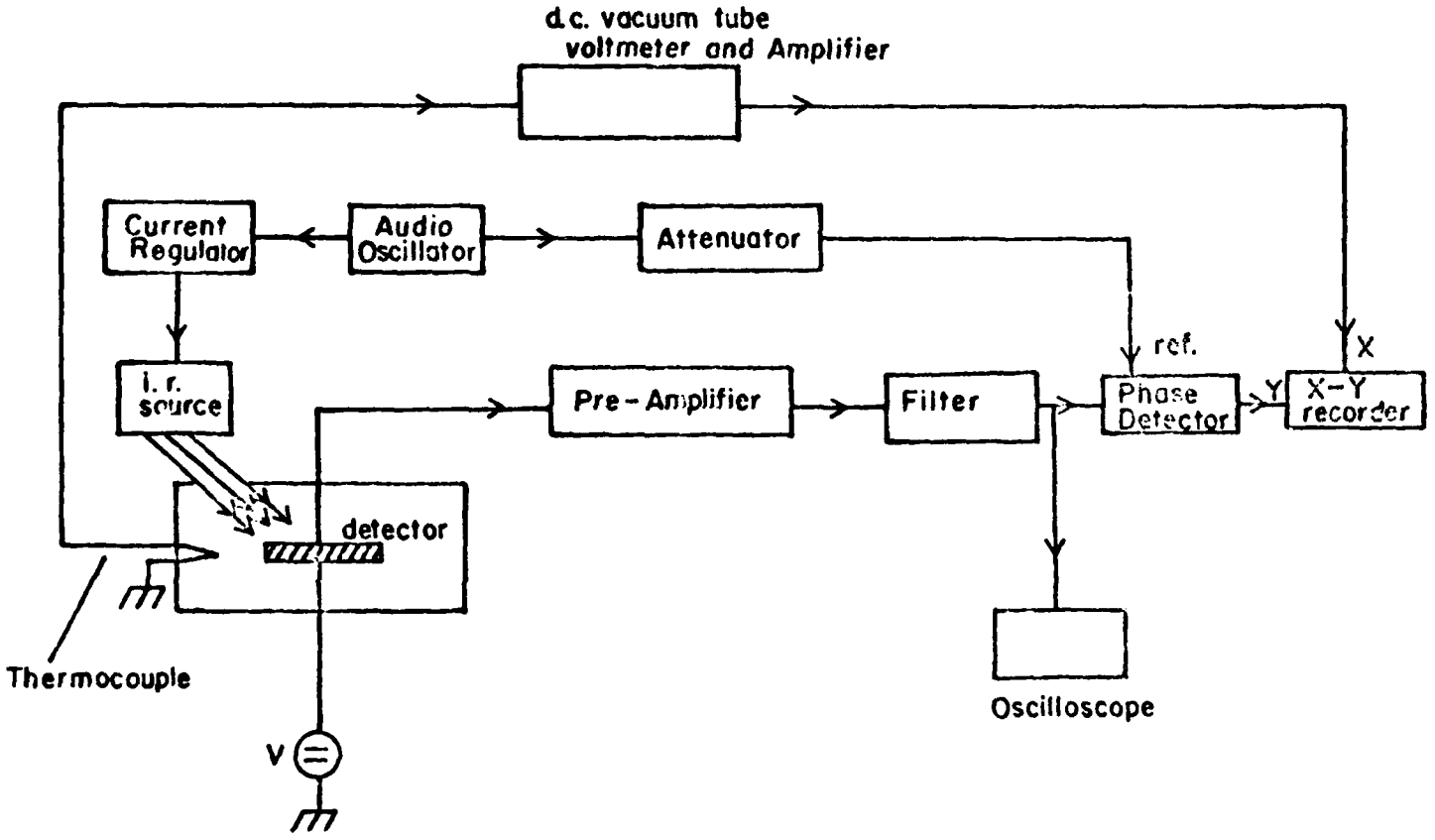

FIG. 3 Experimental set-up for measuring d.c. bolometer sensitivity

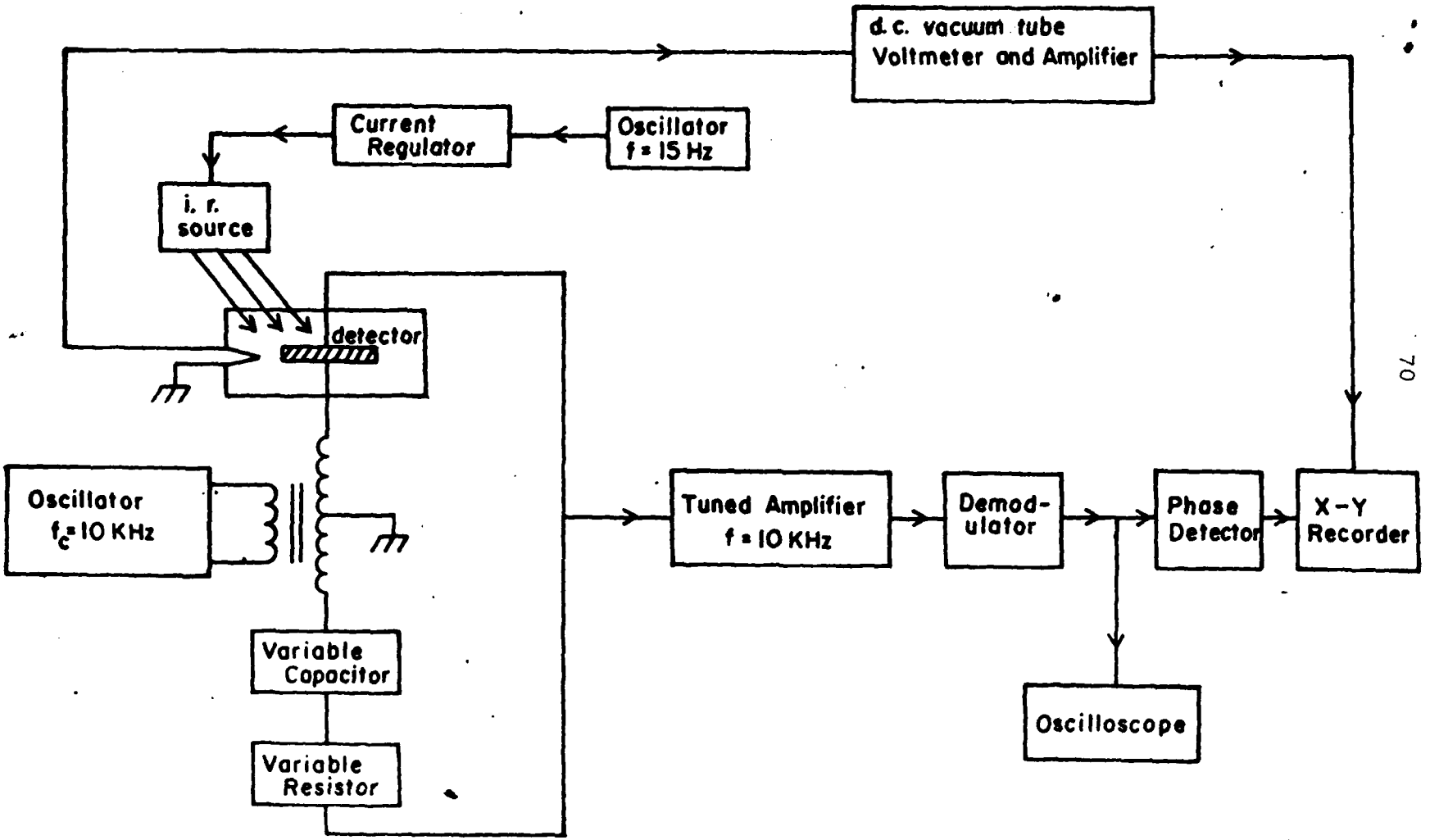

FIG. 4 Set-up for measuring a.c. bolometer sensitivity

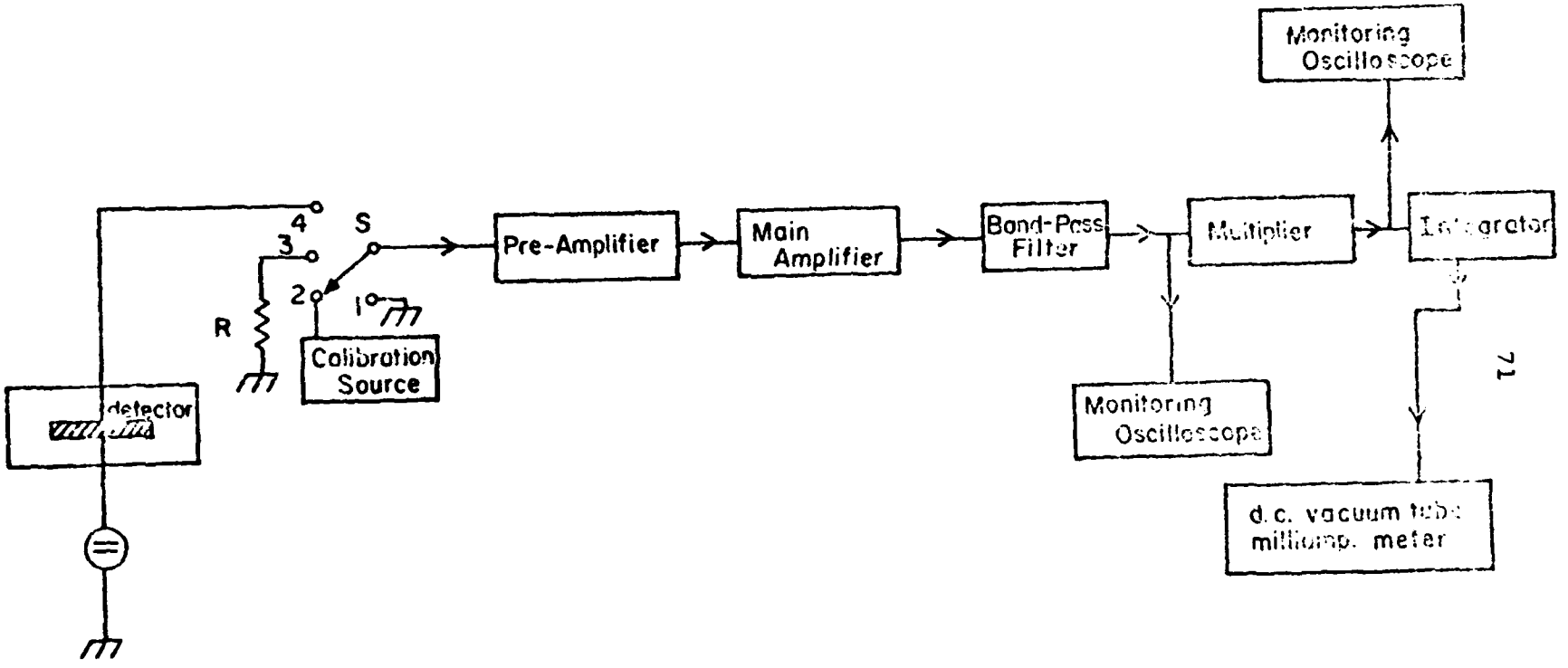

FIG. 5 Set-up for Noise Measurement in d.c. bolometer

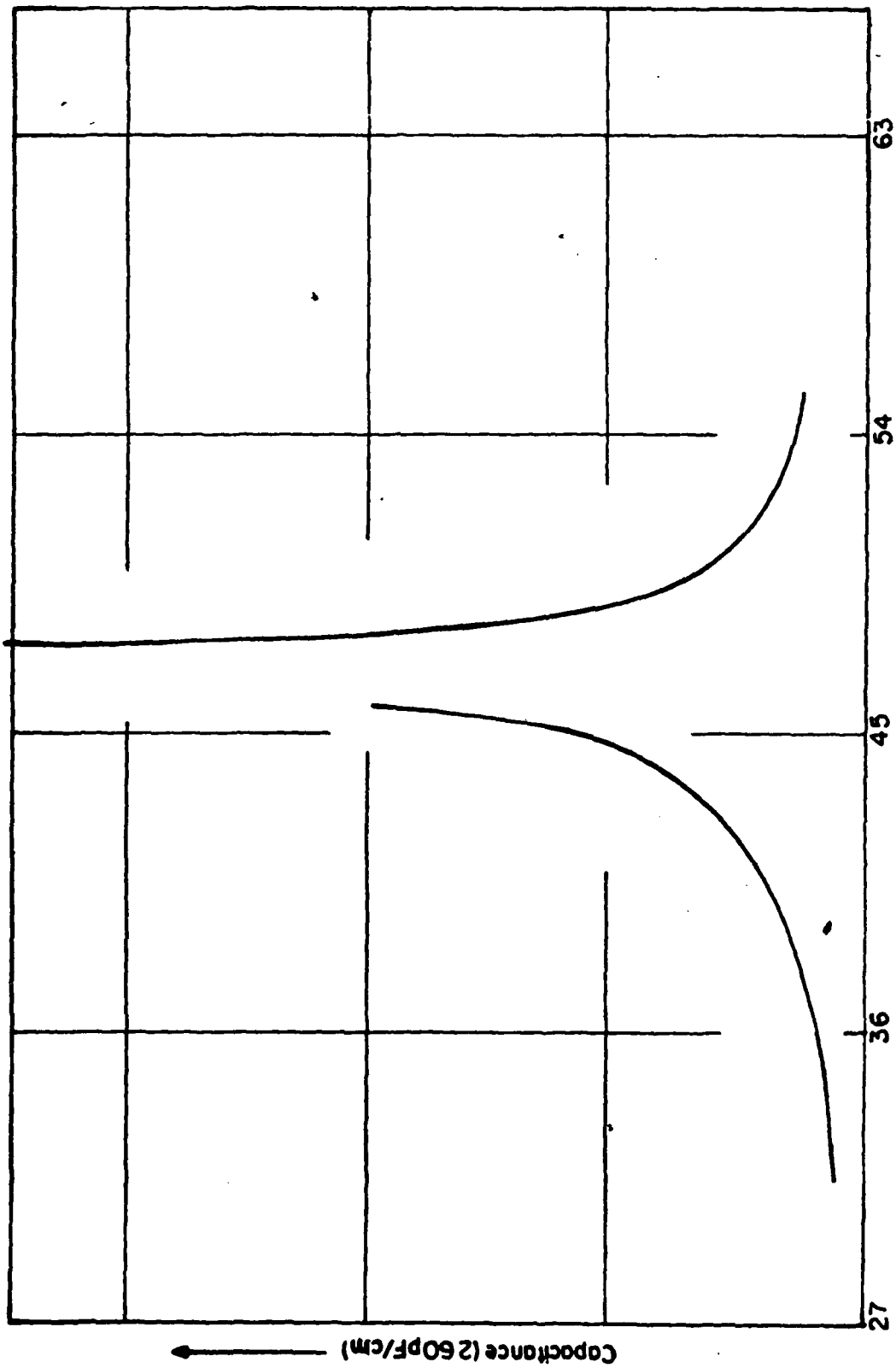

FIG. 6

Capacitance versus temperature in TGS capacitor

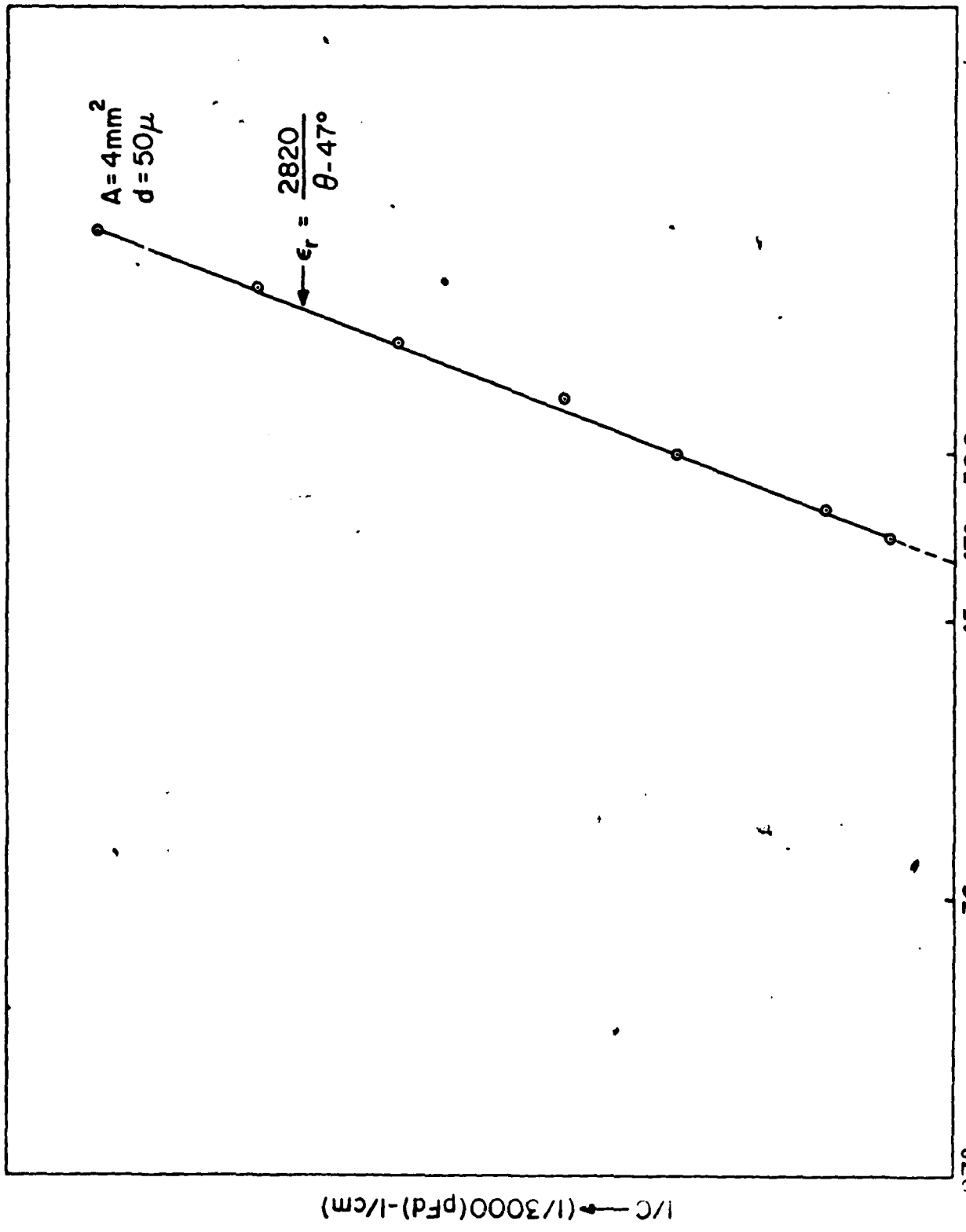

FIG. 7

1/C versus temperature in TGS capacitor

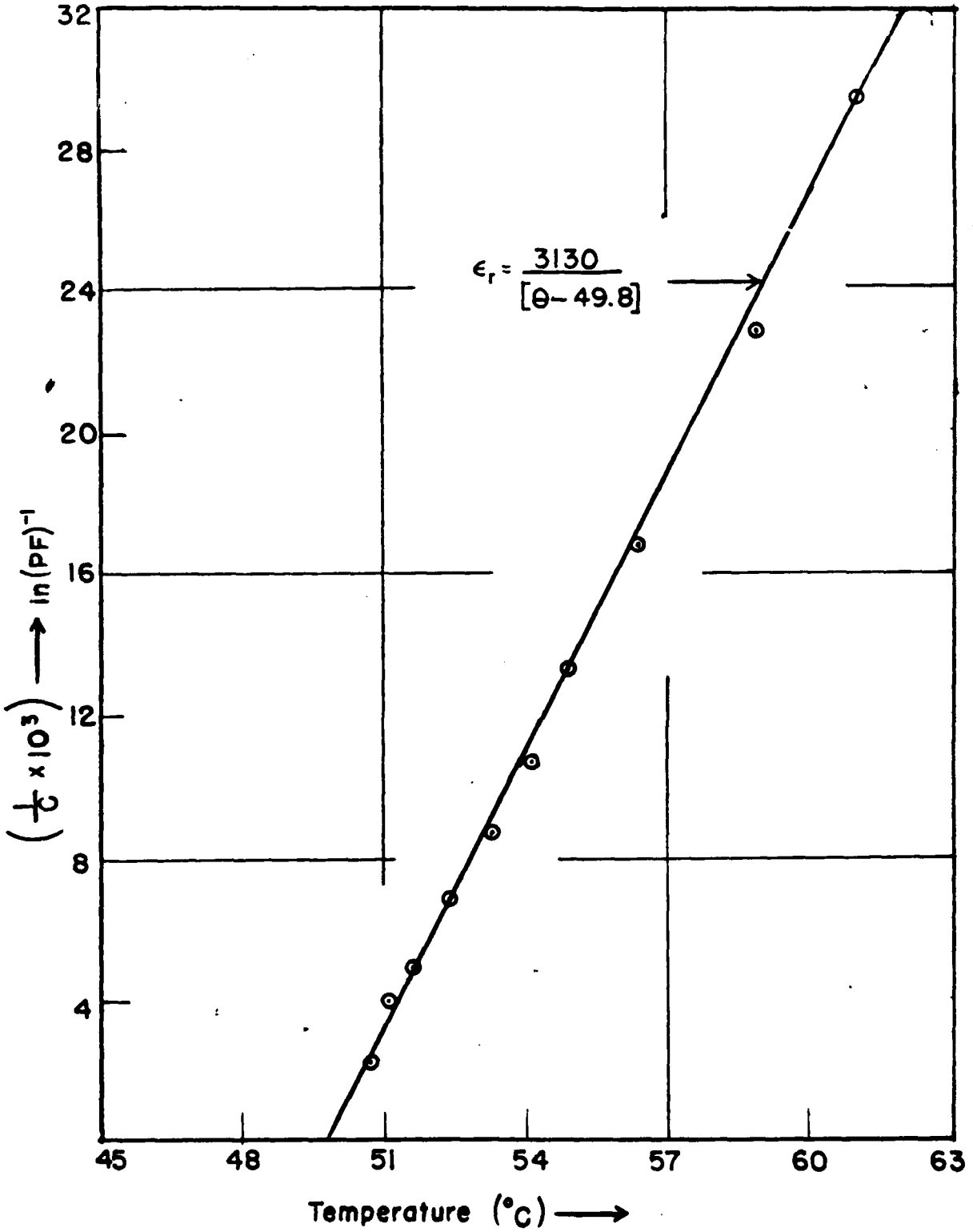

FIG. 8 TGS#42

TGS#42, 1/C versus temperature

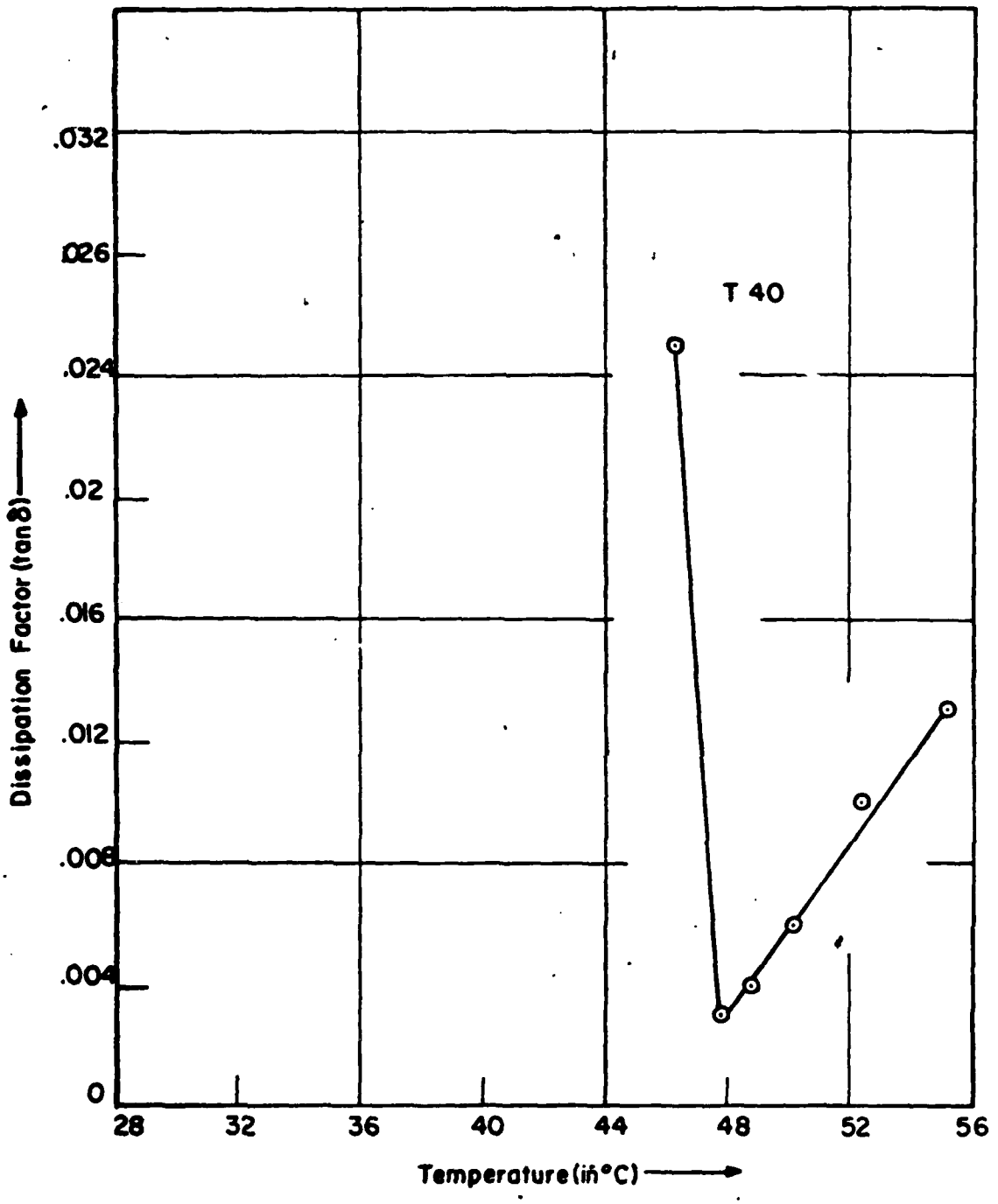

FIG. 9

tan δ versus temperature TGS#40

FIG. 10

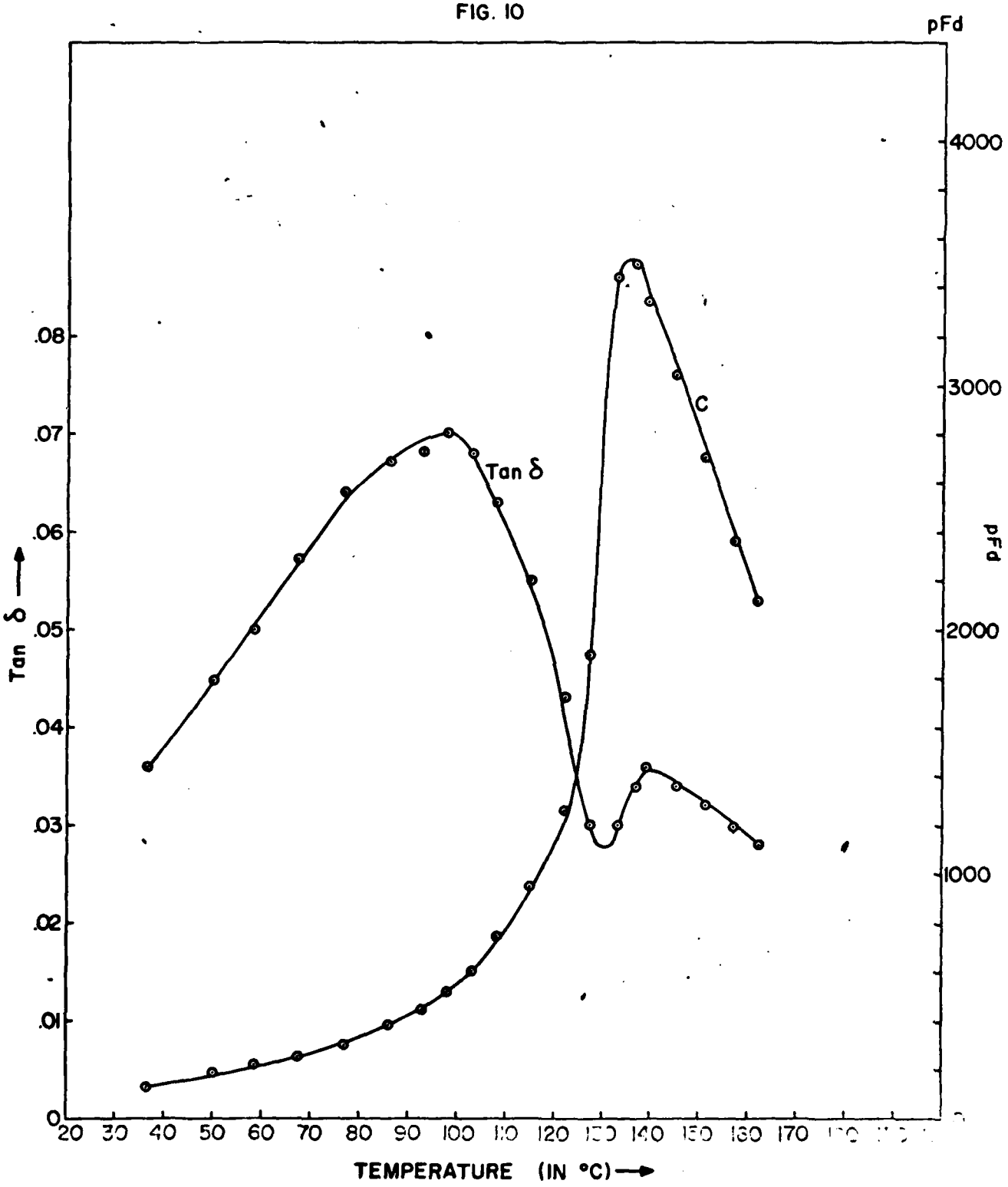

tan δ and capacitance versus temperature for SBN

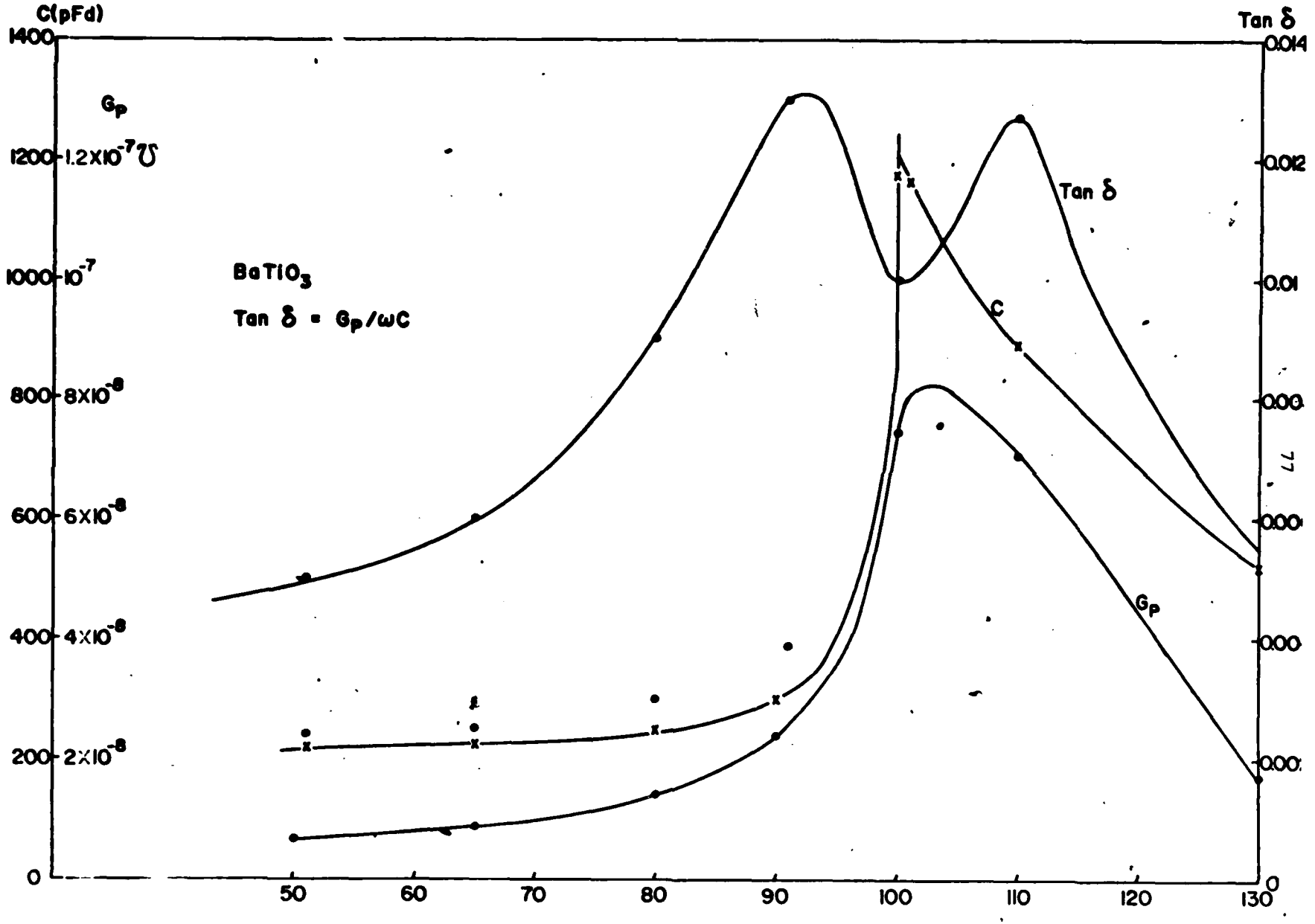

FIG. 11

tan δ, capacitance C and conductance C_p versus temperature for $BaTiO_3$

FIG. 12
Series resistance of $BaTiO_3$ versus temperature

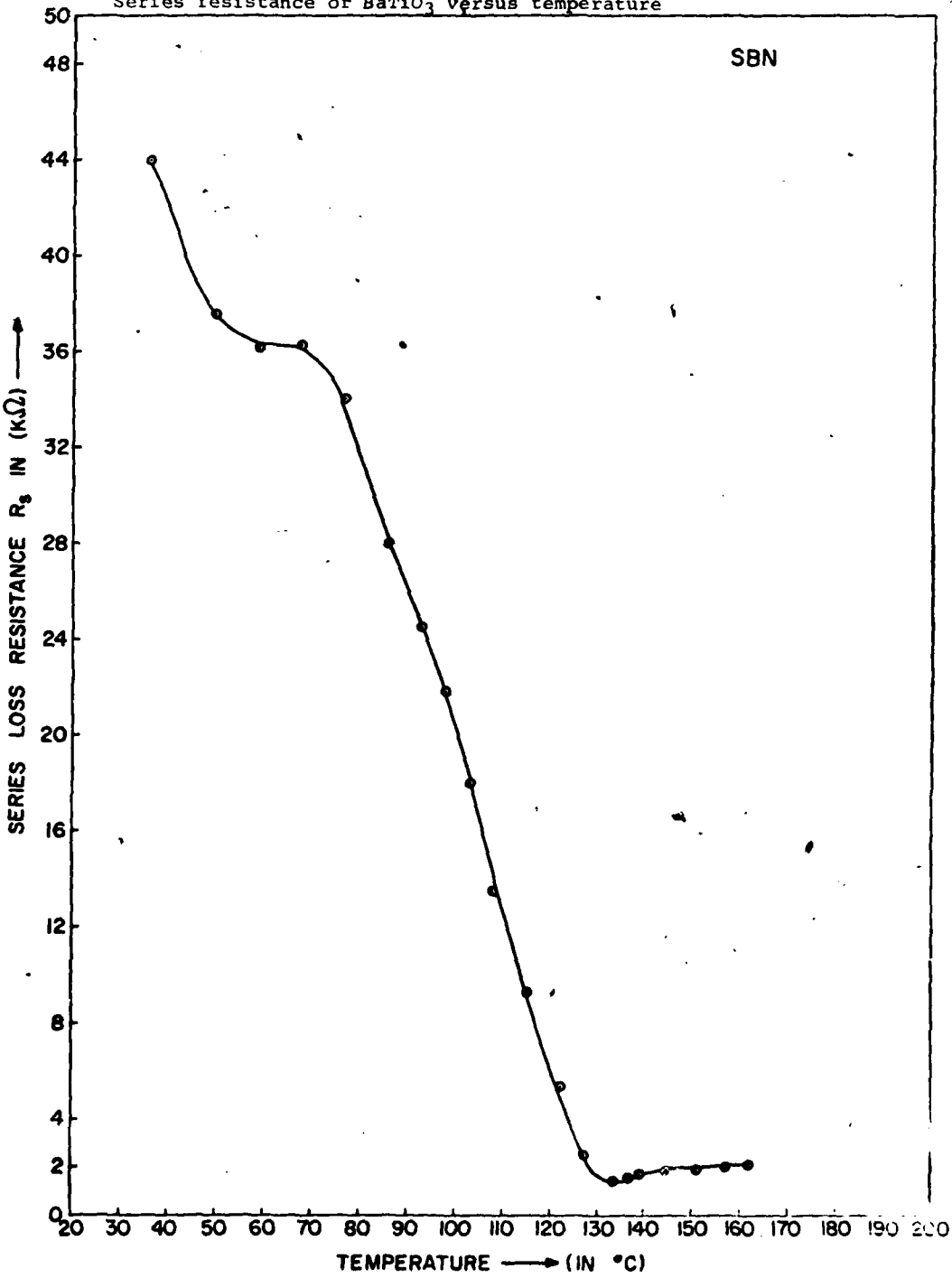

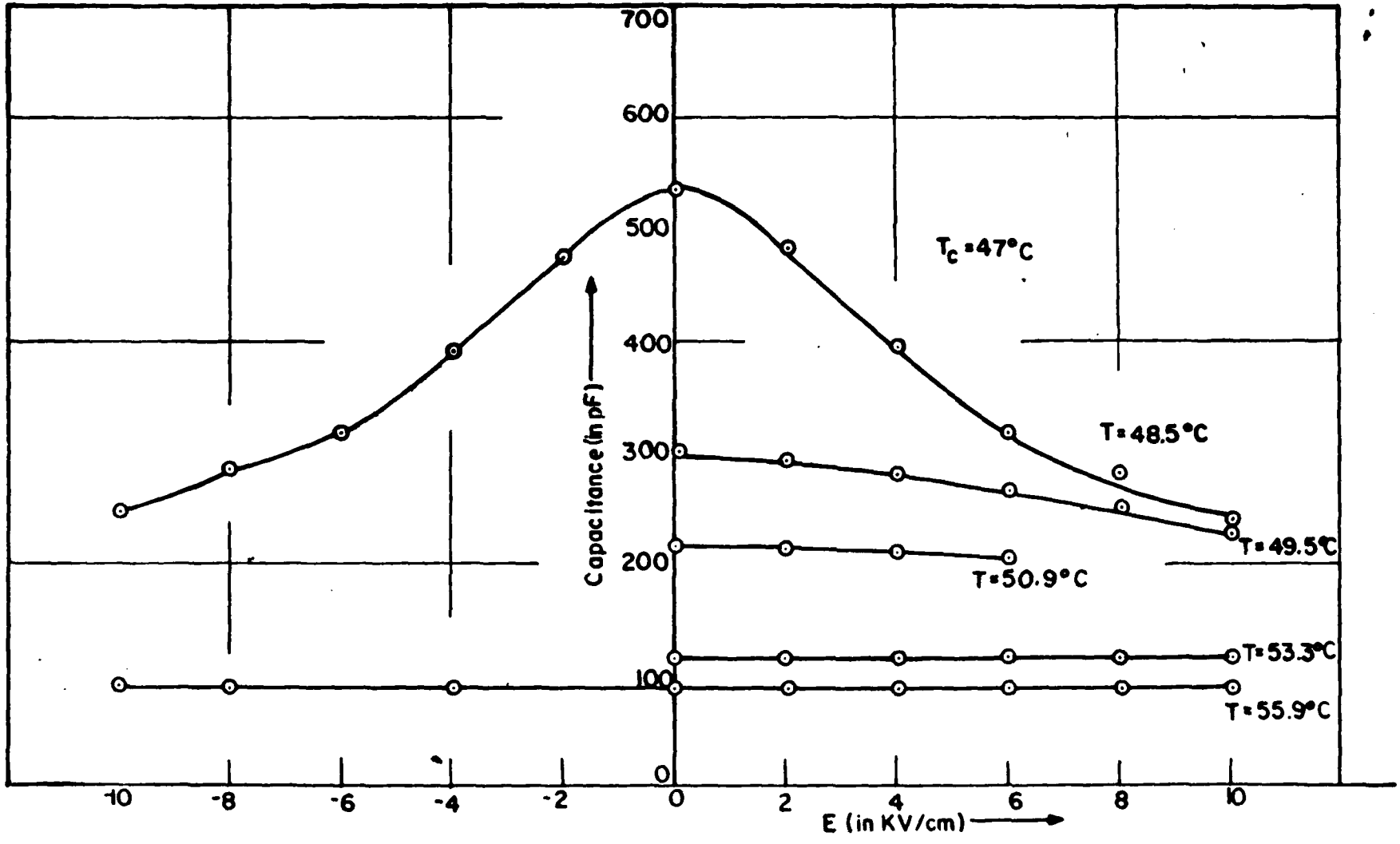

FIG. 13

Capacitance C versus field E in TGS

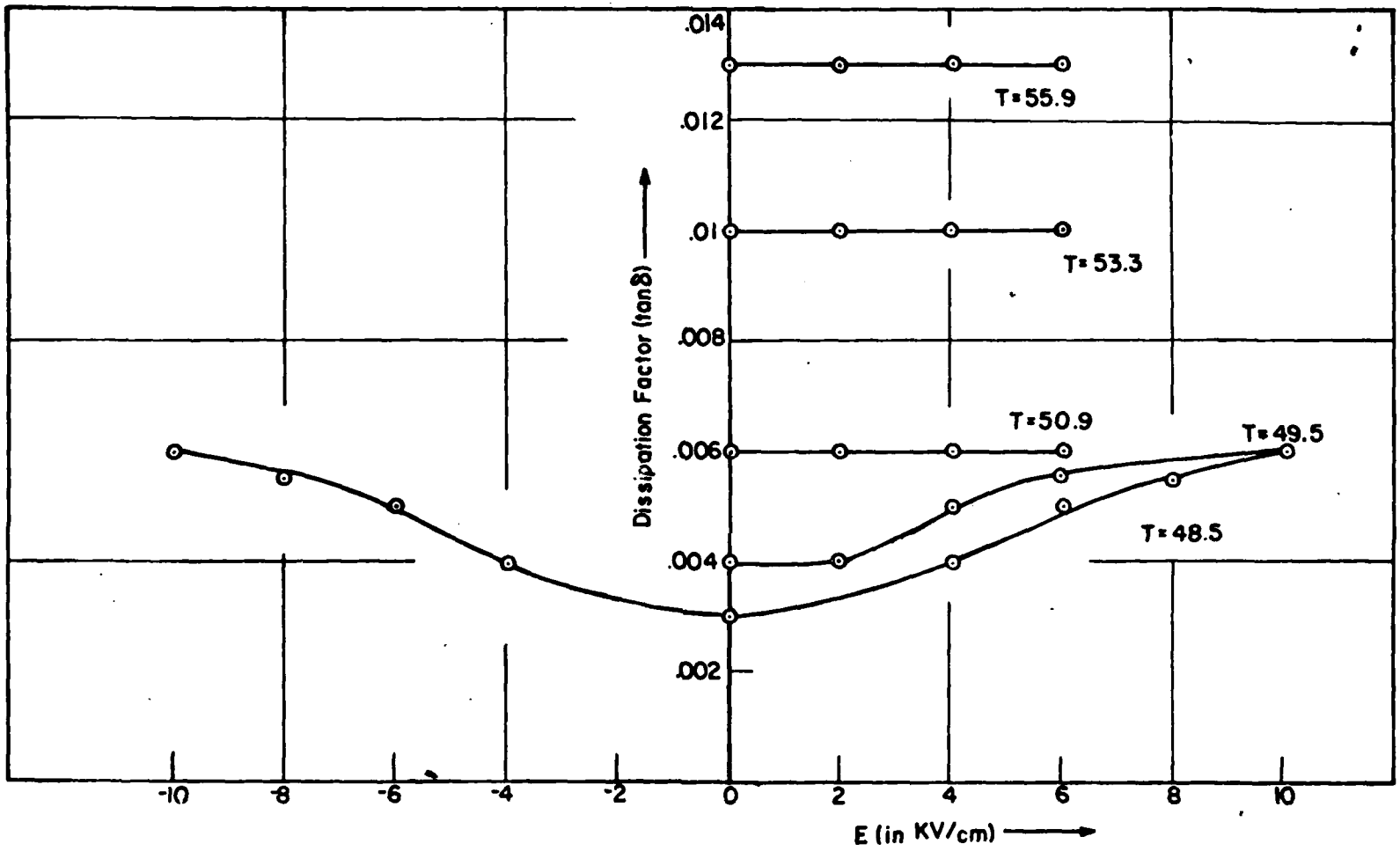

FIG. 14

Dissipation factor tan δ versus field E in TGS

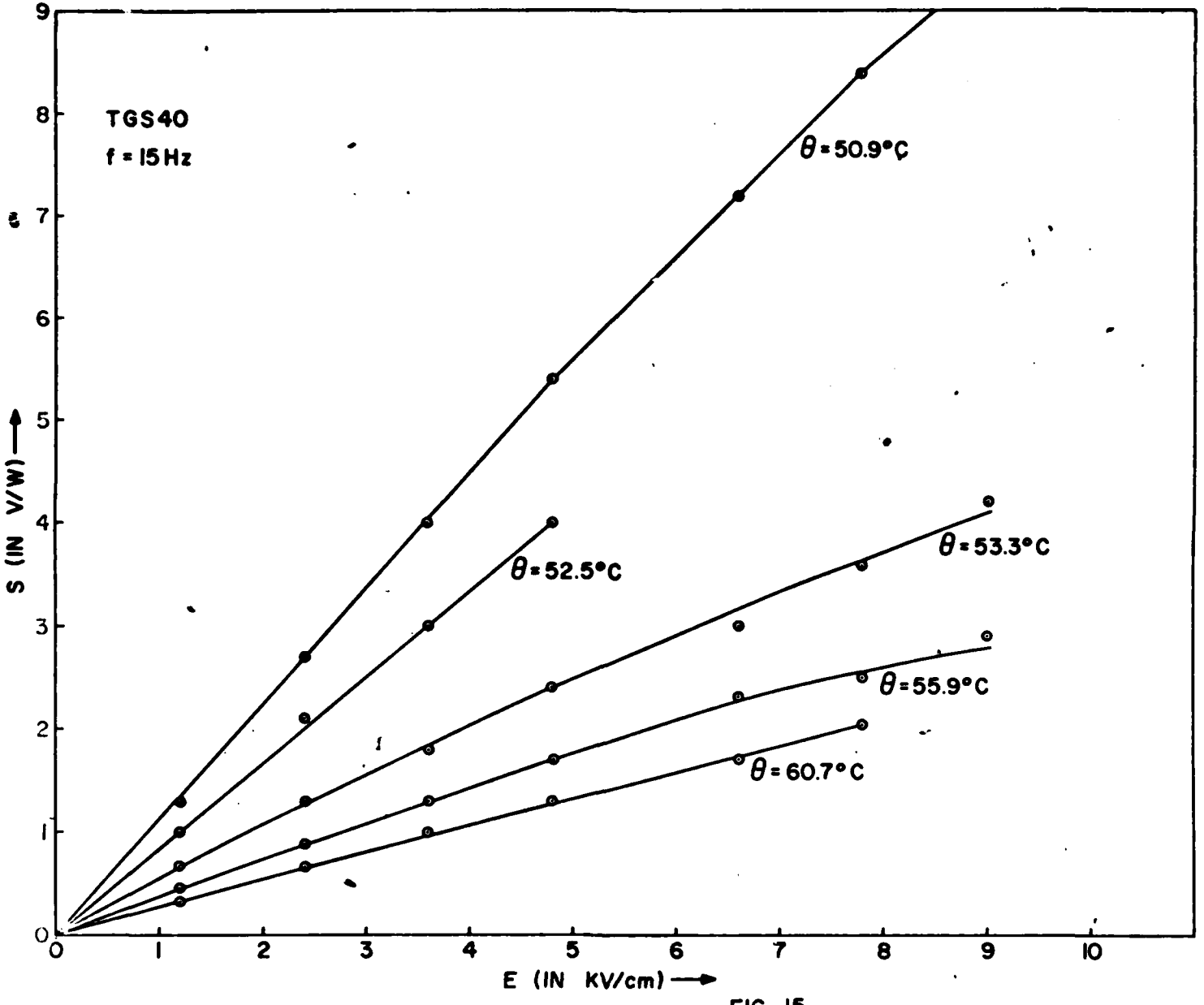

FIG. 15

D.C. bolometer sensitivity for TGS#40 versus E

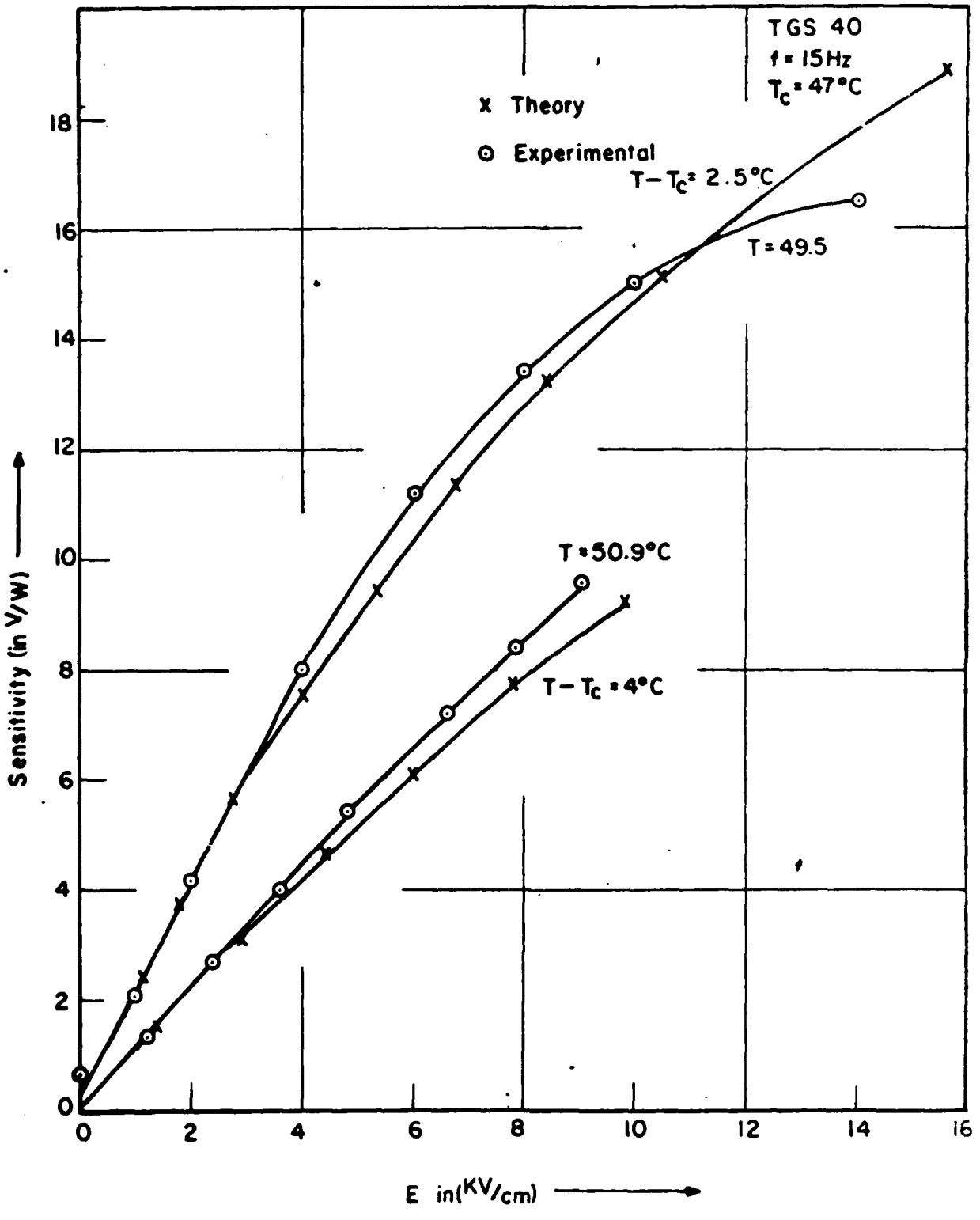

FIG. 16

D.C. bolometer sensitivity for TGS#40 versus E

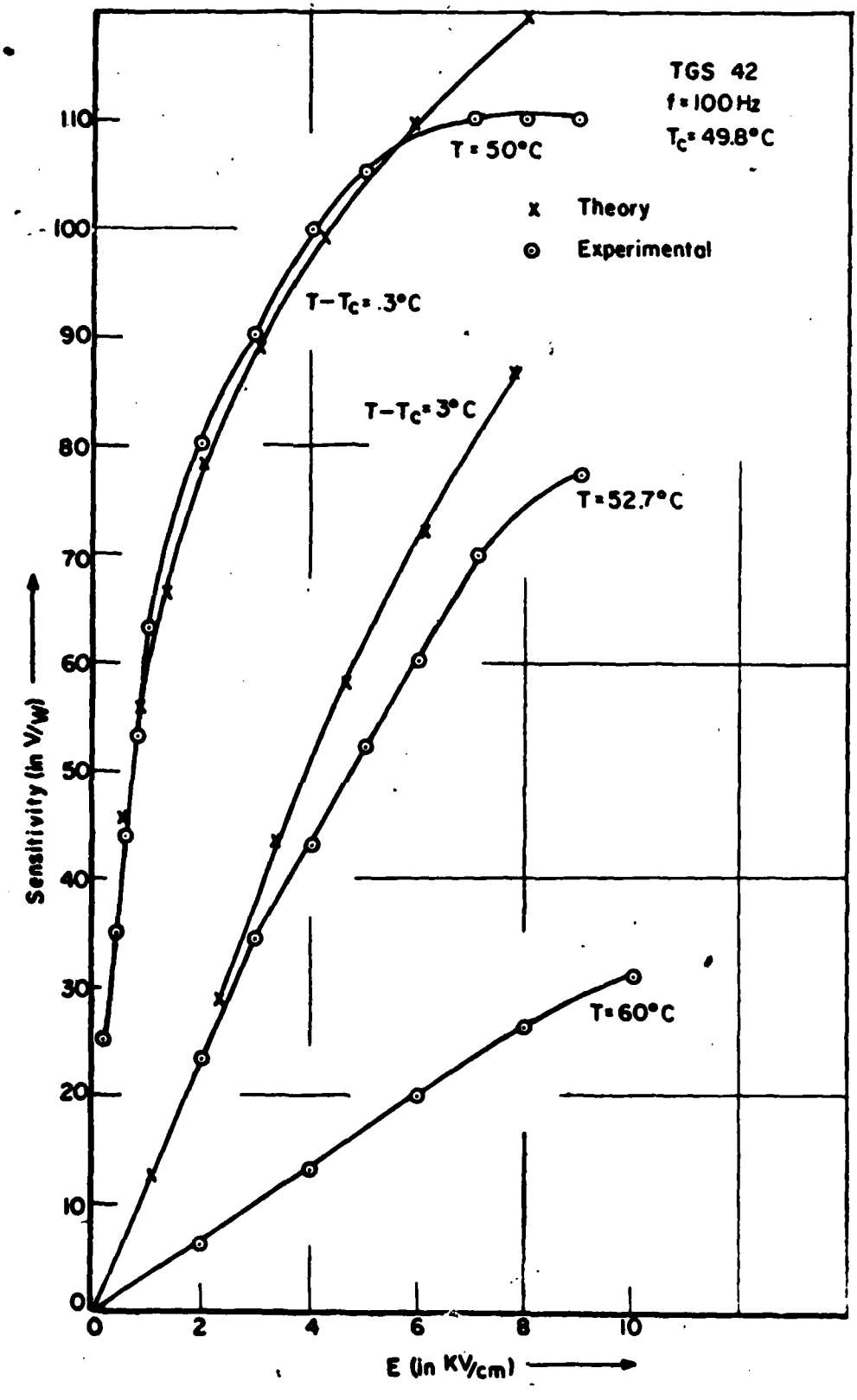

FIG. 17
D.C. bolometer sensitivity versus E for TGS#42

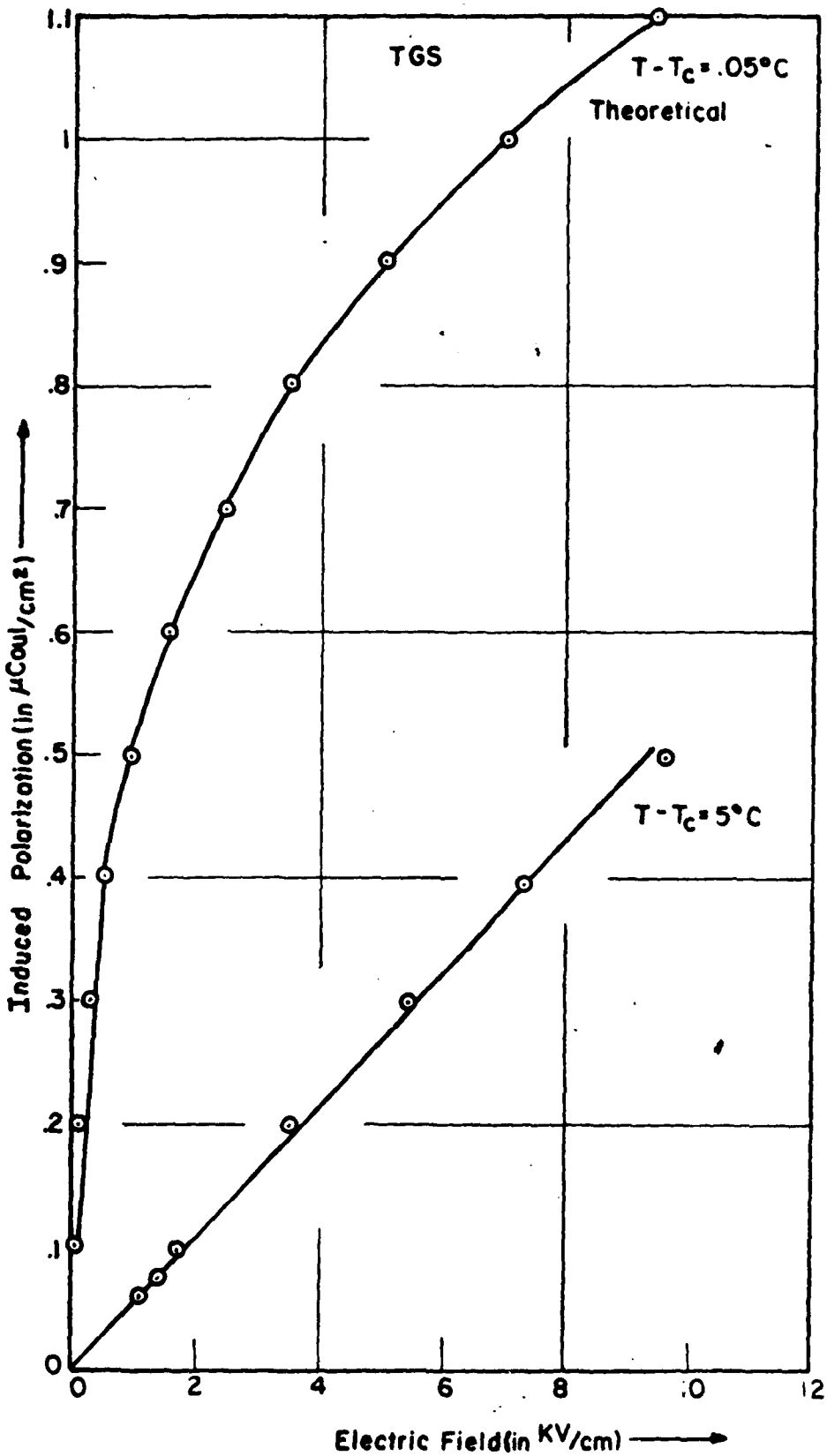

FIG. 18

Induced polarization versus field in TGS

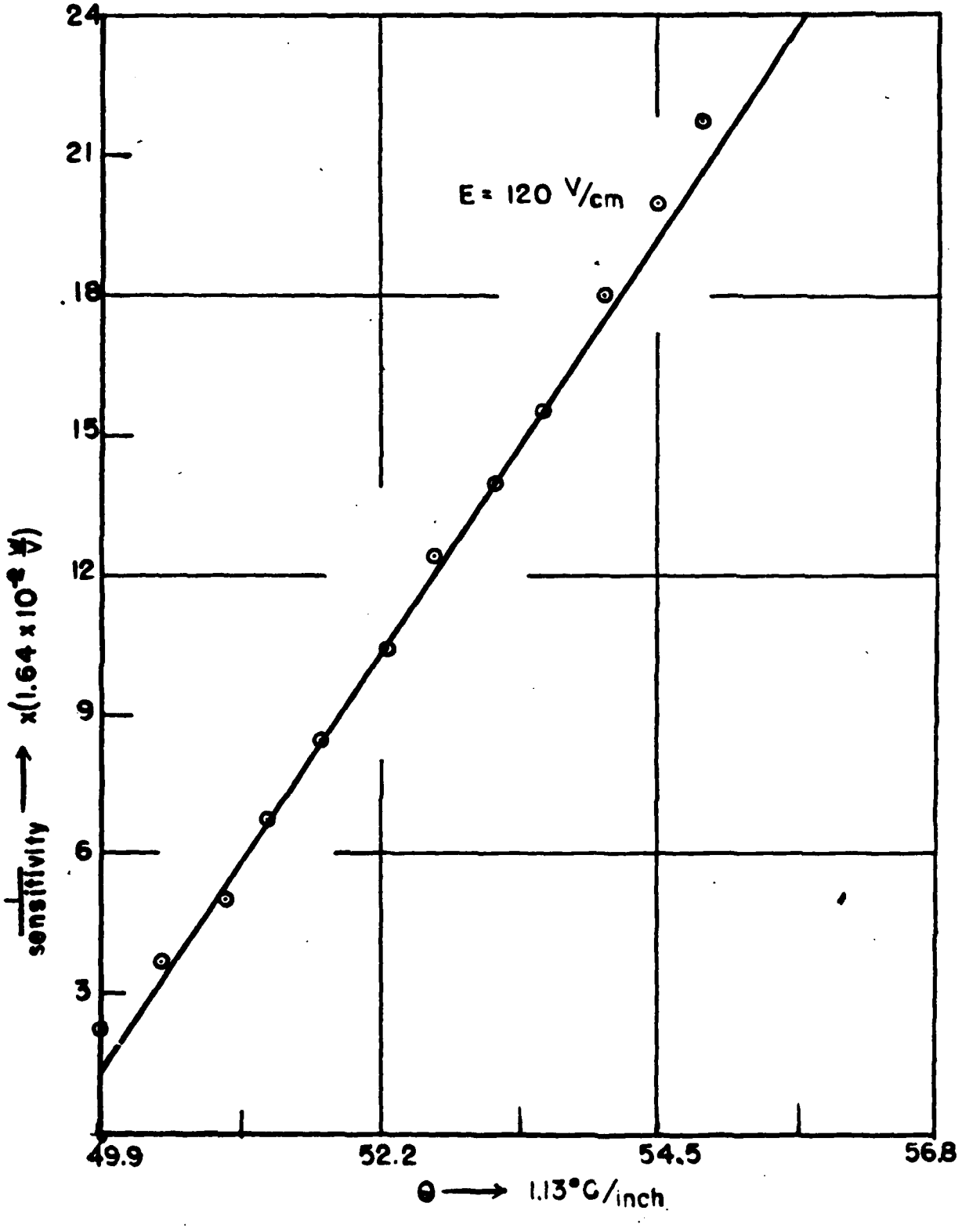

FIG. 19

Inverse of sensitivity versus temperature in TGS

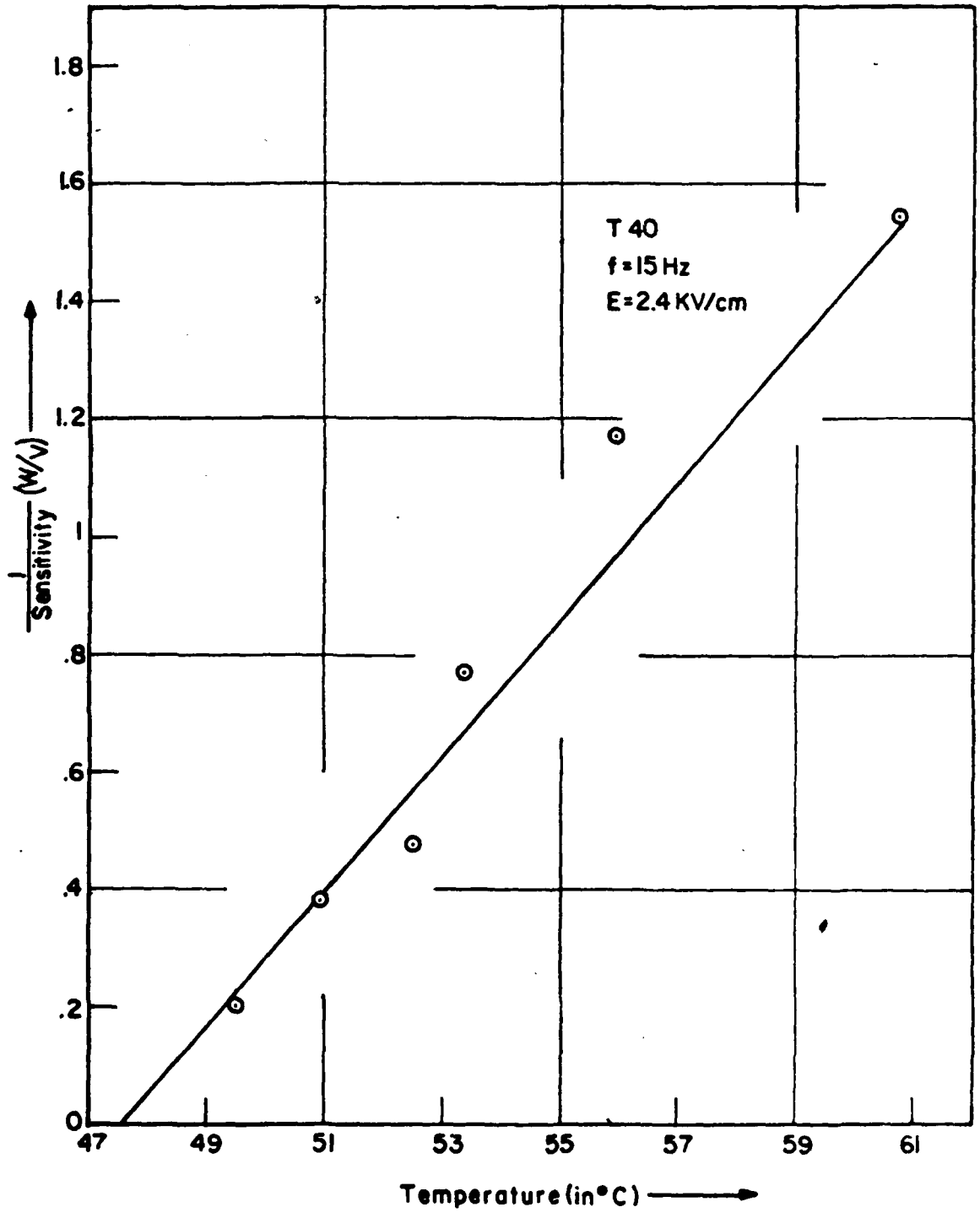

FIG. 20

Inverse of sensitivity versus temperature in TGS#40

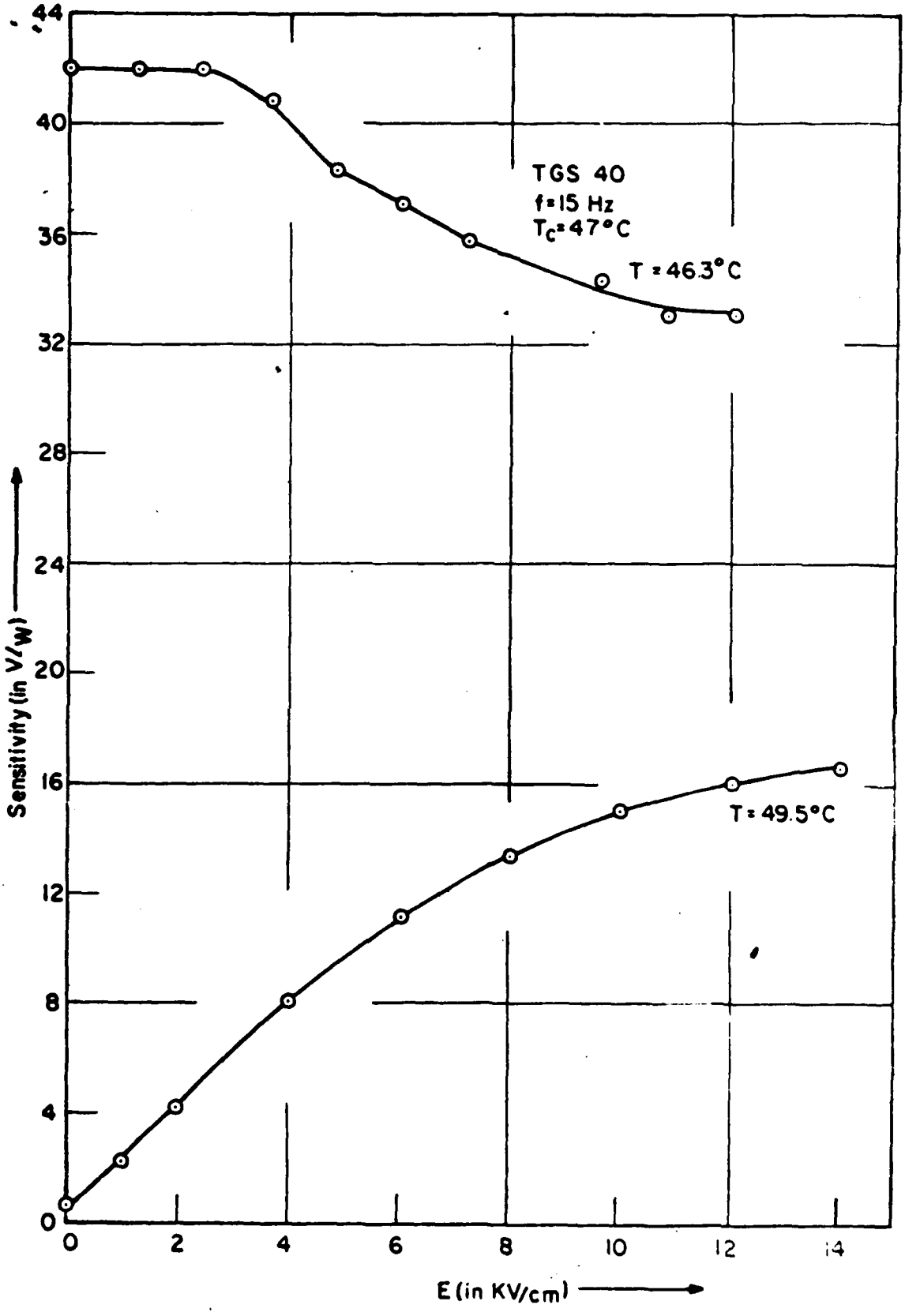

FIG. 21

Pyroelectric sensitivity and capacitive bolometer sensitivity versus field (TGS#40)

AD-A112 855 MINNESOTA UNIV MINNEAPOLIS DEPT OF ELECTRICAL ENGIN--ETC F/G 20/3
INVESTIGATION OF PYROELECTRIC AND PYROMAGNETIC DETECTION.(U)
APR 74 A VAN DER ZIEL DAAK02-72-C-0398

UNCLASSIFIED NL

2 OF 2
AD A
112 855

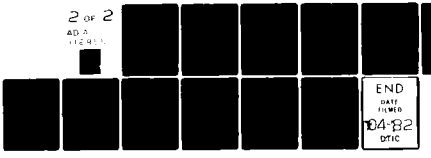

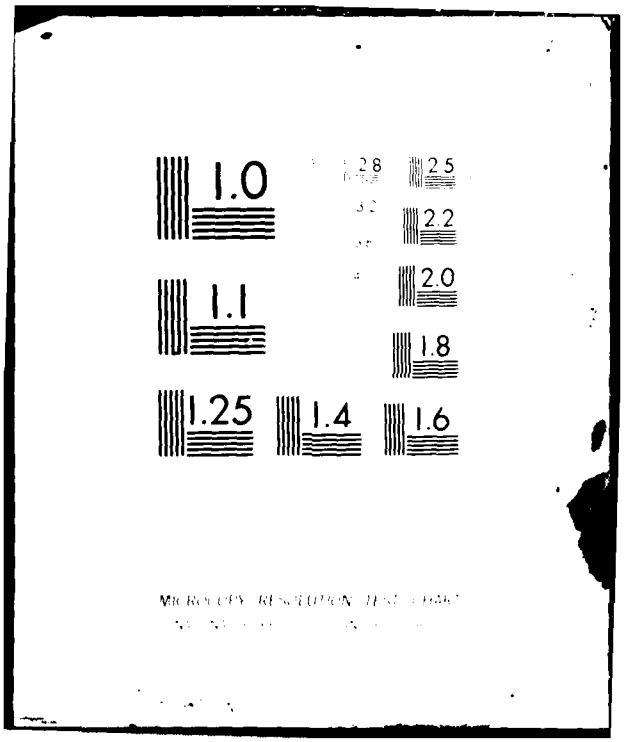
1.0
1.1
1.25
1.4
1.6
2.0
2.2
2.5

FIG. 22(a)

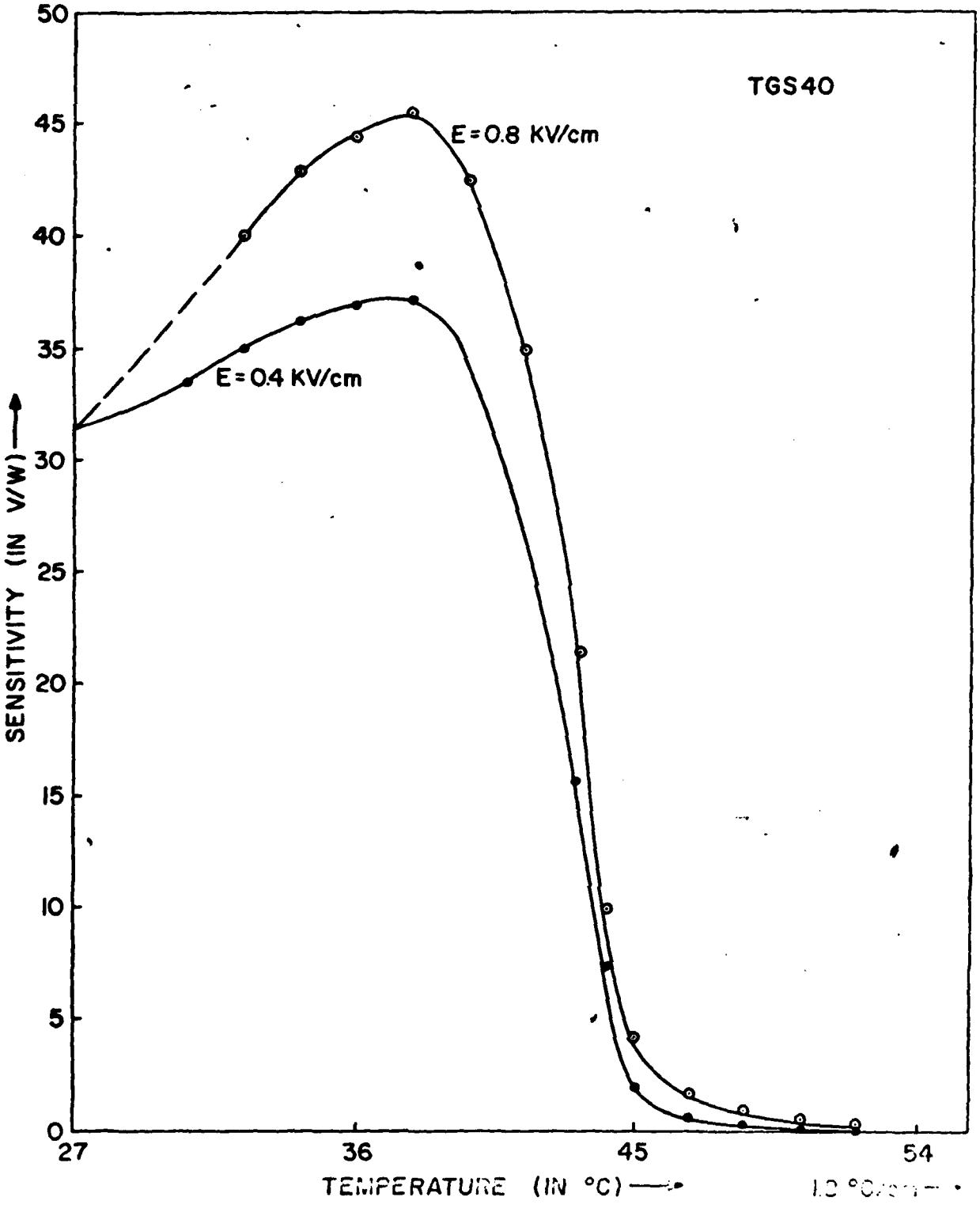

Pyroelectric sensitivity for TGS#40 versus temperature, field as parameter

FIG. 22 (b)

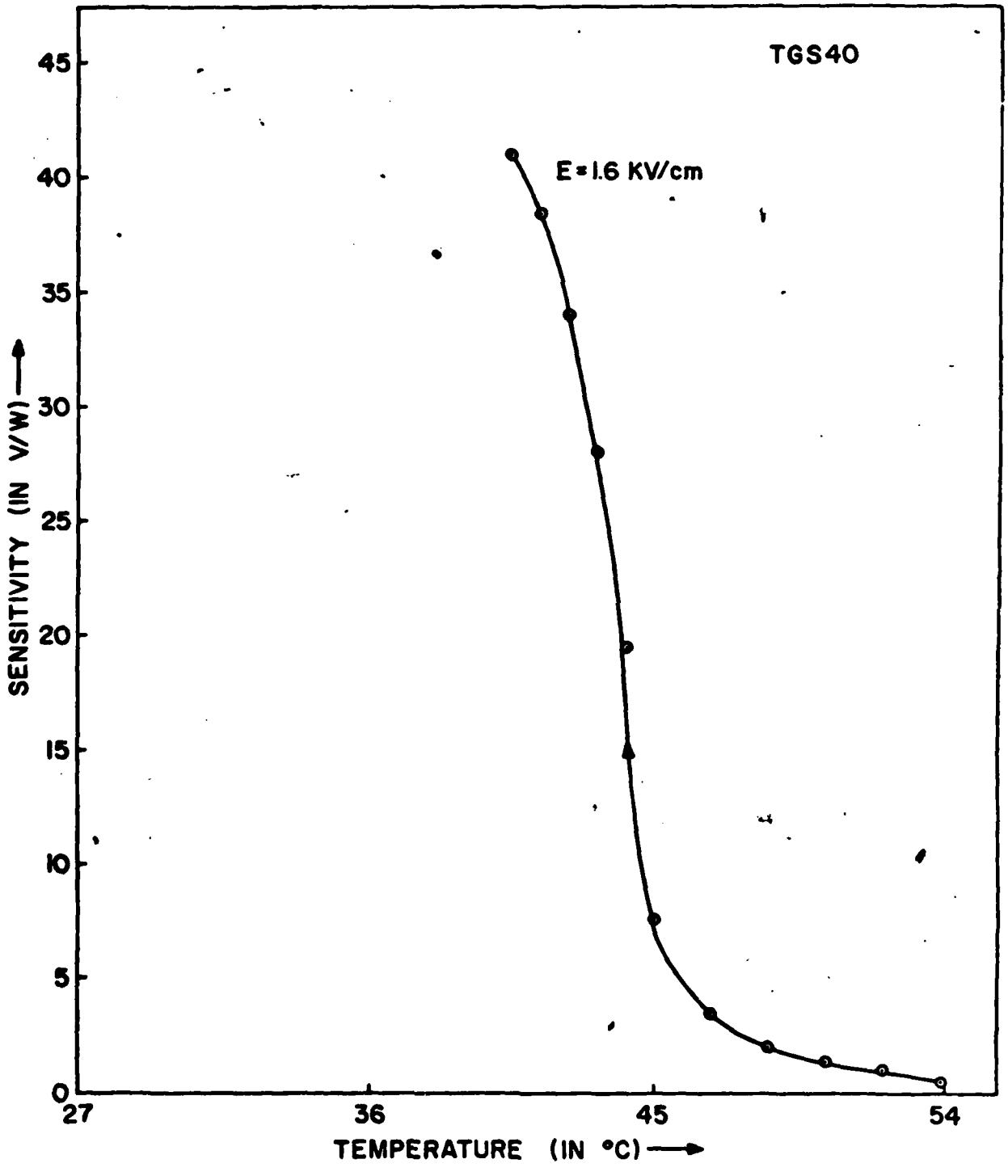

Pyroelectric sensitivity for TGS#40 versus temperature at 1.6 KV/cm

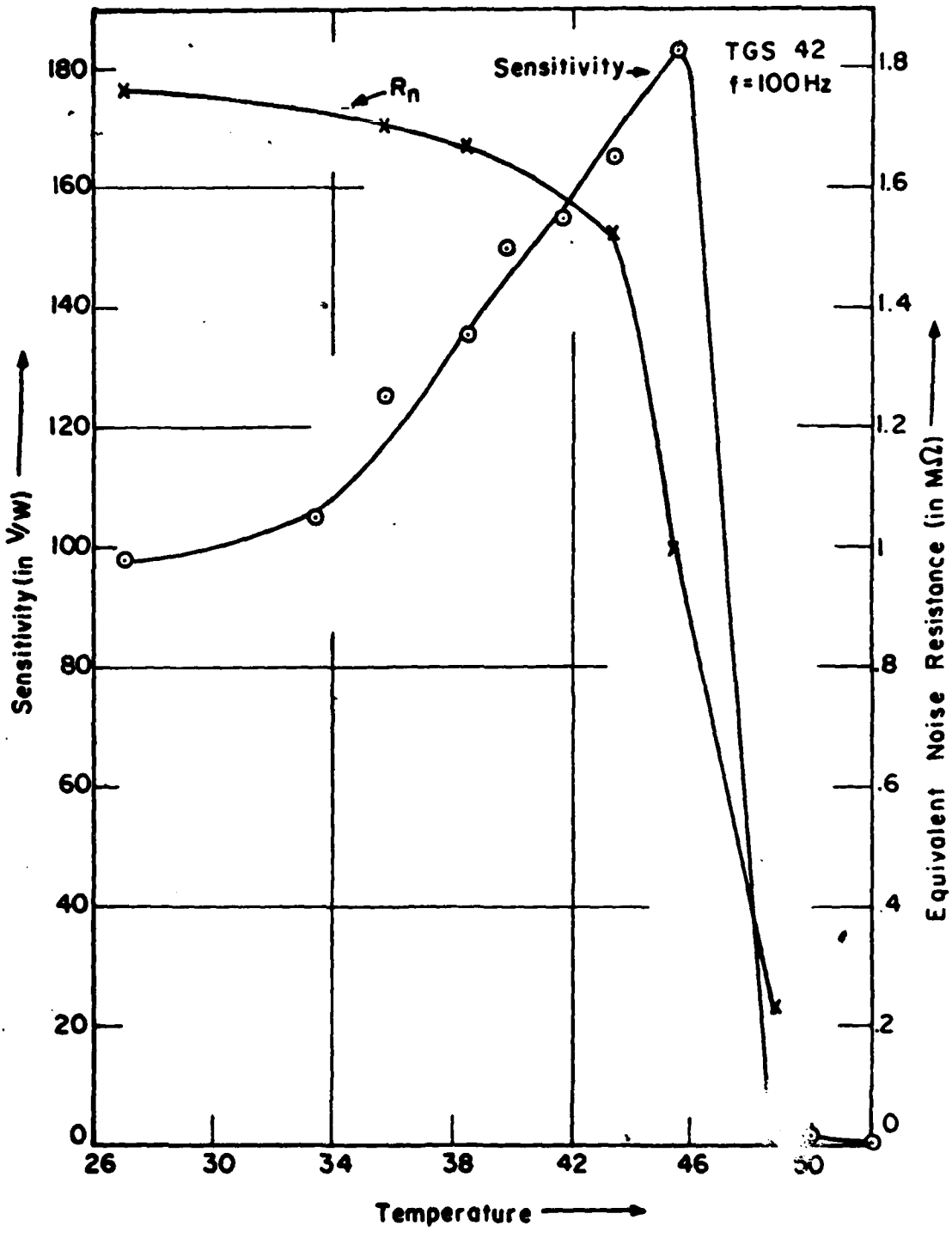

FIG. 23

Pyroelectric sensitivity and noise resistance R_n versus temperature for TGS#42

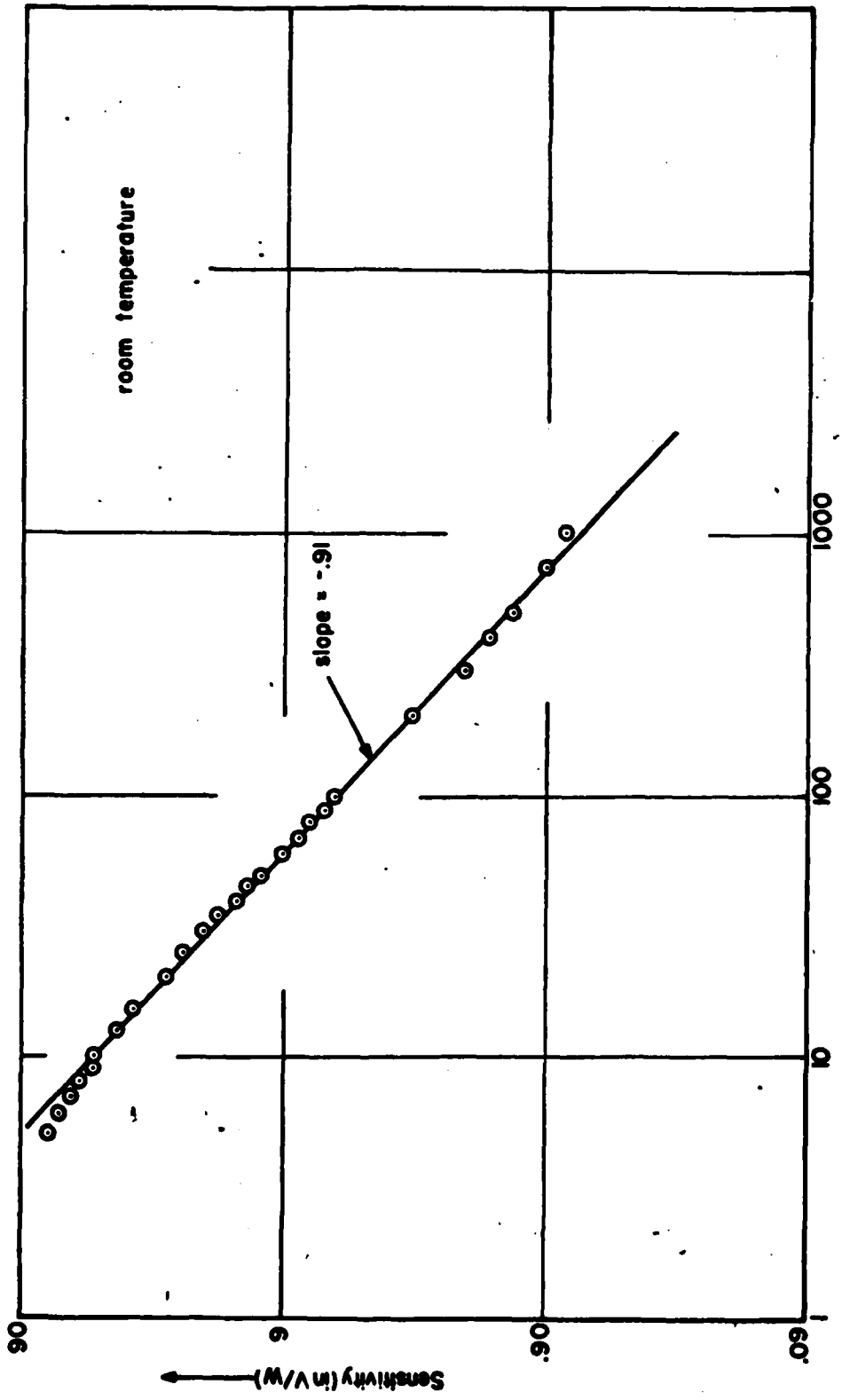

FIG. 24
Sensitivity versus frequency for TGS#40

FIG. 25

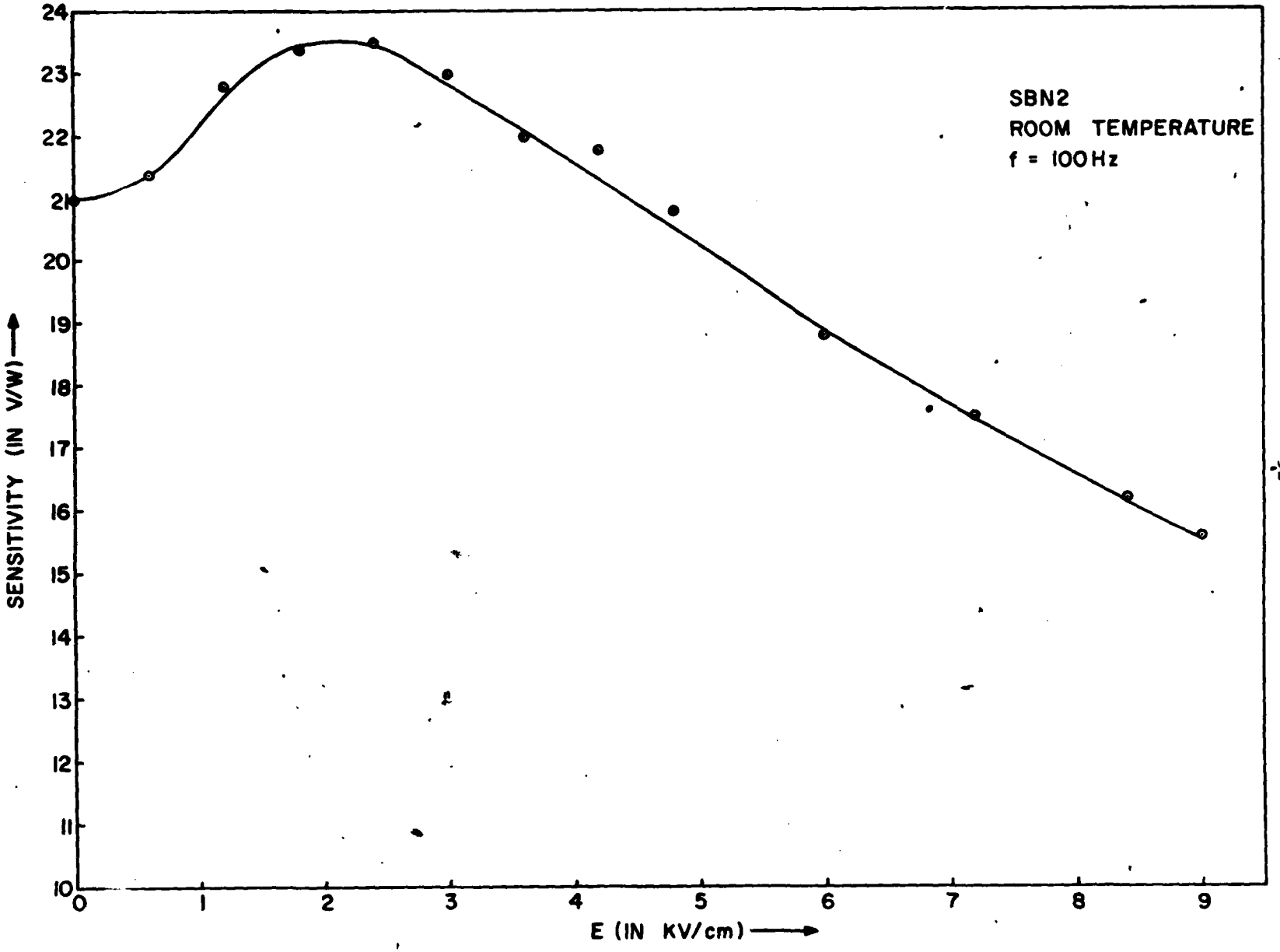

Sensitivity versus field for SBN_2 at room temperature

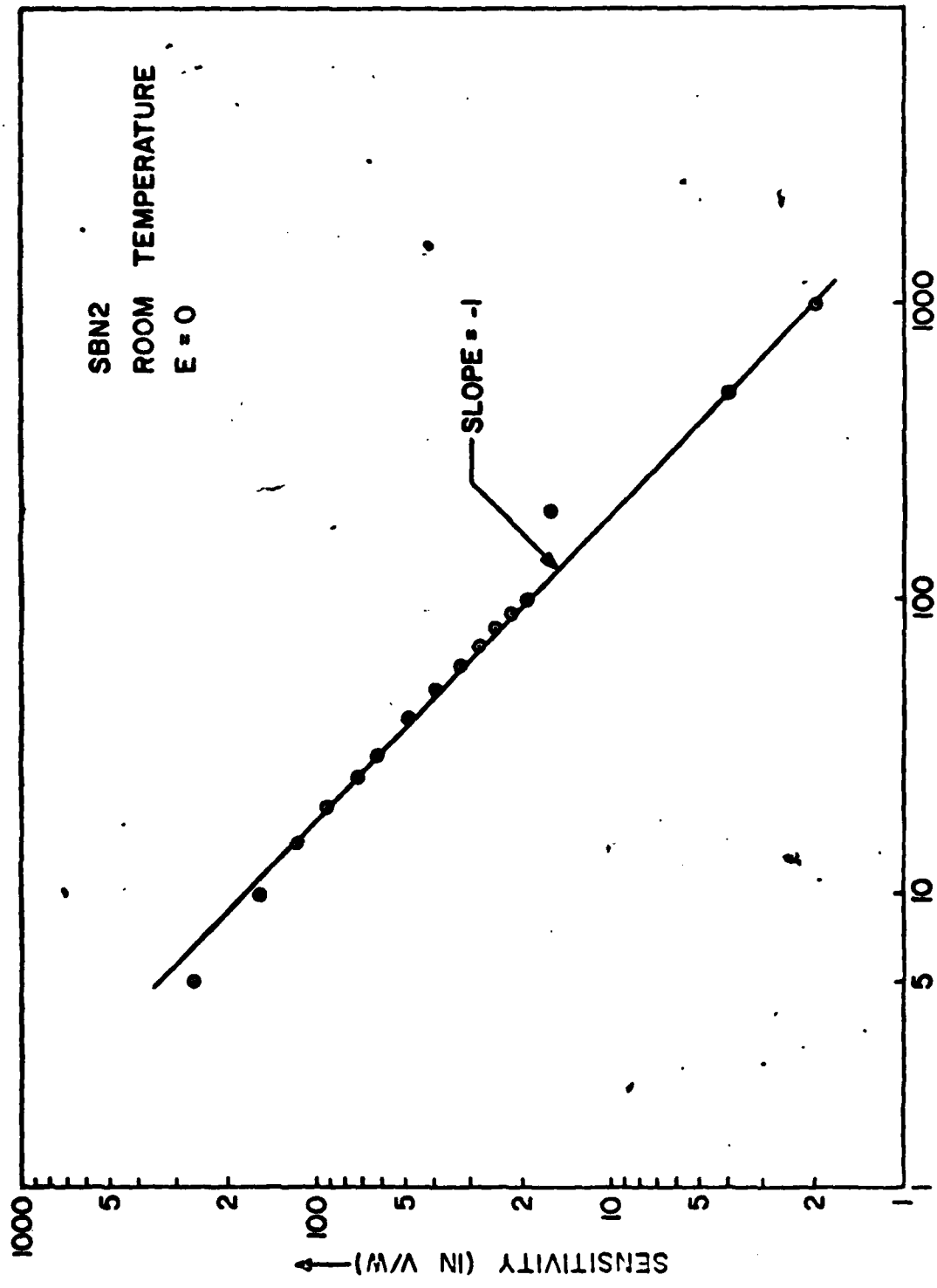

FIG. 26

Sensitivity versus field for SBN_2 at room temperature

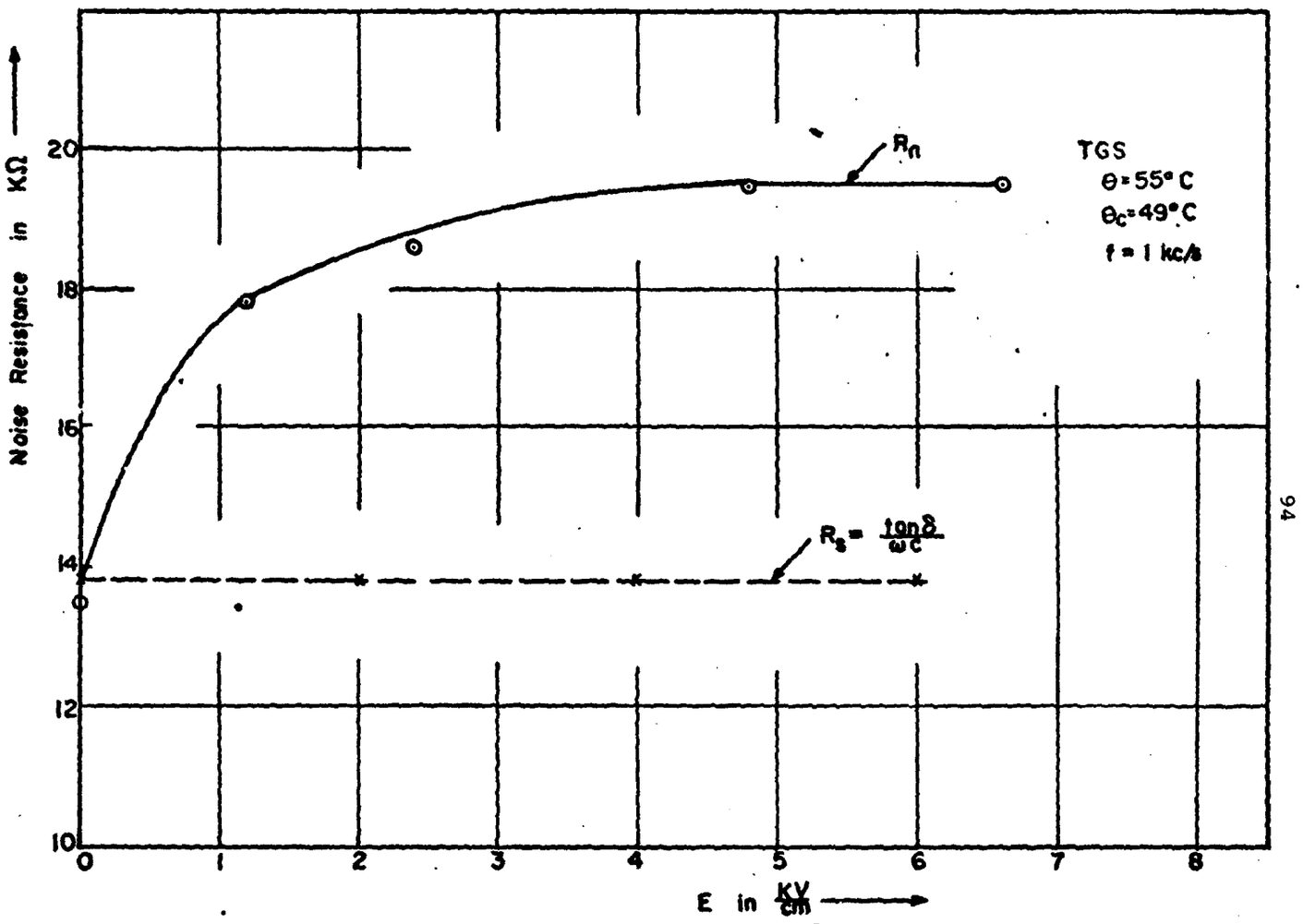

Fig. 27

Noise resistance R_n versus field in TGS#40 at 55°C

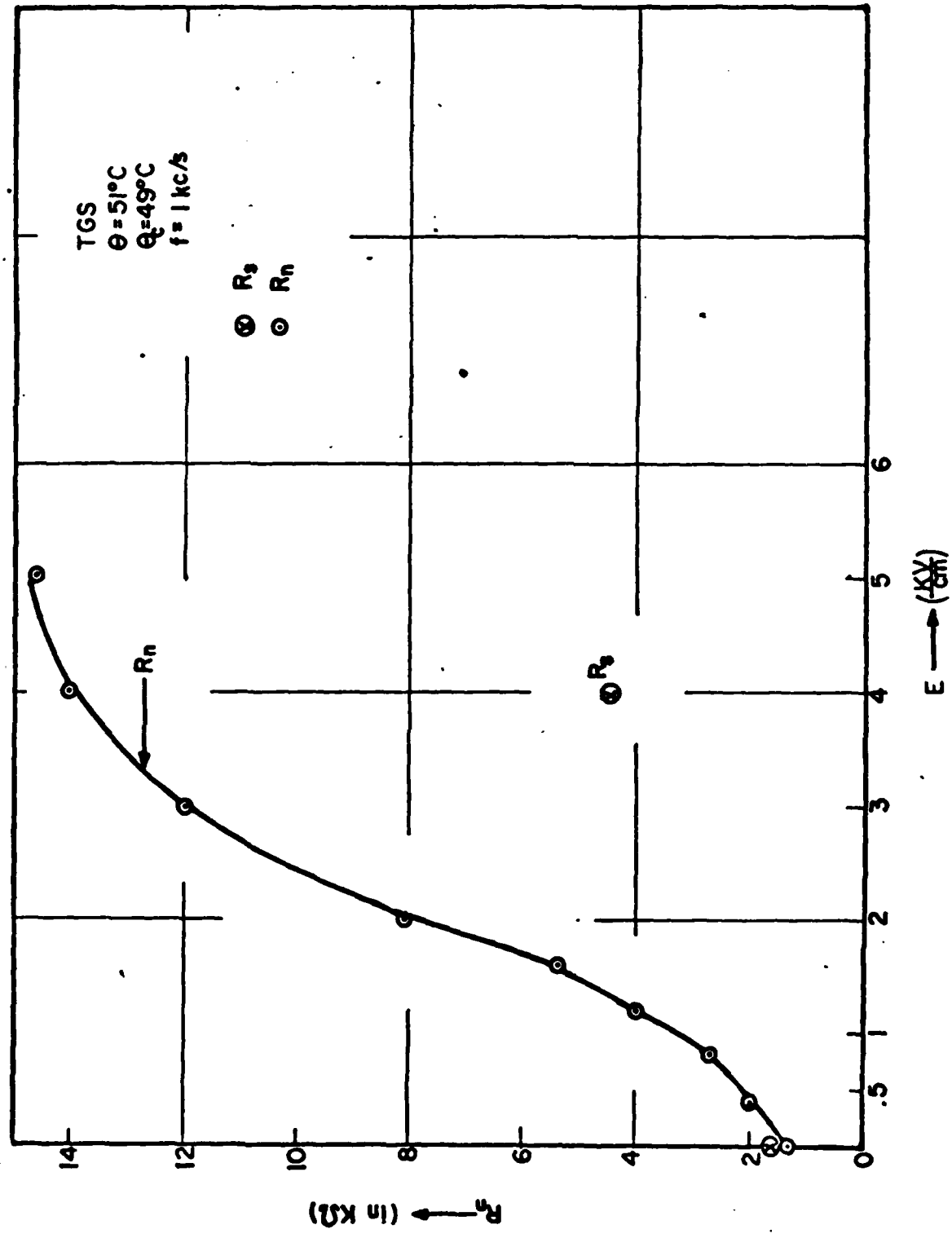

Fig. 28

Noise resistance R_n versus field in TGS#40 at 51°C

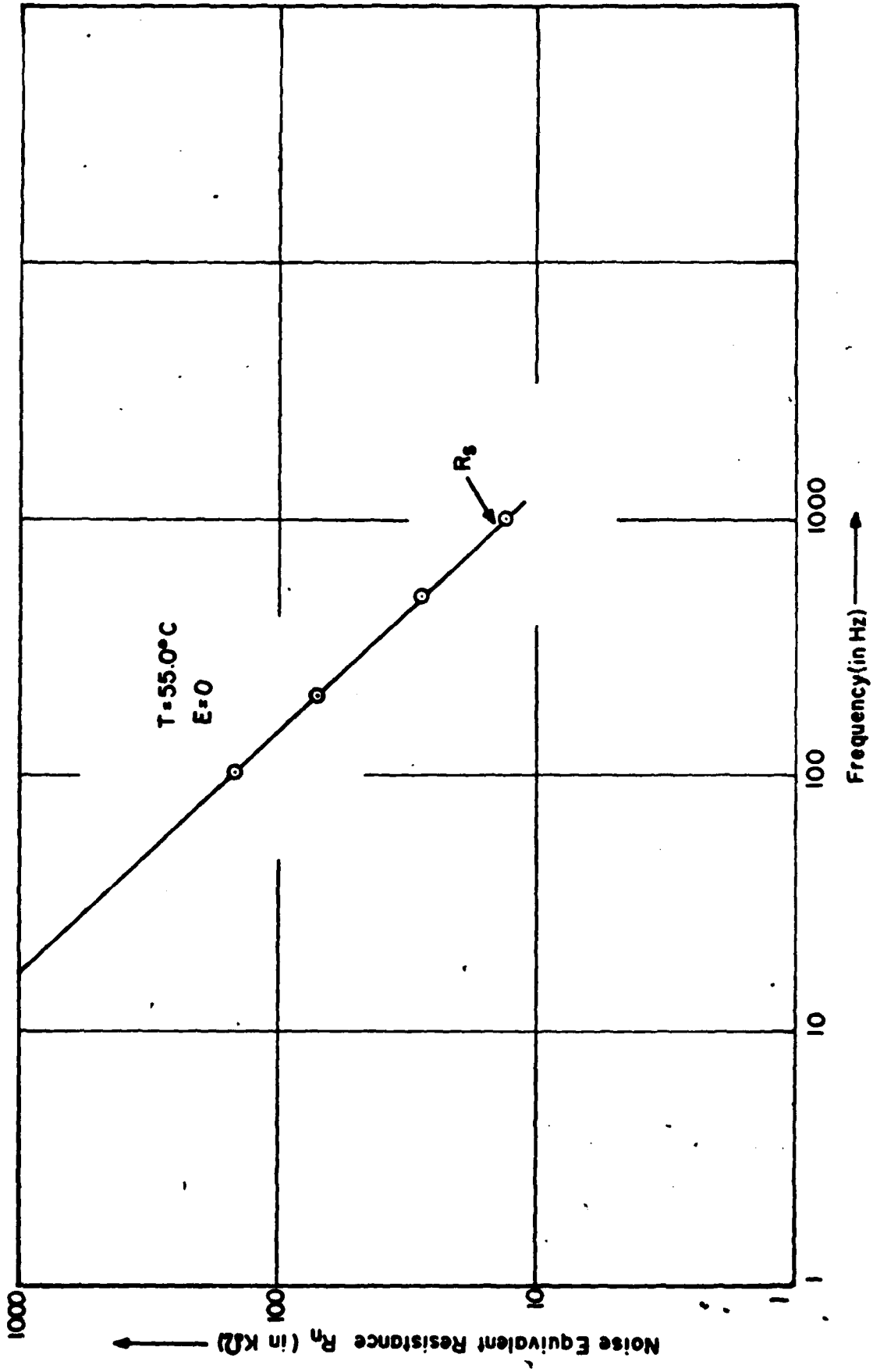

FIG. 29
Noise resistance R_n versus frequency TGS#40

FIG. 30

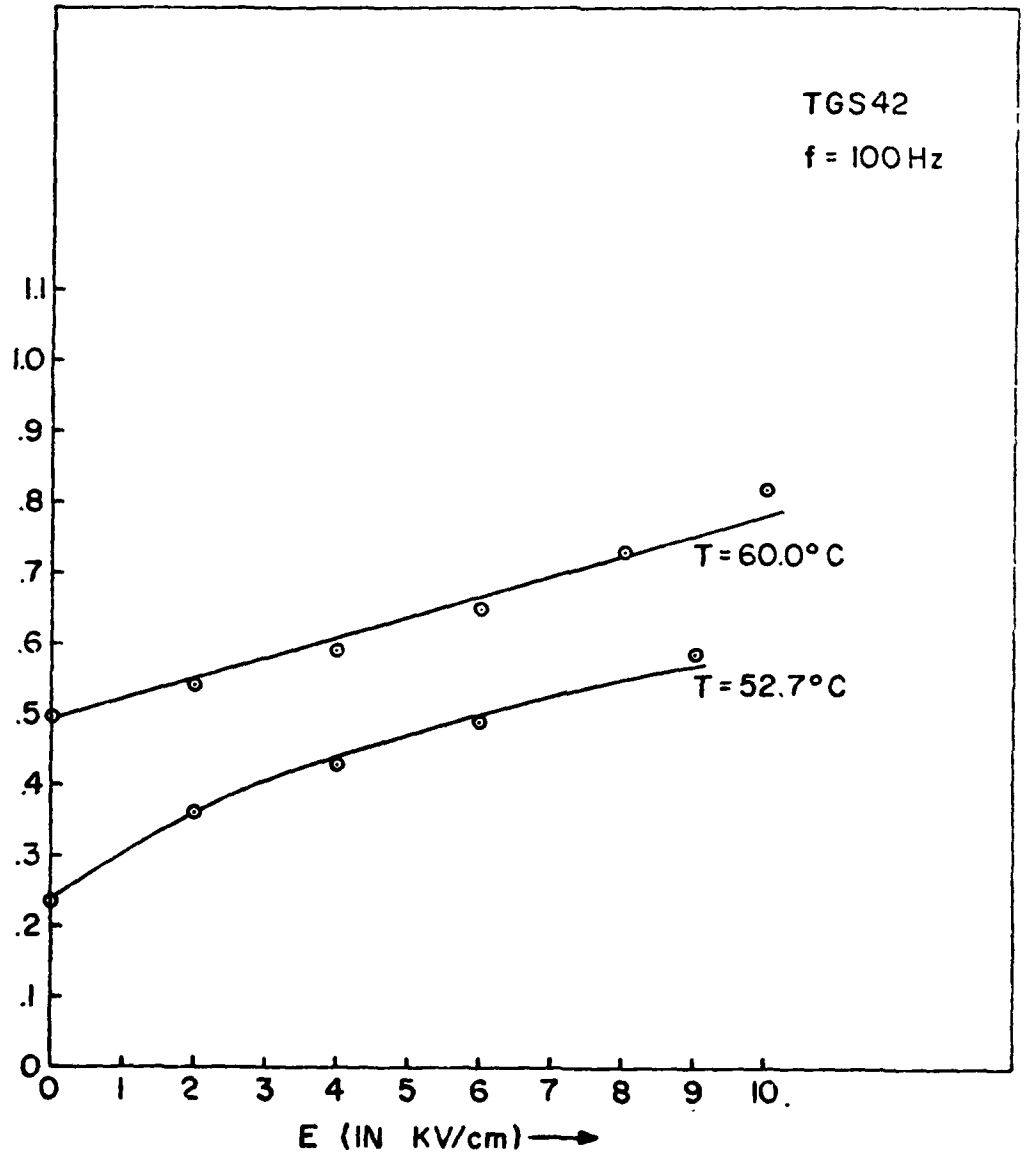

Noise resistance R_n in TGS#42 versus field

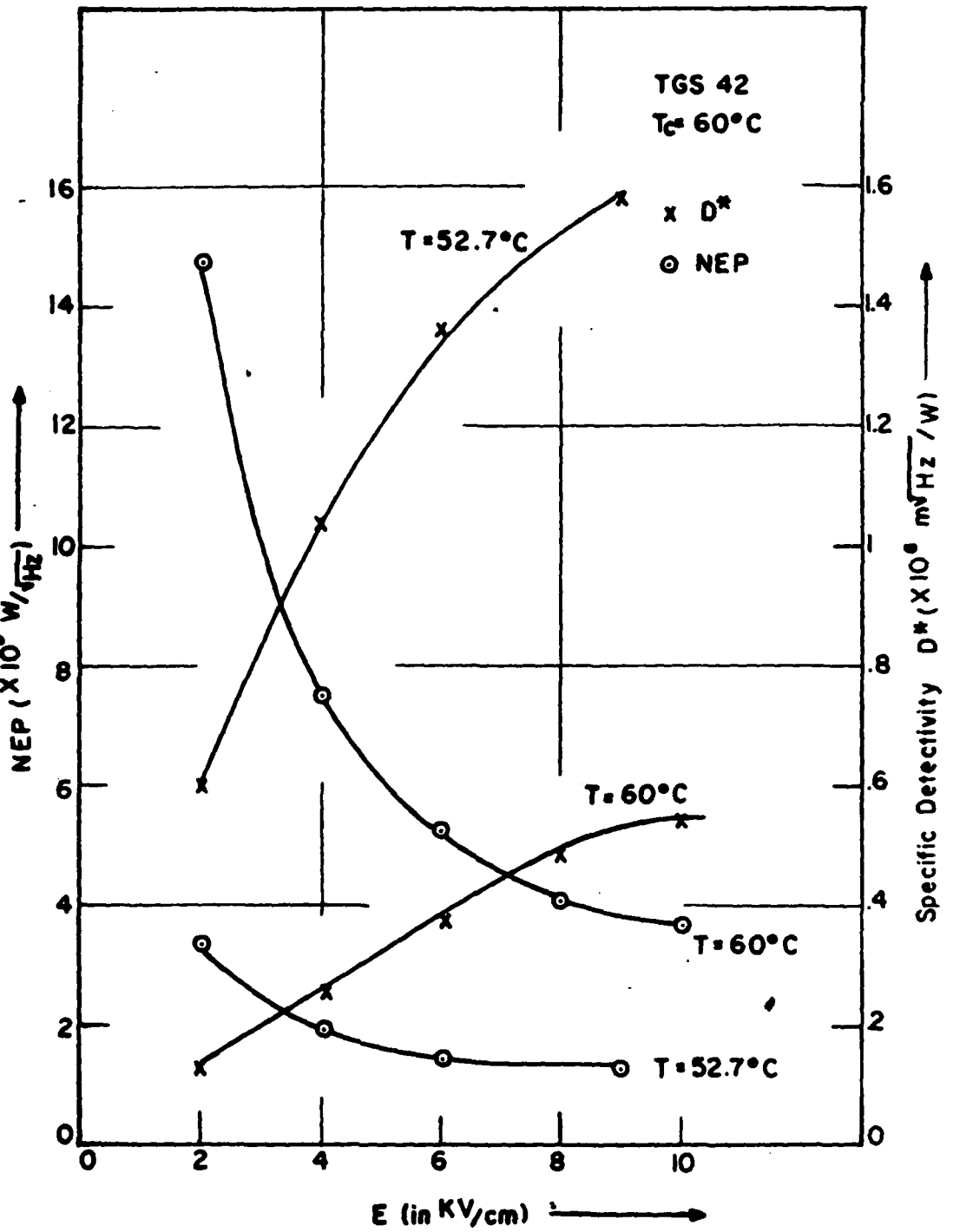

FIG. 31

NEP and D* versus field in TGS#42 for capacitive bolometer mode

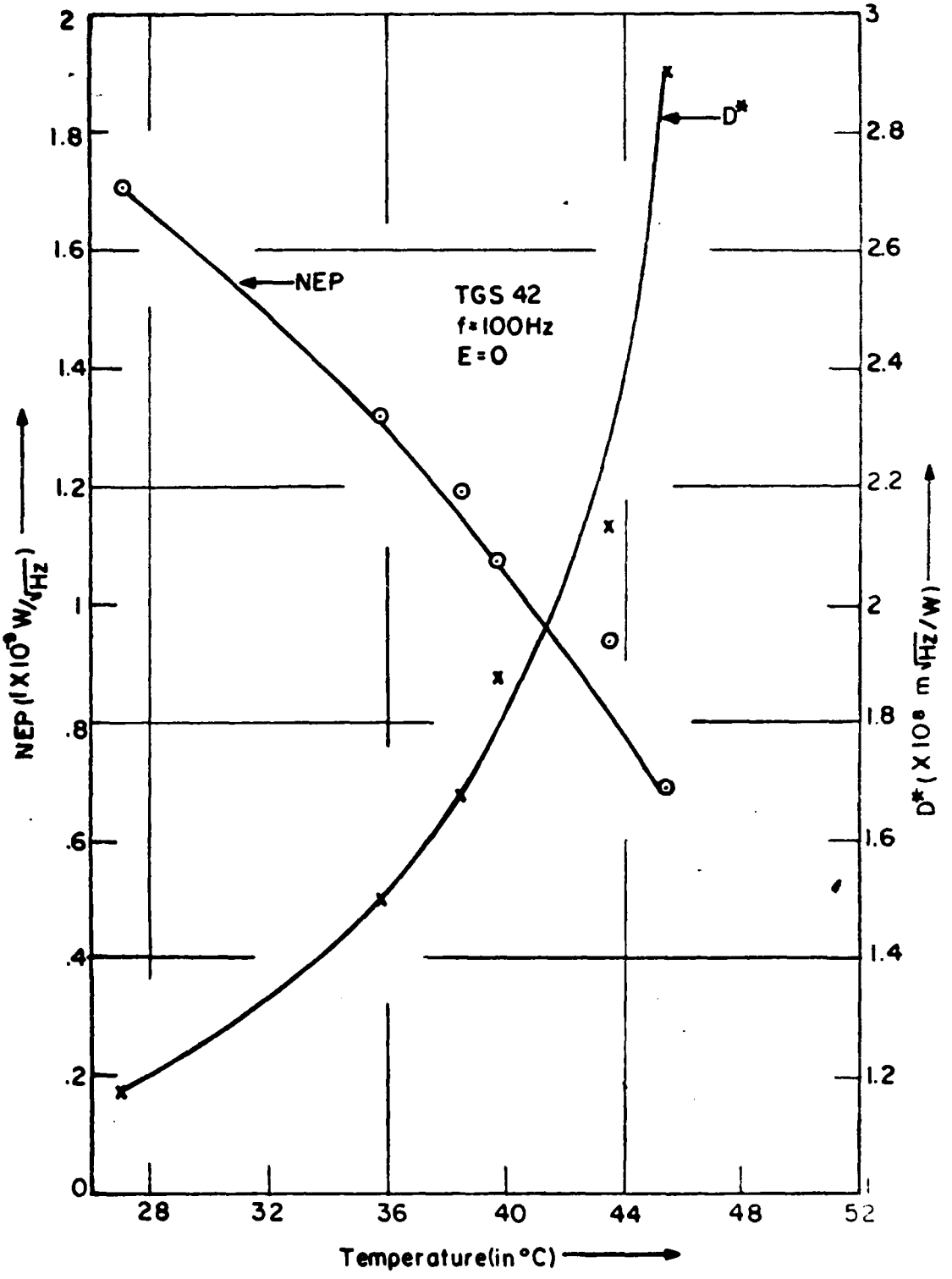

FIG. 32

NEP and D* versus temperature in TGS#42 for zero field

FIG. 33

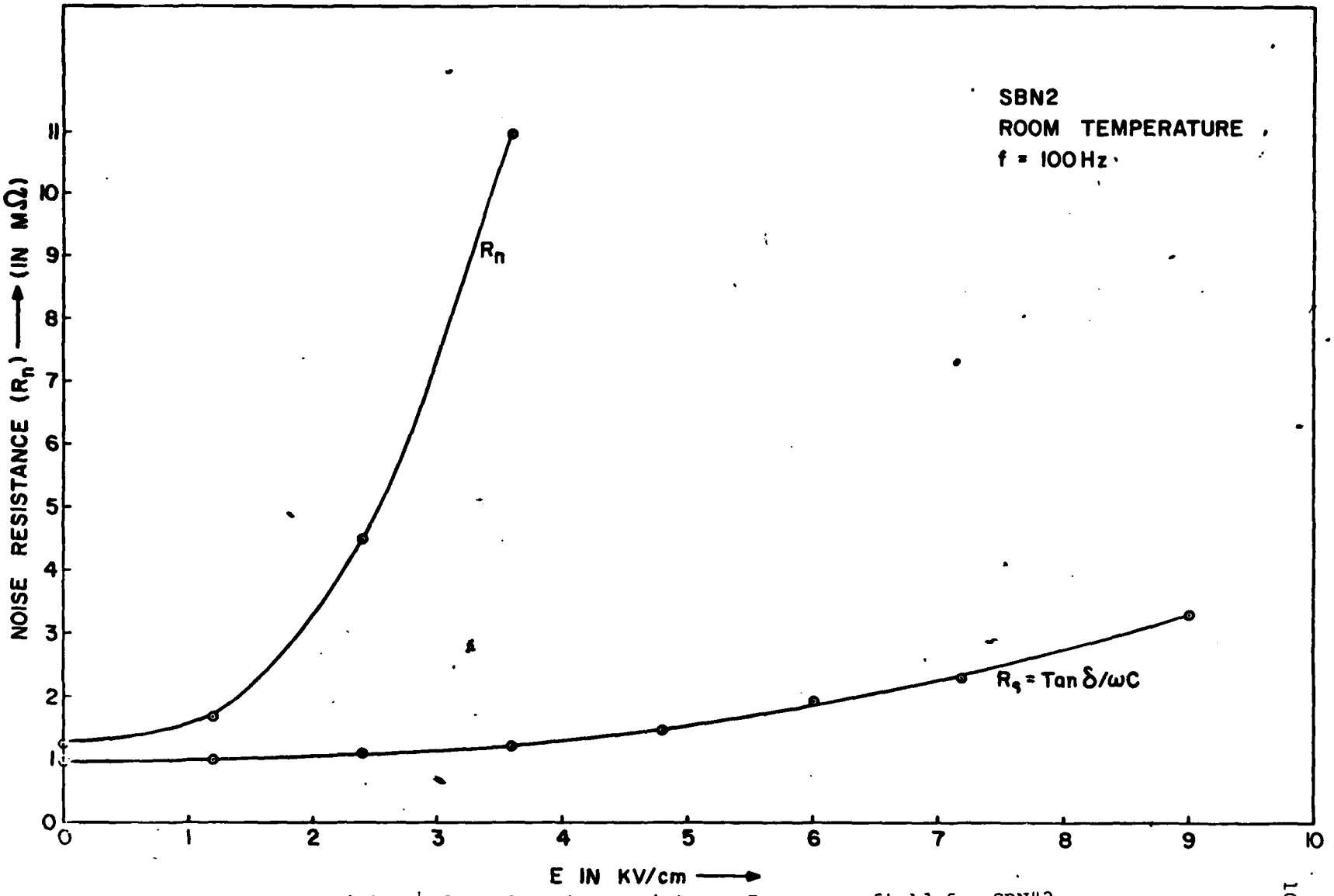

Noise resistance R_n and series resistance R_s versus field for SBN#2

FIG. 34

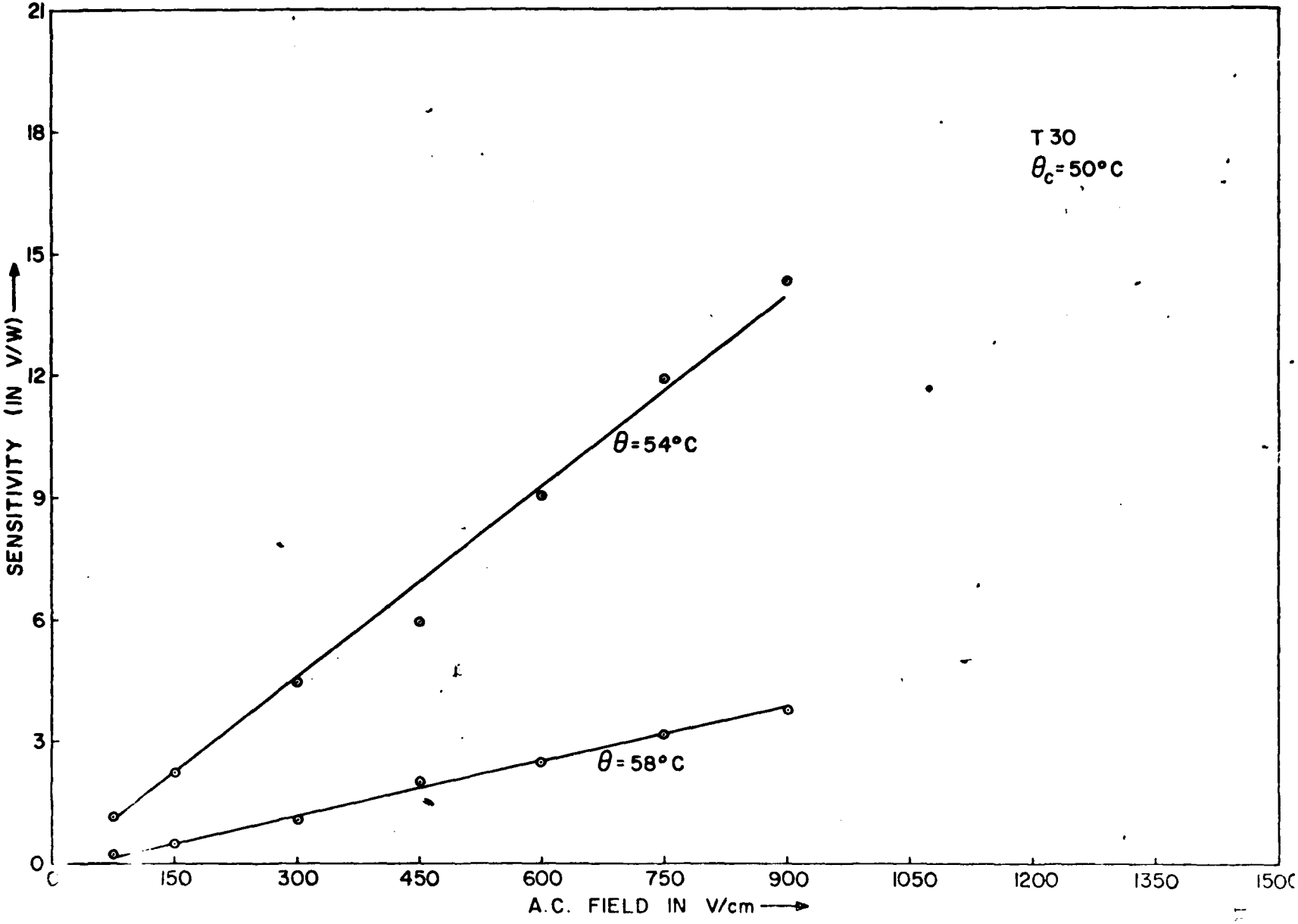

Sensitivity versus a.c. field for TGS#30

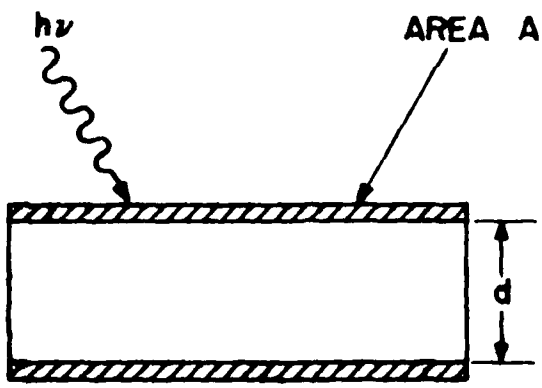

FIG. 35

PYROELECTRIC DETECTOR

Schematic diagram of pyroelectric detector

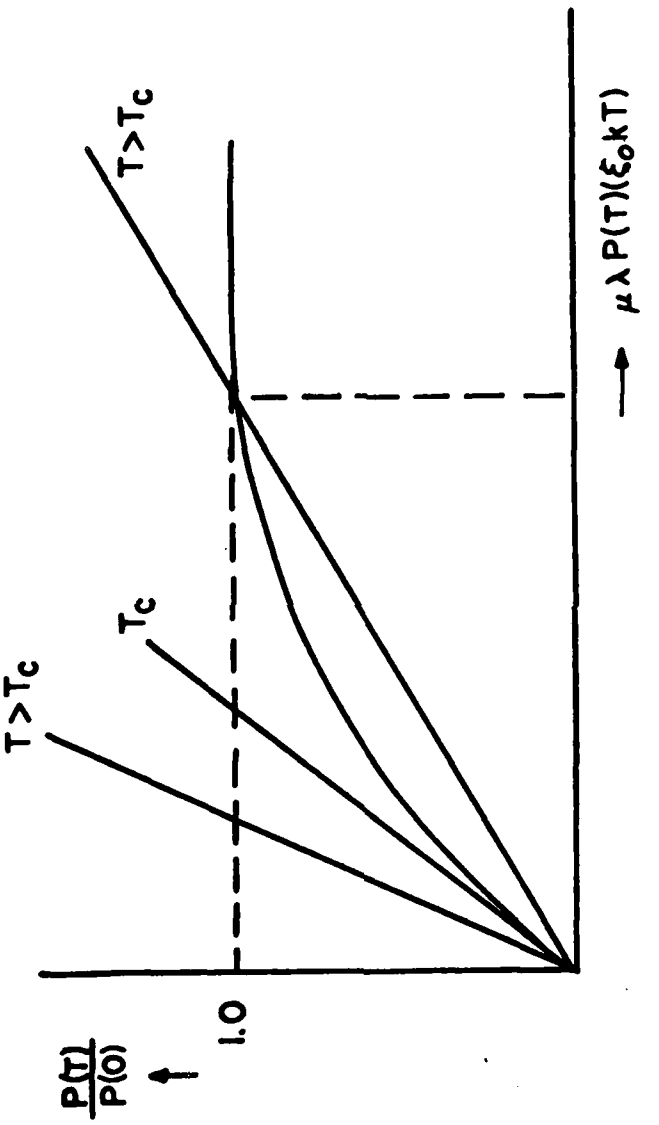

FIG. 36

Graphical determination of the saturation polarization, if any.

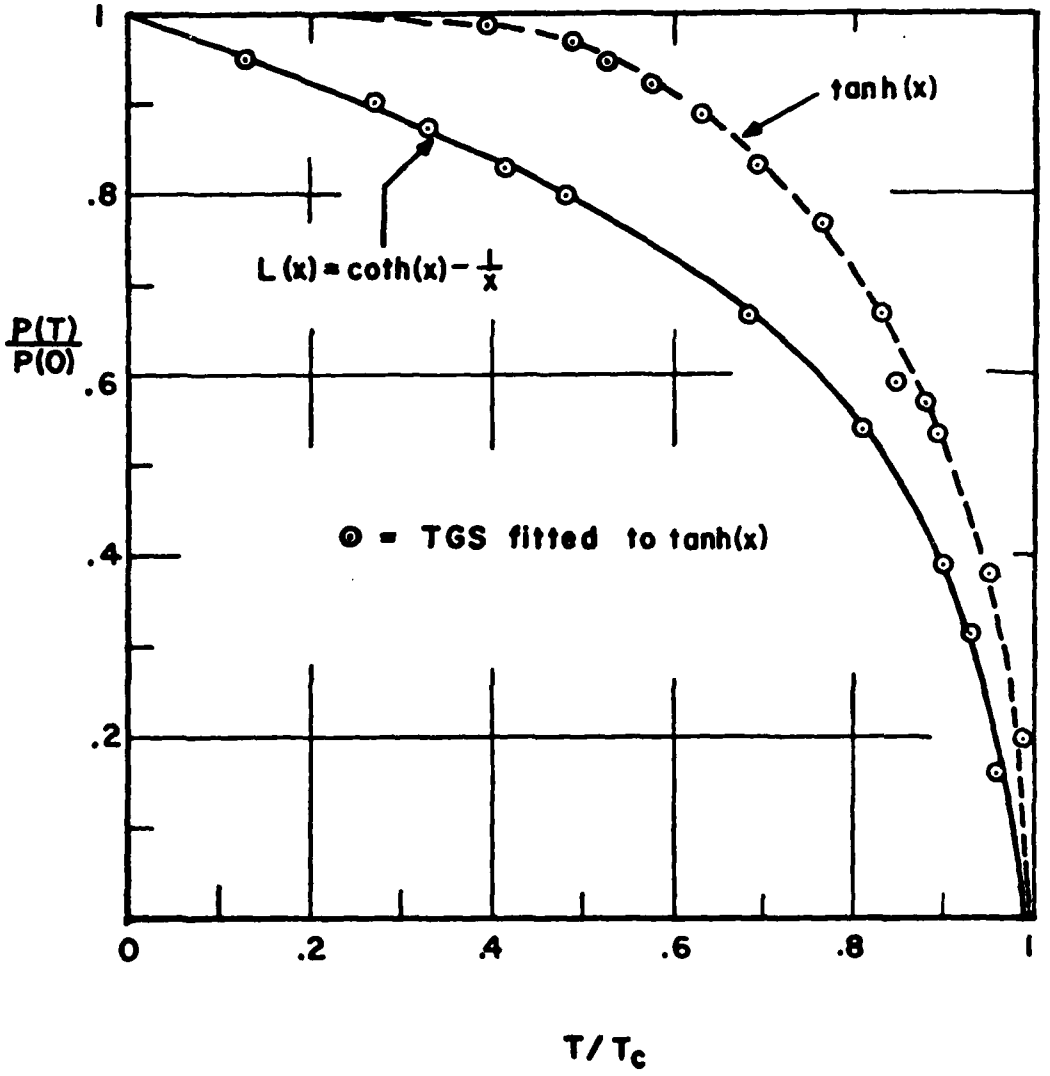

FIG. 37

$P_s(t)/P(o)$ plotted versus T/T_c for the classical and the two-level cases.

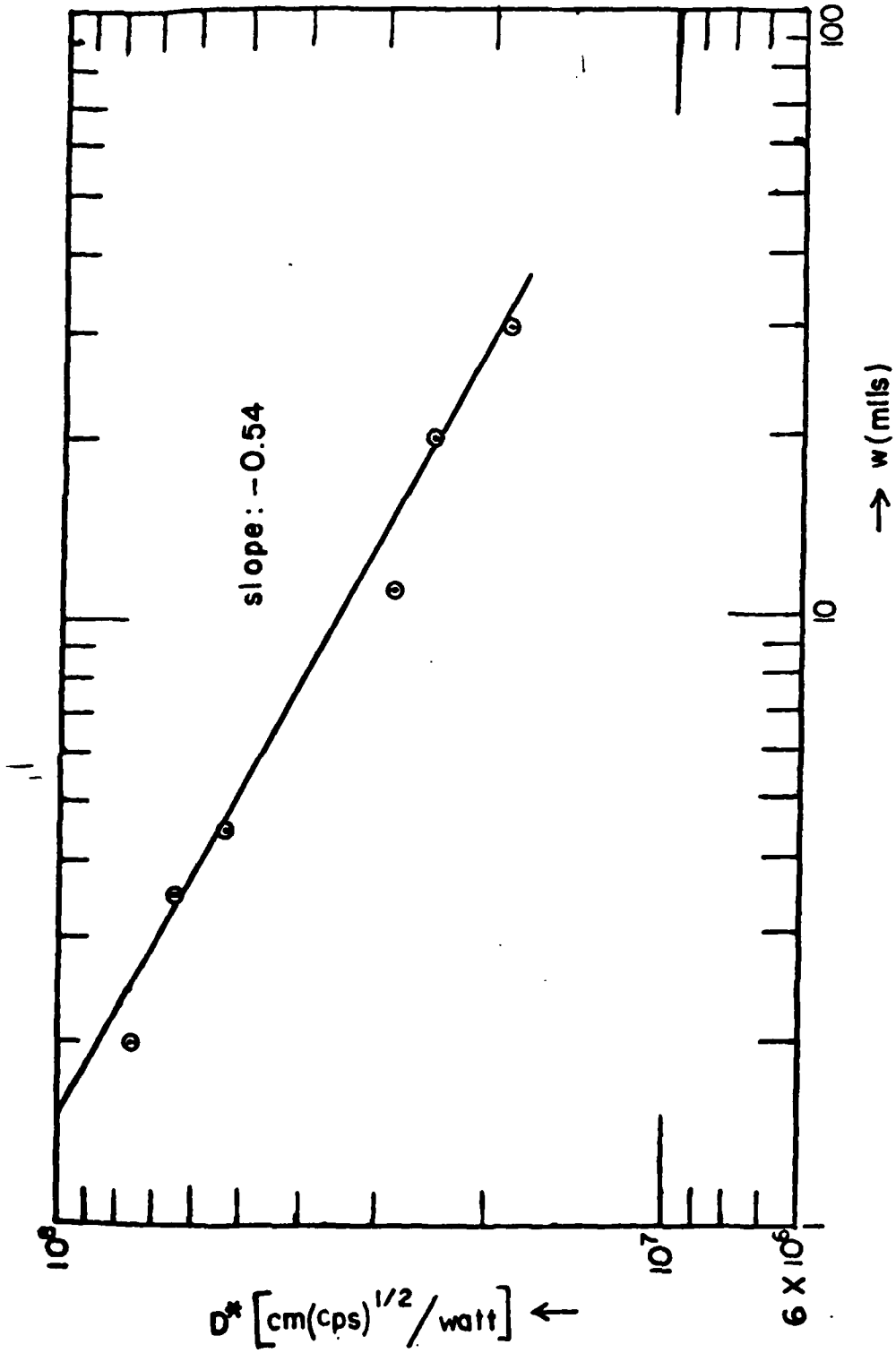

Fig. 38 D* versus w for PLZT samples with Cr-Au contacts

END

DATE
FILMED

04-82

DTIC